IDO/1523-5
Distribution Category UC-66d

UTEC ME 80-122

Comparison Between a Spray Column and a Sieve Tray Column Operating as Liquid-Liquid Heat Exchangers

Annette Keller
Harold R. Jacobs
Robert F. Boehm

MECHANICAL ENGINEERING
UNIVERSITY OF UTAH
SALT LAKE CITY, UTAH 84112

Date Published -- December 1980

PREPARED FOR THE
U. S. DEPARTMENT OF ENERGY
DIVISION OF GEOTHERMAL ENERGY
UNDER CONTRACT NO. E (10-1) 1523

DISCLAIMER

TABLE OF CONTENTS

ABSTRACT

Spray columns, baffle plate columns and perforated plate columns are equipment used in the chemical process industry as mass transfer devices. They also have potential use as heat transfer equipment for extracting energy from corrosive or fouling fluids.

Spray columns are the simplest of the liquid-liquid exchange equipment as they have no internal devices; however, they have proven to be the least efficient as liquid-liquid mass transfer equipment and thus, are not often used in extraction processes. Perforated plate columns are widely used in chemical extraction processes due to the ability to control the number of process stages; i.e. a defined fraction of a stage ~ .5-.7 will exist between each pair of trays.

The purpose of the present work was to compare the performance of a spray column and a sieve tray column as a liquid-liquid heat exchanger. In carrying out these studies a 15.2 cm (6.0 in) diameter column, 183 cm (6.0 ft) tall was utilized. The performance of the spray column as a heat exchanger was shown to correlate with the model of Letan-Kehat which has as a basis that the heat transfer is dominated by the wakeshedding characteristics of the drops over much of the column length. This model defines several hydrodynamic zones along the column of which the wake formation zone at the bottom appears to have the most efficient heat transfer.

The column was also operated with four perforated plates spaced two column diameters apart in order to take advantage of the wake formation zone heat transfer. The plates induce coalescence of the dispersed phase and reformation of the drops, and thus cause a repeti-

tion of the wake formation zone. In the present work, it is shown that the overall volumetric heat transfer coefficient in a perforated plate column is increased by a minimum of eleven percent over that in a spray column. A hydrodynamic model that predicts the performance of a perforated plate column is suggested.

NOMENCLATURE

A	area
C_p	heat capacity
d	diameter of thermocouple bulb
d_p	diameter of droplet
D	diameter of column
f	friction factor
F	duration of continuous phase, drop and wake temperature sequence
g	acceleration of gravity
g_c	gravitational constant
h	convective heat transfer coefficient
H	percent of heat lost from column
k	thermal conductivity
m	volume of wake elements shed per volume of drop and unit length of column
m	mass of thermocouple bulb
$\dot{m}$	mass flow rate
m_w	volume of wake shed
m_p	mass of droplet
M	ratio of wake to drop volumes
M_D	wake volume
Q	volumetric flow rate
r	$(\rho C_p)_d/(\rho C_p)_c$
R	V_d/V_c
Re_d	Reynolds number of thermocouple bulb
Re_D	Reynolds number of column
Re_p	Reynolds number of droplet

t time

t_s time for a droplet to rise through the wake formation zone

T temperature

U experimental temperature

U_V overall volumetric heat transfer coefficient

v_o volume of droplet

V volume

V superficial velocity = Q/A

V' actual velocity

V_T terminal droplet velocity

V_s wake shedding velocity

z height along column axis

α thermocouple time constant

ρ density

ϕ holdup

ϕ_f holdup at flooding

μ viscosity

Subscripts

c continuous phase

d dispersed phase

i inlet

j number of plate

l top of the wake shedding zone

o outlet

s top of the wake formation zone

w wake

z height

INTRODUCTION

Geothermal energy has been utilized for the production of electrical power for a number of years in a few unique vapor dominated reservoirs such as the Geysers in California. The increase in world energy demand has created an interest in developing other geothermal sites. The potential geothermal resources in the Western United States have an estimated potential of producing 385,000 MWe by the year 2000 and could if developed greatly reduce the dependence of other resources.

Geothermal resources occur in three types of reservoirs: vapor dominated, hot dry rock, and liquid dominated. As mentioned, the use of vapor dominated systems for production of electrical power has been successfully demonstrated. Development of hot dry rock reservoirs will require new drilling and energy extractive technology. Liquid dominated systems hold the greatest potential for contribution to U.S. energy self sufficiency within the next fifteen to twenty years as they are estimated to be twenty times more prevalent that vapor dominated systems [1].

Conventional binary cycles appear to be economical for producing electrical power from liquid dominated systems that are low in dissolved solids. However, many geothermal brines are of a corrosive and/or fouling nature being heavily laden with dissolved solids [2]. Non-conventional heat exchange equipment must be developed in order to overcome the fouling problem that would occur in conventional shell and tube heat exchangers. It has been shown that conventional heat exchangers would be the major capital cost item in a plant, other than the cost of drilling the geothermal wells. A type of heat exchanger that would

reduce the volume necessary to support the heat load in addition to eliminating the fouling problem would make the economics of the liquid dominated systems more competitive with other energy sources.

This study concentrates on the design of a direct contact heat exchanger to be used as a preheater in a binary power producing cycle like that shown in Figure 1. The apparatus is a vertical column arranged for counter-current flow of two immiscible fluids. The geothermal brine would flow downward through the column and contact the less dense working fluid which would be dispersed into small drops flowing upward. The drops would be heated by the brine and conversely the brine would be cooled by the drops. Ideally a small temperature difference is possible throughout the column depending upon the thermal capacitance of the two fluids and their relative flow rates. This design eliminates small easily fouled tubes and increases the ratio of the total area of thermal contact to the volume of the heat exchanger.

The preheater typically will carry about 30 percent of the heat duty in the cycle[3], however, it will require a greater volume than the boiler because it will involve sensible heat transfer as opposed to latent heat transfer. A direct contact boiler design has been investigated by Jacobs, Boehm, and Hanson[3]. The brine temperatures in the preheater are significantly lower than in the boiler, thus it is more probable that precipitation of any dissolved solids will occur in it.

Direct contact heat exchange introduces two problems. First, the two fluids must be at the same pressure. If the well pressure is less than the optimum turbine pressure then a brine pressure boost pump will

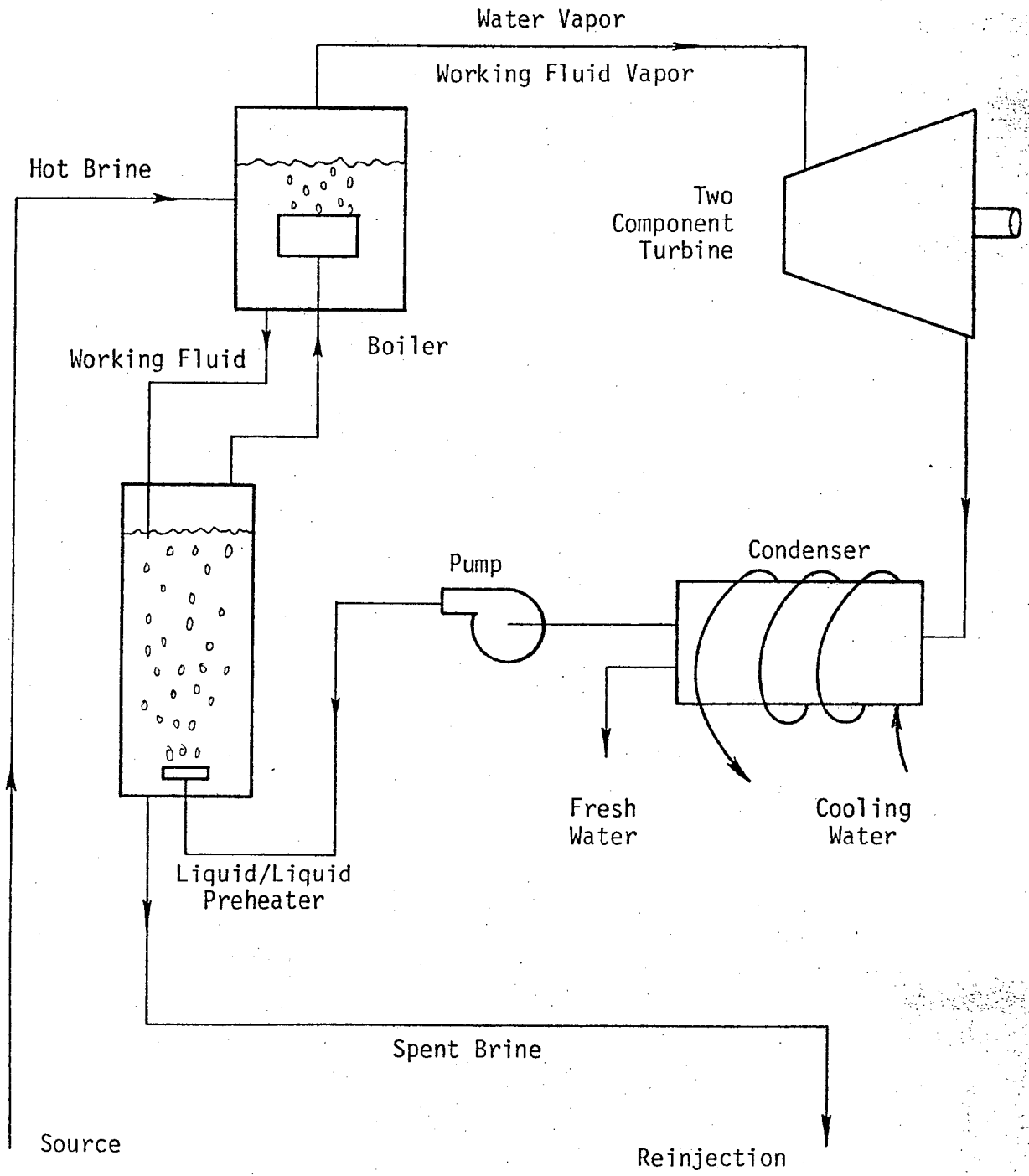

Figure 1. Basic Direct Contact Binary Power Cycle

be necessary. Although this pump will reduce the net work done by the cycle, the closer approach temperatures possible from direct contact heat exchange will help to compensate for the increased pump work.

The other problem involves the choice of a working fluid. The brine and the working fluid will be mutually soluable to some degree so some of the working fluid will be removed with the brine probably necessitating a separation system for working fluid recovery. The accompanying fact that a small amount of brine will be dissolved in the working fluid will have the desirable effect of increasing the available enthalpy of the fluid expanding through the turbine, however, this mixture may require another separation system. Because the equilibrium solubility of the working fluid in the brine will probably increase with decreasing temperatures, the choice of a working fluid will be governed in part by its solubility in the brine at the temperatures present in the preheater. The working fluid must also have suitable thermodynamic properties in order to maximize the power production.

The binary cycle is most efficient when the working fluid is supercritical in the primary heat exchanger and when it leaves the turbine as a saturated vapor[3]. Refrigerants and light hydrocarbons have desirable thermodynamic properties. The hydrocarbons become favorable when working fluid availability and total economics are considered, however; the exact fluid selection will depend on the characteristics of the particular well. Although the heat transfer properties of hydrocarbons are poor, the decreased size and therefore cost of the direct contact heat exchange system will compensate for this.

Possible working fluids that have been considered by Jacobs, Boehm,

and Hanson[3] include pentane, isobutane propane, hexane, R-111, R-113, and R-114. Some cyclic hydrocarbons have also been found to meet the requirements. Pentane, hexane, and isobutane are preferred due to their low relative cost and due to their low solubility in the brine.

There are several types of counter-current flow devices that have conventionally been used for mass transfer which could also serve as direct contact liquid-liquid heat exchangers. These include spray towers, baffled towers, perforated plate towers, and wetted-wall-towers. Spray towers are the simplest design and have high throughput, however, they have the disadvantage of possible strong back mixing. Baffled towers reduce back mixing however they would cause coalescence of the dispersed phase. The perforated plate tower has a lower throughput, however, it has been shown to be about twice as efficient for mass transfer as the baffled tower. The wetted-wall-tower would reduce the amount of volume necessary for separation of the two fluids, but this is at the expense of the surface area available for heat transfer.

The problem with back mixing in a spray tower can be solved by keeping the ratio of tower heighth to diameter large. It appears that values of 7 to 10 for this ratio are adequate. However, the heat transfer coefficients observed in spray towers do not appear to be large. In some portions of a spray tower Letan and Kehat have indicated that the heat transfer is reduced by a wake shedding mechanism. Reduced heat transfer on a volumetric basis may thus result from a tall tower, however as previously noted a tall tower is required to prevent back mixing. Thus, a perforated plate tower may be more desirable despite the lower throughput as it could lead to the requirement of a signifi-

cantly lower volume heat exchanger. The purpose of the present work is to evaluate the prior conclusions and models concerning spray columns and to evaluate the relative performance when perforated plate internals are added. As most of the existing data have been obtained using kerosene as the dispersed phase, it was also used in the present work despite the fact that it is not a likely geothermal binary working fluid. Further it is a safer fluid to use in the laboratory being less volatile than pentane, isobutane or hexane.

In this thesis results for the spray tower were compared with the results of Letan and Kehat, and Plass. The tower was then run with four perforated plates and the results were compared to determine the extent to which the heat transfer is improved by reducing the amount of back mixing.

PREVIOUS WORK

A heat exchange system that has been designed for a particular geothermal site must be optimized in terms of power produced per existing unit flow of geothermal fluid. Previous experimental heat transfer results have therefore been correlated in terms of the ratio of the working fluid flow rate to the existing brine flow rate, and in terms of the holdup, which is defined as the volumetric fraction of the dispersed phase in the column. Holdup is a function of the fluid flow rates and the particle Reynolds number of the droplets in the dispersed phase.

The heat transfer that is being measured occurs in the volume of the exchanger above the dispersion plate at the working fluid inlet and

below the level of the continuous phase in the column. Above this level, referred to as the interface, the dispersed phase droplets coalesce and the two fluids are no longer in contact.

The experimental results in Plass have been presented in terms of an overall volumetric heat transfer coefficient as defined below*

$$U_V = \frac{Q \rho c_p \Delta T}{V \Delta Tm} \qquad (1)$$

The volume in Equation (1) refers to the volume discussed above, and the log mean temperature difference is taken about the boundaries of this volume. It can be shown that the thermal contact area per unit volume in the column is given by $6\phi/d_p$. This relationship can be used to relate the volumetric heat transfer coefficient to a surface coefficient:

$$U_V = \frac{6\phi U}{d_p} \qquad (2)$$

Heat tranfer correlations obtained from experiments where the flow is laminar may be applied to columns of varying sizes as long as the flow conditions are laminar, however, results obtained from turbulent flow systems may only be applied to identical systems. The Reynolds number of the column is given by[4]

$$Re_D = \frac{V_c \rho_c D}{\mu_c}(1 - \phi)^{1.5} \left[1 + \left(\frac{\rho_d}{\rho_c} - 1\right)\right].$$

For a value of Re_D less than 2300 flow is laminar otherwise it is turbulent.

Plass conducted experiments in a 6 inch (18.24 cm) diameter column

---

* See notation

utilizing Chevron Insulating Oil as the dispersed phase. A dispersion plate with an array of 3.18 mm (0.175 in) holes and one with 1.60 mm (0.063 in) holes for which average droplet diameters were 6.40 mm (0.253 in) and 3.10 mm (0.122 in) respectively, were tested.* The following correlation, based on the entire volume above the distribution plate, was obtained[5].

$$U_{vt} = 45000\ (\phi - 0.05)\ e^{-0.57R} + 600 \text{ Btu/hr ft}^3\text{°F}\ (\phi > 0.05)$$
$$U_{vt} = 12000\phi \text{ Btu/hr ft}^3\text{°F}\ (\phi < 0.05) \qquad (3)$$

Letan and Kehat have developed a model for a direct contact heat exchanger based on experimental results obtained using a 15.2 cm (6.0 in) diameter column. Kerosene was used as the working fluid, and it was dispersed into 3.50 mm (0.137 in) diameter droplets. Two modes of operation referred to as dispersed packing and dense packing of droplets were investigated. It was found for both modes that the heat transfer in the column is controlled by the fluid mechanics of the system and not by the resistance to heat transfer inside or at the surface of the drops. The wakes of the drops play a dominate role in the fluid mechanics of the system. It was also found that, although, lower flow rates are required for a dense packing mode, more heat is transferred, and; therefore, this mode is more desirable. However the dense mode is difficult to obtain in practice.

Letan and Kehat have divided the spray column into five hydrodynamic regions as shown in Figure 2: (1) wake formation, (2) intermediate,

---

* These droplet diameters were obtained from correlations in the literature.

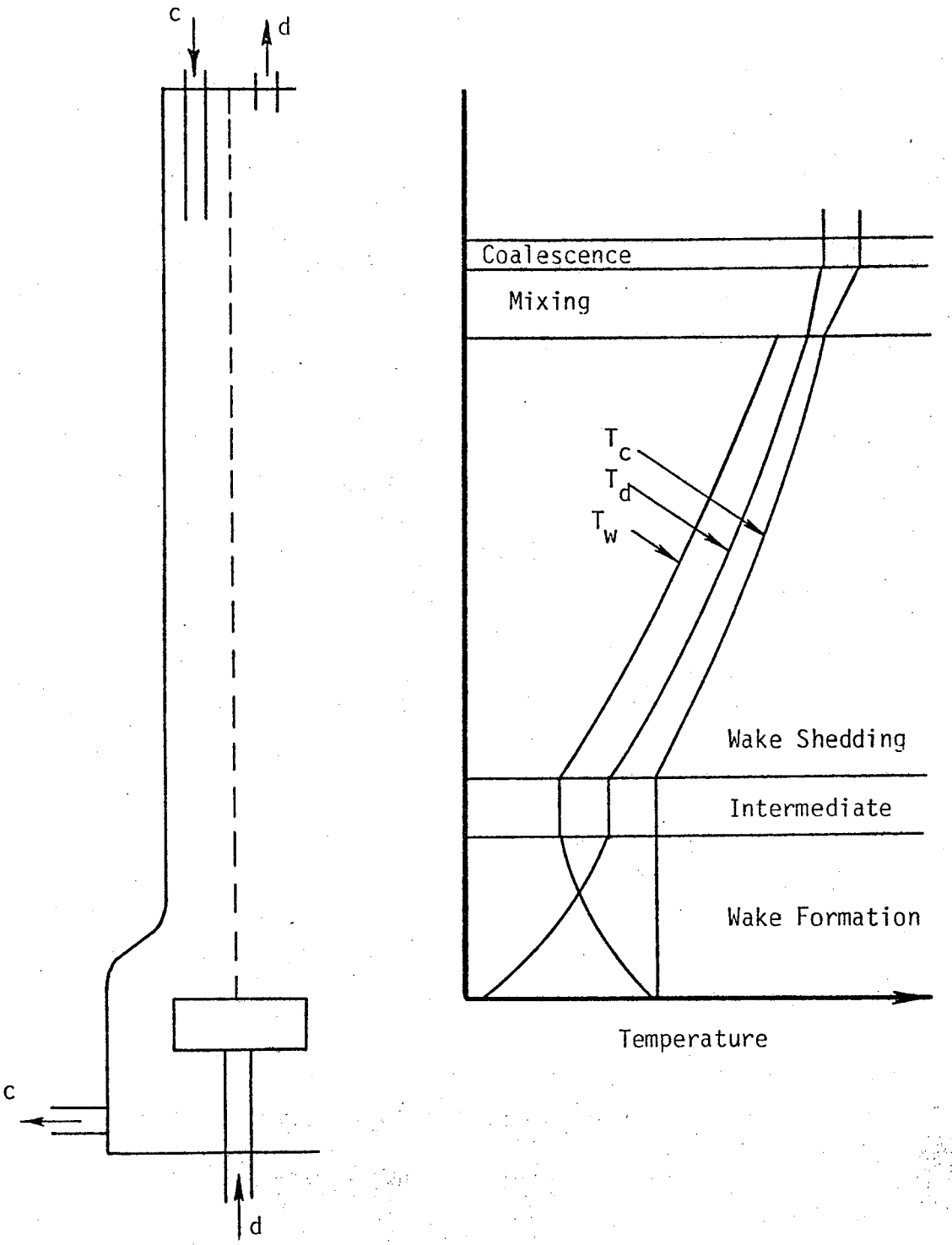

Figure 2. Physical Model of Heat Transfer in a Spray Column Proposed by Letan and Kehat

(3) wake shedding, (4) mixing, and (5) coalescence. The wake formation zone occurs a short distance above the dispersion plate where boundary layer separation begins to occur on the drop. This disturbance causes turbulent motion in the continuous phase close to the boundary of the drop enhancing wake to drop heat transfer, and it causes the drop to oscillate resulting in turbulent mixing inside the drop. The fluid in front of the boundary layer separation point remains at the local continuous phase temperature while the fluid in the highly mixed zone behind the separation point quickly comes to thermal equilibrium with the drop and then is carried upward as a wake.* It is in this zone that most of the wake to drop heat transfer occurs; however, conduction and convection from the wake to the continuous phase are negligible compared to that higher in the column.

The intermediate zone occurs only in the dispersed mode of packing when the wake has reached its maximum volume, and no mass or therefore heat, is transferred into or out of the wake. In the dense packing mode a temperature jump of the continuous phase occurs instead, due to the backmixing that occurs in the wake shedding zone. In the next zone wake shedding occurs such that the flow rate of the continous phase into the wake through the boundary layer equals the flow rate of the continuous phase expelled from the wake. The elements that are shed from the wakes have been effectively backmixed with the continuous phase modifying its temperature and reducing the driving force for heat

---

* Because this boundary layer fluid gives up heat to the drop and then joins the wake which is made up of colder fluid from lower down in the column, the drop temperature eventually exceeds the wake temperature.

transfer. This zone represents the greatest portion of the column.

Near the continuous phase inlet there is a zone where all drops, the incoming continuous phase, and wakes returning from the coalescence zone are mixed. This mixing causes a temperature jump in both phases as shown in Figure 2. Finally the drops approach the upper interface and coalesce. The wakes are detached and flow back down to the mixing zone.

The hydrodynamics that have been found to occur in these zones clarify the desired role of perforated plates in improving the heat transfer efficiency of a column by reducing the distance in the column over which fluids are backmixed and by causing the wake shedding zone to reoccur above each plate.

Letan and Kehat have also examined the effects of fluid properties, column height and droplet size. The relationship between the volumetric flow rates, the fluid properties, and the thermal driving force can be seen from a steady state energy balance around the column.

$$Rr = -\frac{\Delta Tc}{\Delta Td} \tag{4}$$

where

$$R \equiv \frac{Qd}{Qc}$$

and

$$r \equiv \frac{(\rho c_p)_d}{(\rho c_p)_c}$$

They showed theoretically that the optimum value of the ratio of thermal capacities of the two streams Rr is equal to unity, and their experimental results support this conclusion. However, this value cannot

necessarily be selected in the geothermal power cycle as other factors may set the flow ratio and the fluid selection. From their model it was also concluded that for long columns the closest approach temperatures are obtianed for values of $Rr \leq 1$[6]. In addition the continuous phase temperature jump at the inlet is minimized for $Rr \leq 1$ in. long columns. The effect of backmixing is reduced in long columns as the distance that a wake is carried upward becomes small in relation to the column length. A parametric study of Letan showed that increased droplet size increased the required length and decreased the required diameter of the column[7].

A semi-empirical relationship between the slip velocity and the holdup has been obtained by Richardson and Zaki[8]. It is expressed in terms of the terminal velocity of the droplets as shown:

$$V_S = V_T (1 - \phi)^m \qquad (5)$$

where

$m = 3.65$ $\qquad Re_o < 0.2$

$m = (4.35\ Re_o^{-0.03} - 1)$ $\qquad 0.2 < Re_o < 1$

$m = (4.45\ Re_o^{-0.1} - 1)$ $\qquad 1 < Re_o < 500$

$m = 1.39$ $\qquad 500 \leq Re_o$

and $$V_T = \frac{1}{f}\left[\frac{4}{3} d_p \frac{(\rho_d - \rho_c)}{\rho_c}\right]^{1/2} = \frac{Re_o\ \mu_c}{d_p\ \rho_c}$$

where

$$f = \frac{24}{Re_o} \qquad Re_o < 0.1$$

$$f = \frac{18.5}{Re_o^{0.6}} \qquad 2 < Re_o < 500$$

$$f = 0.44 \qquad 500 < Re_o < 2 \times 10^5$$

$$f = 0.2 \qquad 2 \times 10^5 < Re_o$$

The slip velocity is defined as

$$V_s = V_d' + V_c' \quad , \tag{6}$$

and from the definition of superficial velocity it can be shown that this is also equal to

$$V_s = \frac{V_d}{d} + \frac{V_c}{(1 - \phi)} \quad . \tag{7}$$

Lapidus and Elgin[9] have combined Equations (5) and (7) and made a plot of the holdup ϕ against the superficial velocity of the continuous phase V_c with the superficial velocity of the dispersed phase V_d as a parameter. They have shown that there are two regions on the plot corresponding to dense packed operation and dispersed packed operation separated by a flooding line representing the disruption of stable flow condition. At flooding:

$$\left.\frac{\partial V_c}{\partial \phi_f}\right|_{V_d} = 0 \tag{8}$$

and the value of ϕ_f can be found from carrying out this differentiation[10]. Experimental results in this study will be compared with the predictions of Equations (5) and (7).

Letan and Kehat have developed a theoretical model for predicting the axial temperature profiles of both phases in the column assuming plug flow. Equations are generated from energy balances taken around the drops and wakes in each of the previously described regions of the column[11],[12]. Two parameters dealing with the wake volume are required to solve the equations for the dispersed packing mode and three

are required for the dense packing mode.

In this thesis the effects of the hold up and the flow rate ratio will be investigated. Experimental results will be compared to the predictions of Letan and Kehat and Plass.

EXPERIMENTAL

A 183.0 cm (6.0 ft) tall, 15.2 cm (6.0 in.) diameter, uninsulated schedule 80 pipe was used as the heat exchanger column. The water inlet pipe extended 43.2 cm (17.0 in.) down from the flange at the top of the column. Water entered the column through 16 axial holes in the inlet pipe. The distribution plate at the kerosene inlet was contained in a bell-shaped pressure vessel welded to the bottom of the column as shown in Figure 3. The surface of the plate was 24.1 cm (9.49 in.) below the bottom of the column. In an experiment performed by Dr. H. R. Jacobs at the University of Utah a variety of perforated plates were tested to optimize throughput and droplet uniformity. It was found that the flat perforated plate shown in Figure 4 was desirable and that 1.93 mm (0.760 in.) diameter perforations produced droplets of nearly the same diameter as those in the experiments of Letan and Kehat (3.50 mm, (0.138 in.)). This type of plate was used for the distribution plate and also for the perforated plate baffles.

Several windows were placed in the column so that droplets could be observed and so that the interface location and holdup could be measured. The inlet and outlet temperatures as well as the axial temperature profile inside the column were measured by 3.16 mm (0.124 in.) ungrounded, shielded, type K Omega thermocouples. Fast response 0.25 mm (0.01 in.) grounded, shielded, type K Omega thermocouples

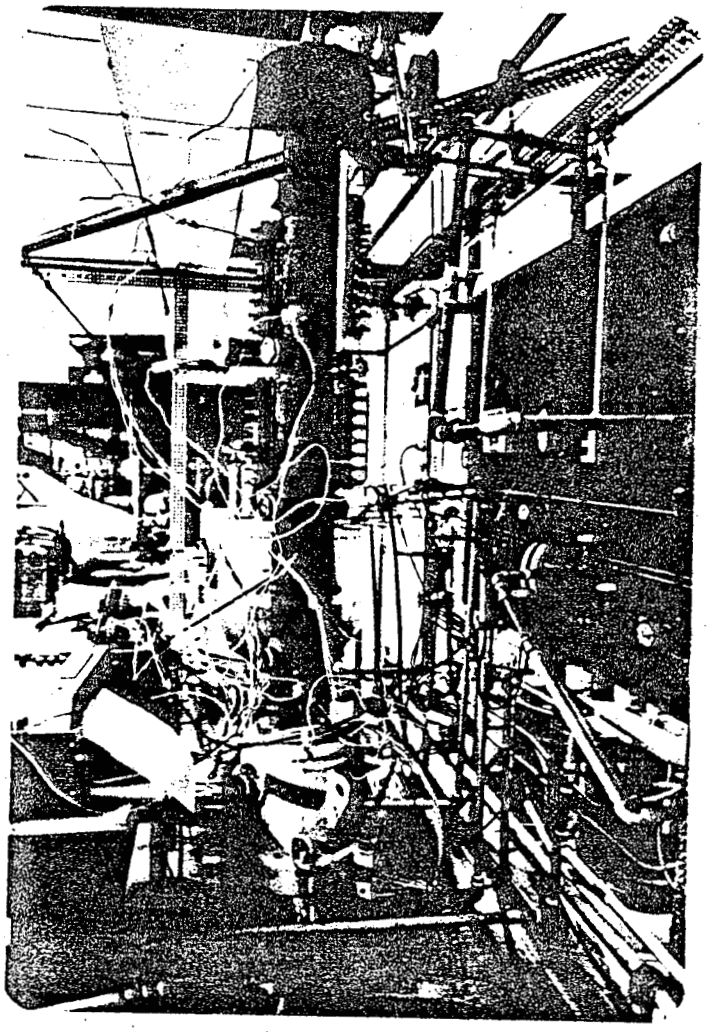

DIRECT CONTACT
HEAT EXCHANGER

FIGURE 3

PERFORATED PLATE

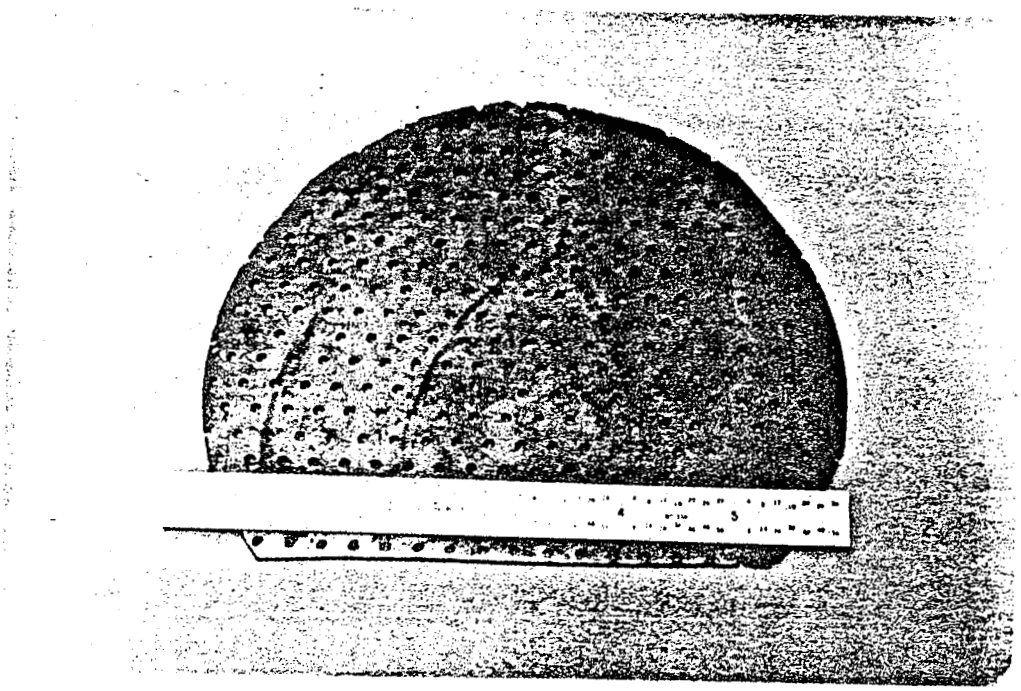

FIGURE 4

were used to measure temperature differences caused by the passage of the droplets and their wakes. Figure 5 shows the thermocouples and the windows.

Four perforated plate baffles were used to convert the column from a spray tower to a perforated plate tower. The plates shown in Figure 6, were spaced 30.5 cm (6.0 ft) apart. A 15.2 cm (6.0 in.) down spout provided a flow region for the downward flowing water to flow past the plates while the kerosene coalesced beneath the plates. The resulting flow pattern is shown in Figure 7.

A Cat Model 1010 piston pump was used to pump water from a 151 liter (40 gal) steam jacketed kettle through the column and back into the kettle. The water temperature was controlled by a Van Waters and Rogers thermoregulator which operated a solenoid valve on the steam line. A similar pump forced kerosene from a tank, through the column, through a shell and tube heat exchanger where it was cooled by cold water, and back to the tank. Flow was measured by CE Invalco 19 mm turbine-type flow meters installed on the column outlet lines for both kerosene and water. The hot water kettle and pump are shown in Figure 8 and the kerosene tank is shown in Figure 9.

Data was taken under steady-state operating conditions for the column first operated as a spray tower and then as a perforated plate tower. The arrangement of the thermocouples in the column is shown in Figures 10a and b. In Figure 10a the thermocouples labeled with an "s" subscript, indicating slow response, measure an average temperature; and the ones having an "f" subscript, indicating fast response, measure temperature differences. In Figure 10b the thermocouples just under

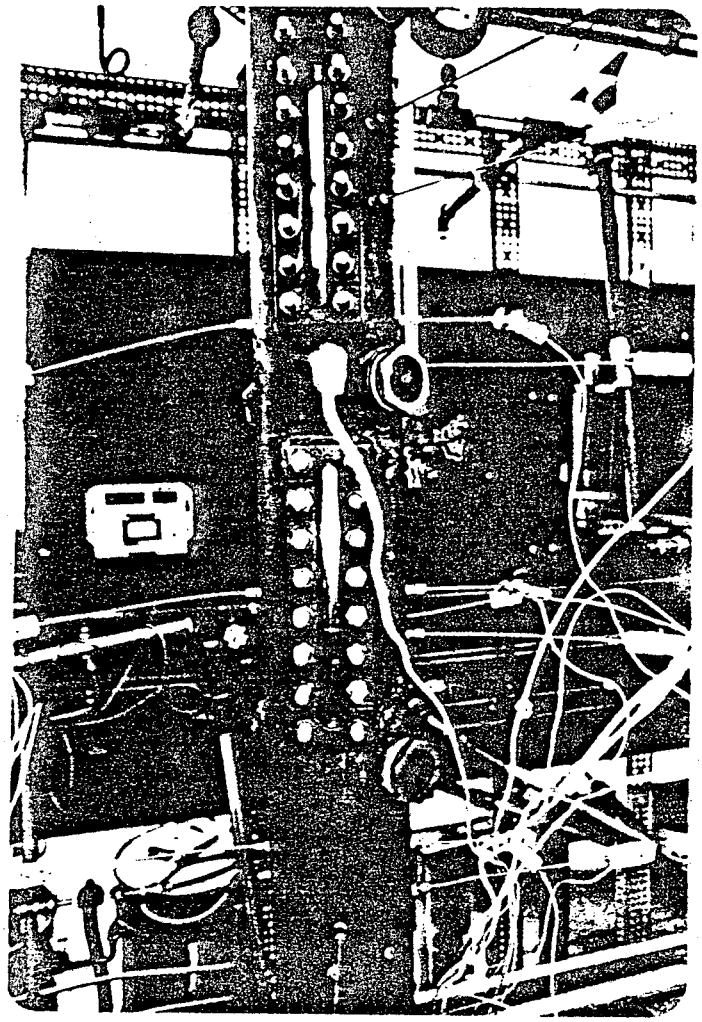

THERMOCOUPLES
AND WINDOWS

FIGURE 5

PERFORATED PLATE BAFFLE

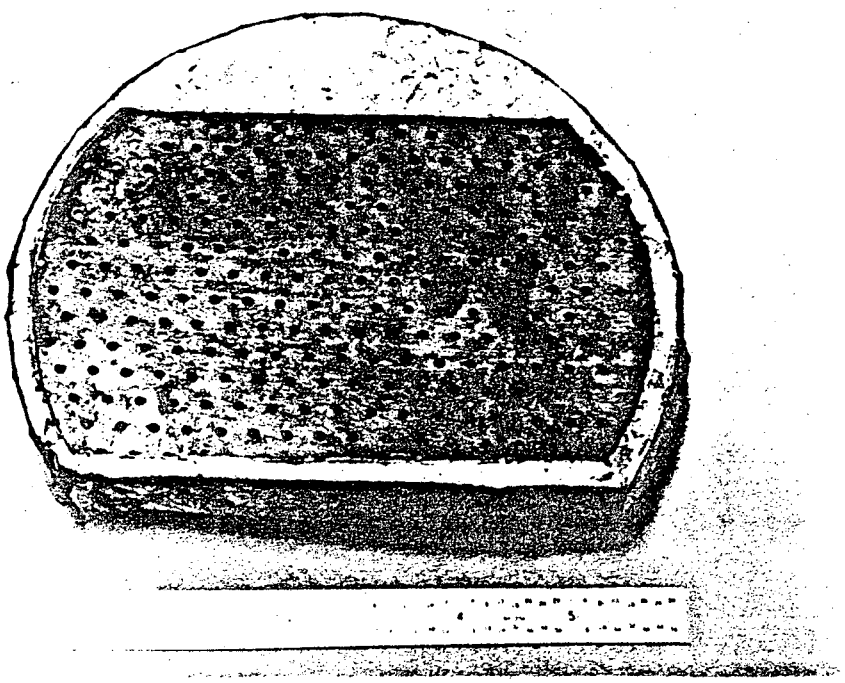

FIGURE 6

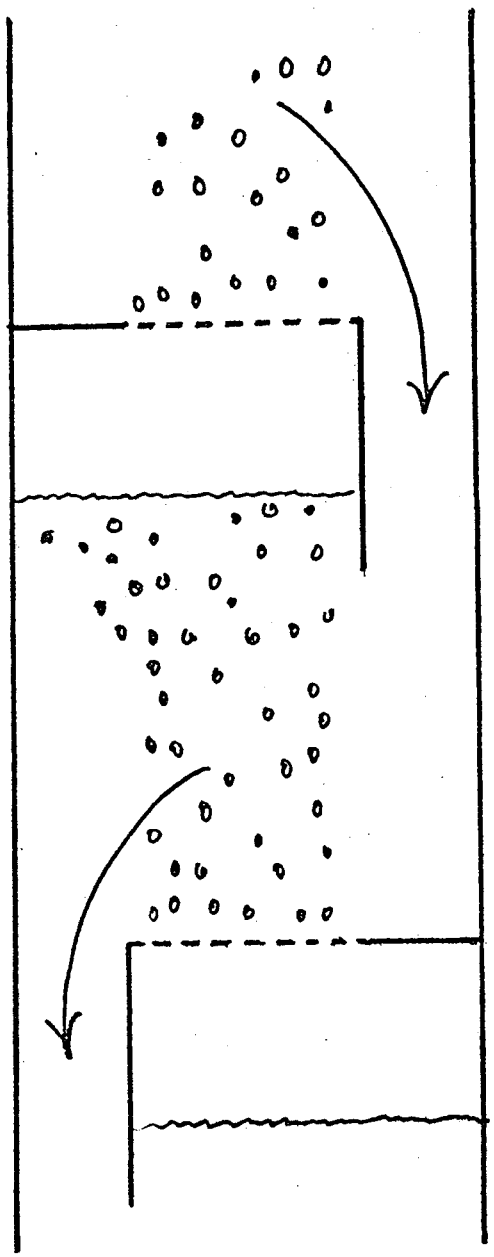

Figure 7. Perforated Plate Flow Pattern

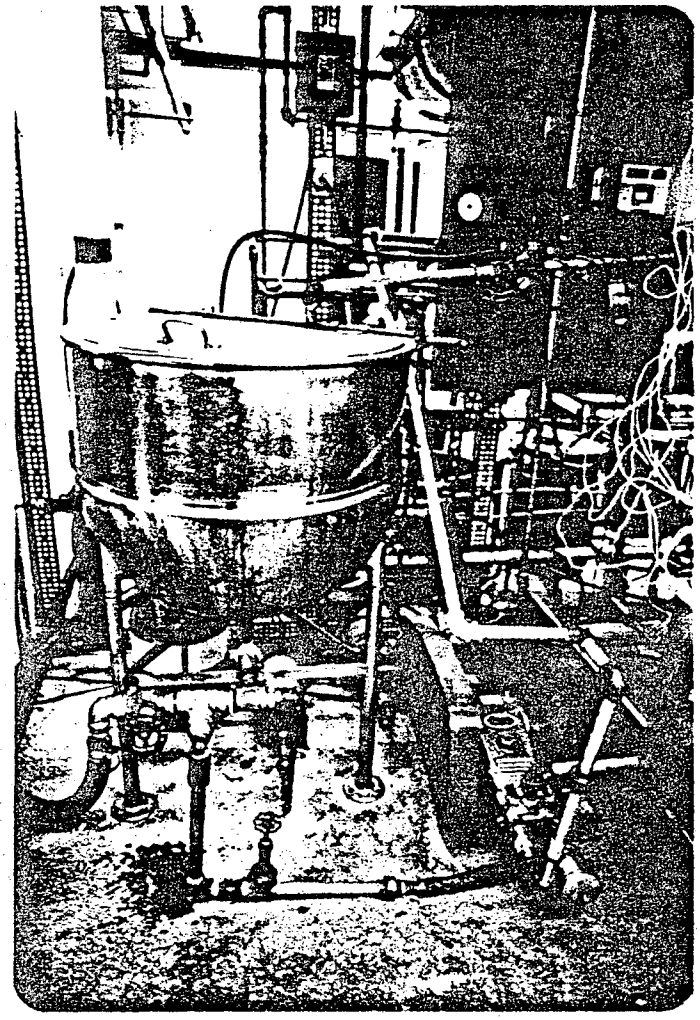

Figure 8. Hot Water Kettle

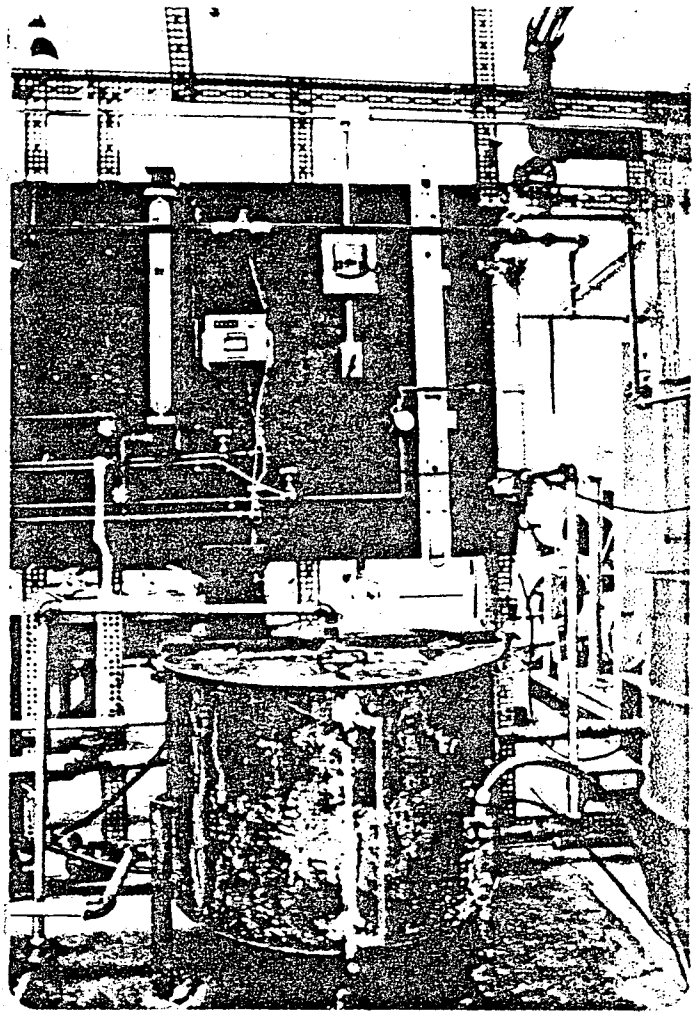

Figure 9. Kerosene Tank

Thermocouple Locations

Slow Response

Fast Response

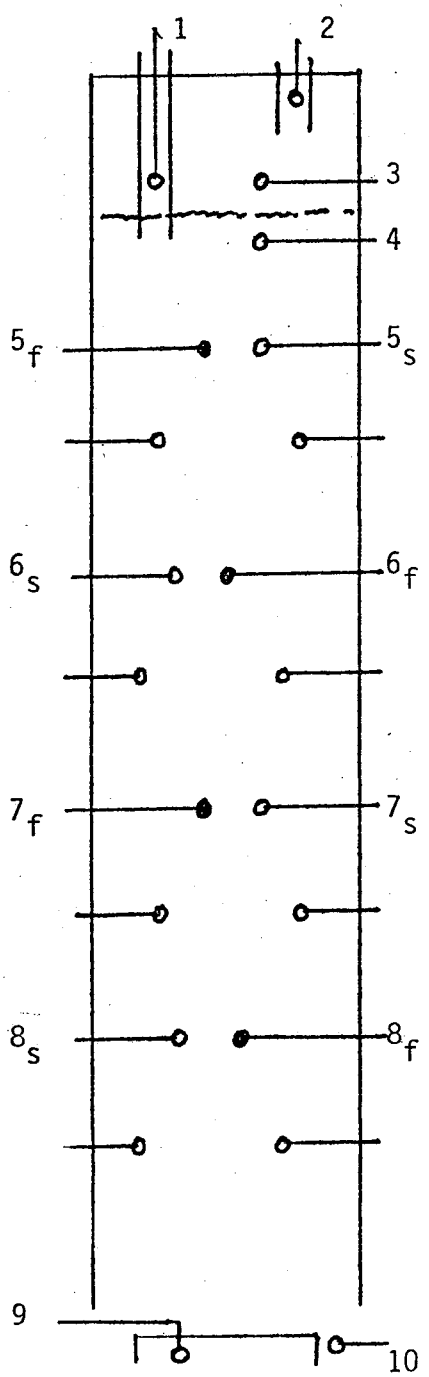

Figure 10a. Spray Column

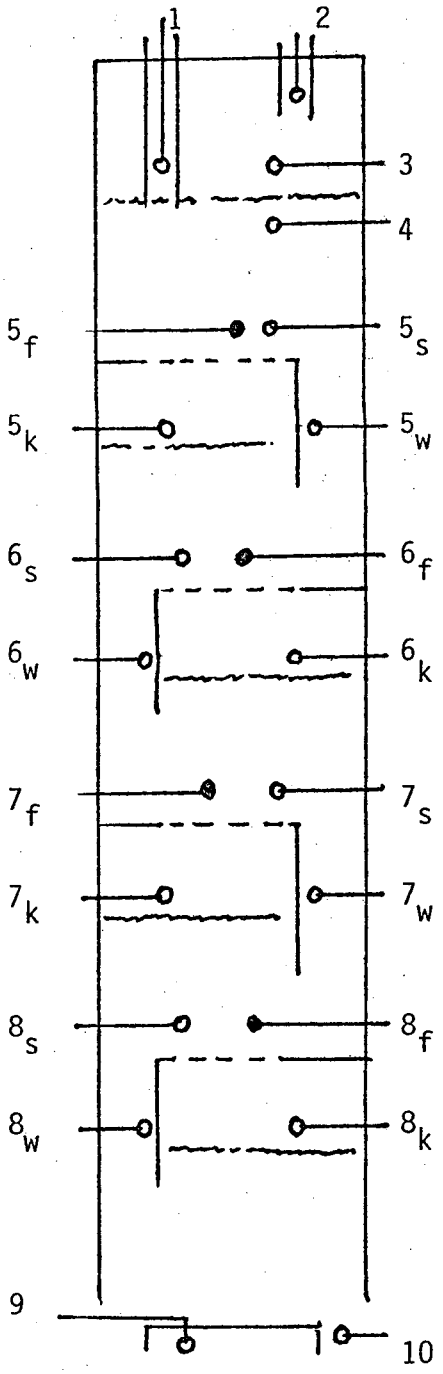

Figure 10b. Perforated Plate Colum

each plate have been relabeled with "w" and "k" subscripts, and they measure the temperature of the continuous phase in the downspout and the coalesced kerosene respectively.

Data from all the thermocouples were recorded on the Fluke Model 2044B data logger which sampled the outputs every .38 seconds. A Houston Model 6452 strip chart recorder was also used to record the output of the fast response thermocouples. The recording instruments are shown in Figure 11.

Fluid flow rates, column pressure, and the level of the kerosene-water interface in the column were also noted. At the end of each run, both pumps and all inlet and outlet valves were simultaneously shut off. Once all the kerosene droplets has risen and coalesced, the new kerosene-water interface level was noted. The ratio of the new interface level to the level during operation provided means of calculating the hold up. An overall view of the experimental apparatus is shown in Figure 12.

ANALYSIS OF RESULTS

Data was taken for a range of flow ratios, R, in the dispersed packed mode of operation and is tabulated in Appendix D. Attempts to obtain data for the dense packed mode of operation were unsuccessful because the location of the interface became very unstable and steady state operation could not be achieved. Values of the Rr product were generally restricted to the range of .24 to .60. The ideal range of $Rr \approx 1$, according to Letan, was not often achieved due to the formation of kerosene-water emulsions at high kerosene flow rates.*

* For kerosene flow rates exceeding 0.265 lit/sec (4.20 gal/min), emulsions formed almost immediately, probably caused by turbulence due to the velocity of the jet at the distribution plate. This flow rate corresponds to a jet velocity of 25.3 cm/s (0.83 ft/sec).

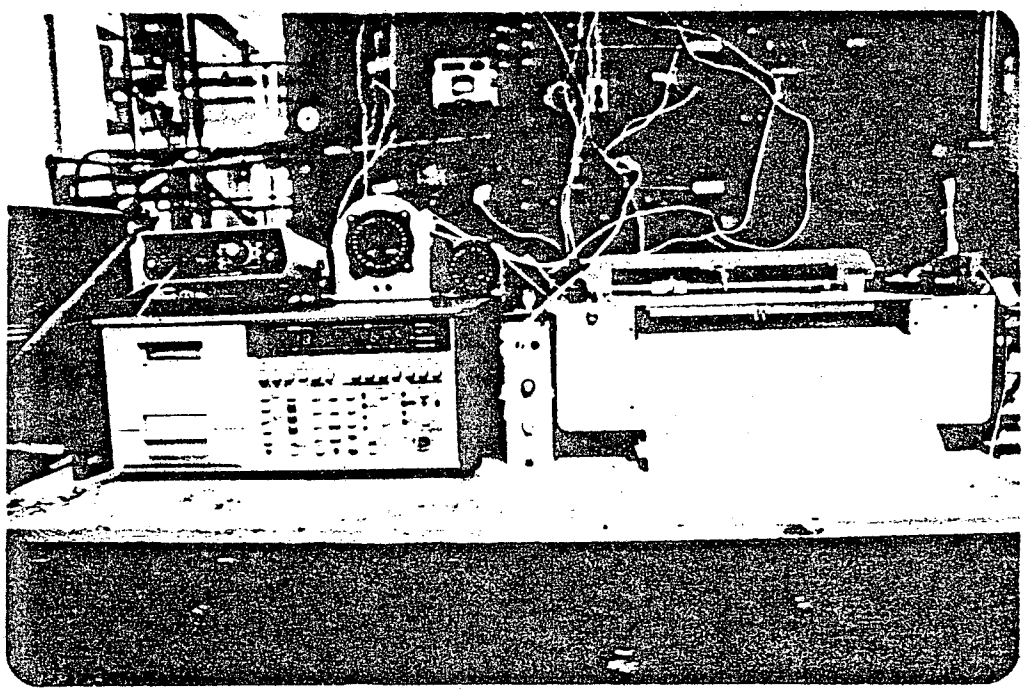

Figure 11. Recording Instruments

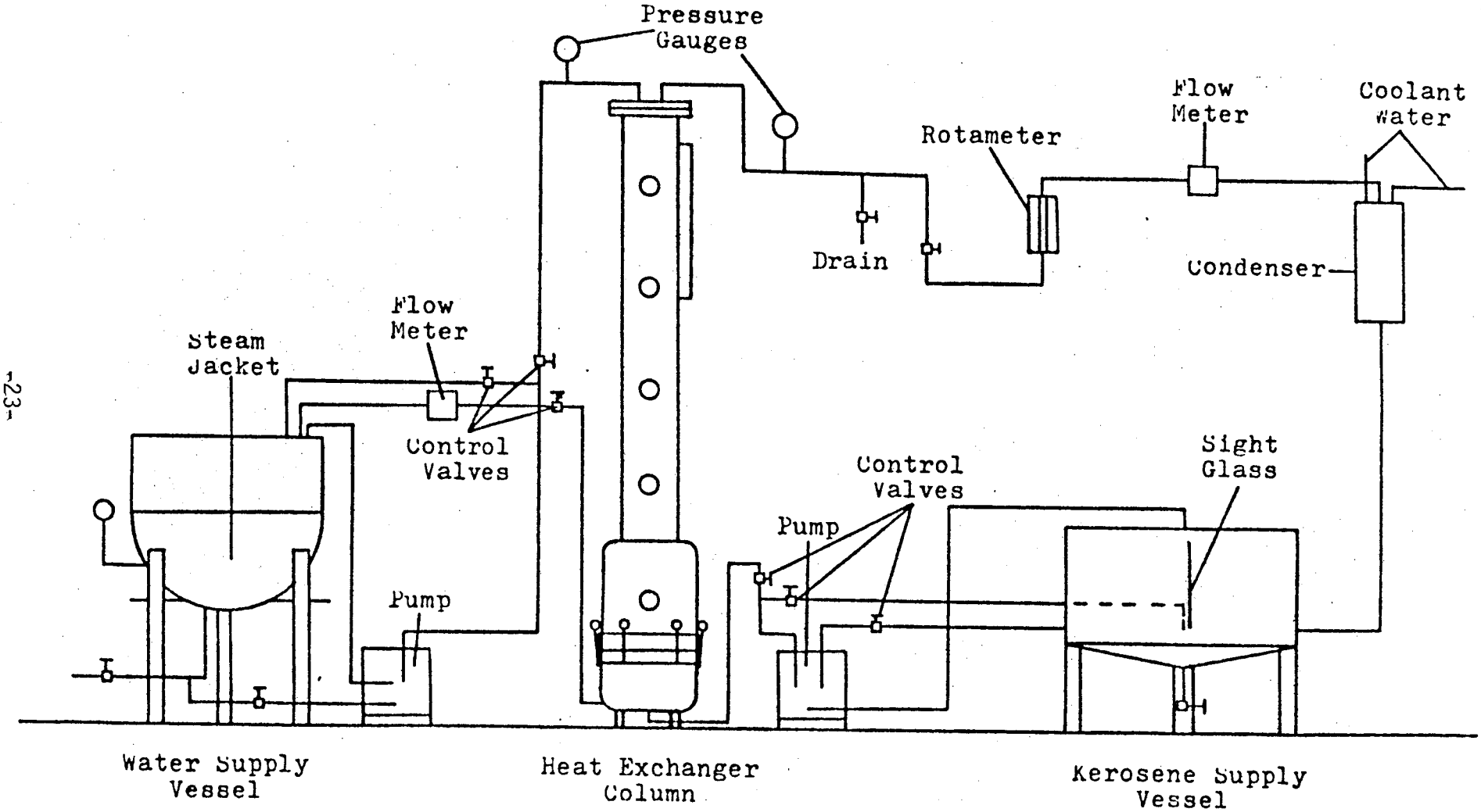
Pressure Gauges
Flow Meter
Coolant Water
Rotameter
Drain
Condenser
Flow Meter
Steam Jacket
Control Valves
Control Valves
Sight Glass
Pump
Pump
Water Supply Vessel
Heat Exchanger Column
Kerosene Supply Vessel

Figure 12

The Reynolds number in the column was approximately 1300 for a typical hold up value of 0.10. This value corresponds to laminar flow based on Letan's suggested correlation for Re_D. Therefore, the model propoed by Letan and Kehat should apply to the present apparatus.

The first step in the analysis was to determine the actual continuous phase, droplet, and wake temperatures from the thermocouple outputs.* For each run the slow response thermocouple outputs were averaged over time, and the maximum and minimum outputs of the fast response thermocouples were each averaged over time. These results were then corrected to account for the thermocouple response time.

Because the fast response thermocouples were small the temperature gradient inside the thermocouple bulb was ignored and first order response was assumed. The maximum and minimum recorded temperatures correspond the the continuous phase and the wakes respectively. If the actual temperature variation is assumed to be a step change from the continuous phase temperature to the wake temperature, the experimental and actual temperatures are related approximately by:

$$U_c = [U_w - T_c]\, e^{-\alpha_c t_c} + T_c \tag{9}$$

$$U_w = [U_c - T_w]\, e^{-\alpha_w t_w - \alpha_d t_d} + T_w \tag{10}$$

where

$$t_c = F\,(1 - \phi - \phi M)$$

$$t_d = F\phi$$

$$t_w = F\phi M$$

F = duration of sequence

$\alpha = hA/M\, c_p$

---

* The thermocouples were periodically surrounded by the continuous phase, droplets, and wakes. From the output of the fast response thermocouples on the strip chart recorder, it appeared that a reasonable frequency for this sequence was .5 seconds.

The convective heat transfer coefficient in the time constant was calculated from the following correlation[13] for the conditions of each run.

$$\frac{hd}{R} = 2 + [0.4\ Re_d^{0.5} + 0.06\ Re_d^{0.67}]\ P_r^{0.4}\ (\mu_s/\mu_w)^{0.25}$$

$$3.5 < Re_d < 7.6 \times 10^4$$

$$0.7 < Pr < 380$$

The thermal capacity of the thermocouple bulb was determined from information provided by the manufacturer.

The slow response thermocouples were shielded by 0.32 cm (0.125 in.) copper tubing, and their outputs corresponded with the maximum temperatures recorded by the fast response thermocouples. The correction for the fast response thermocouples at these maximum temperatures was very samll because the thermocouples were exposed to the continuous phase for a long enough time to equilibriate. Therefore, it was assumed that the slow response thermocouples were measuring the continuous phase temperature and 'did not see' the passing drops and wakes.

SPRAY COLUMN

Temperature Profiles

Model of Letan and Kehat - The experimental continuous phase and wake temperature profiles, corrected for thermocouple response time were plotted together with the three profiles from the model of Letan and Kehat as a function of column height above the dispersed phase injection plate. The energy balances that they used to derive the profiles for the dispersed packed mode of operation are shown below.

Wake Formation Zone:[14] No heat is transferred to the continuous phase in this zone so its temperature remains constant. The temperature of the droplet at the top of this zone can be determined by integrating the heat balance on the drop, shown in Figure 13a, over the entire zone:

$$T_{ds} = (T_{di} - T_{co}) \exp(-M/r) + T_{co} \tag{11}$$

The variable "M" represents the ratio of the wake volume to the drop volume. The wake volume is one of two experimental parameters in the model. The balance around the entire zone in Figure 13b gives the wake temperature at the top of the zone:

$$T_{ws} = r/M\,(T_{di} - T_{ds}) + T_{co} \tag{12}$$

Intermediate Zone: No heat transfer occurs.

Wake Shedding Zone: Since this zone represents the longest portion of the column, it is desired to obtain the temperature profiles as functions of z. Letan and Kehat accomplished this by dividing the heat balances in Figures 13c and 4 by dz. Solvable equations were obtained by defining a second experimental parameter:

$$m \equiv \frac{1}{v_D} \frac{dM_w}{dz} \tag{13}$$

so m represents the mass of wakes shed per volume of drop and length of column. The resulting equations are:

$$\frac{dT_d}{dz} + \frac{m}{r}(T_d - T_c) = 0 \tag{14}$$

$$\frac{dT_w}{dz} \quad \frac{m}{r}(T_w - T_d) = 0 \tag{15}$$

$$\frac{dT_c}{dz} + \frac{m}{P}(T_w - T_c) = 0 \qquad (16)$$

where $P = 1/R + M$

Letan and Kehat solved these three equations simultaneously to obtain the temperature profiles in this region.

Mixing zone: In this zone it is assumed that all outgoing streams are at the same temperature. The balance in Figure 13e can be simplified to

$$T_{ci} = [R(r + M) + 1]\, T_{cl} - R(rT_{dl} + MT_{wl}) \qquad (17)$$

and

$$T_{cl} = T_{do}$$

The continuous phase inlet temperature can also be obtained from a balance around the entire column, as shown:

$$T_{ci} = T_{co} - Rr(T_{di} - T_{do}) \qquad (18)$$

Length of the Wake Shedding and Intermediate Zones - In order to compare plots of the experimental and calculated temperature profiles it was necessary to determine the length of the wake formation zone plus the intermediate zone. From the experimental results of Letan and Kehat the length of these two zones, particularly the intermediate zone, seems to decrease with increasing values of R and ϕ. Their experimental result for $R \approx 1$ and $\phi = 0.6$, which is in the present range of operation, was a total length of about 70 cm (27.7 in.).

From a survey of the literature it appears the velocity at which the transition from non-oscillating to oscillating drops occurs coincides approximately with the start of wake shedding[15]. This transi-

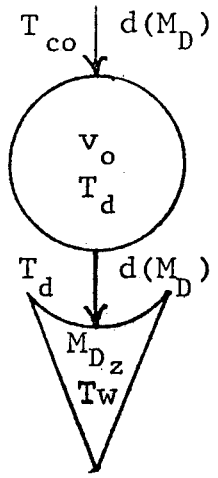

$$(\rho C_p)_c \ (T_{co} - T_d) \ dM_D = v_o (\rho C_p)_d \ dT_d$$

Figure 13a. Wake Formation Zone: Drop and Wake

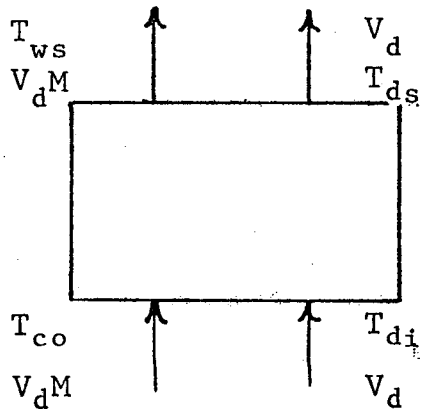

$$V_d M \ (\rho C_p)_c \ (T_{co} - T_{ws}) = V_d \ (\rho C_p)_d \ (T_{ds} - T_{di})$$

Figure 13b. Wake Formation Zone: Overall Balance

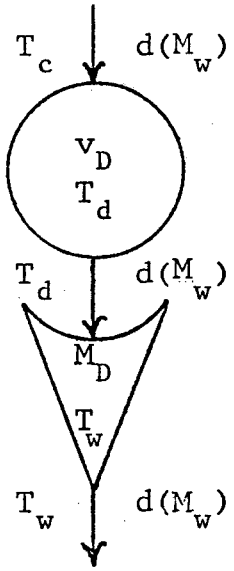

$$(\rho C_p)_c \ (T_c - T_d) dM_w = v_D \ (\rho C_p)_d \ dT_d$$

$$(\rho C_p)_c \ (T_d - T_w) dM_w = M_D \ (\rho C_p)_c \ dT_w$$

Figure 13c. Wake Shedding Zone: Drop and Wake

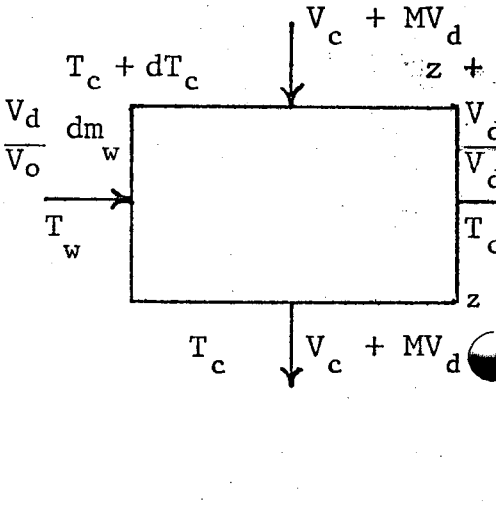

$$(V_c + MV_d)(\rho C_p)_c \ dT_c = V_d \ (\rho C_p)_c \ (T_c - T_w) \ \frac{dm_w}{V_o}$$

Figure 13d. Wake Shedding Zone: Continuous Phase

$$MV_d(\rho C_p)_c T_{w1} + V_d(\rho C_p)_d T_{d1} + V_c(\rho C_p)_c T_c$$

$$= [(V_c + MV_d)(\rho C_p)_c + V_d(\rho C_p)_d]T_{c1}$$

Figure 13e. Mixing Zone: Overall Balance

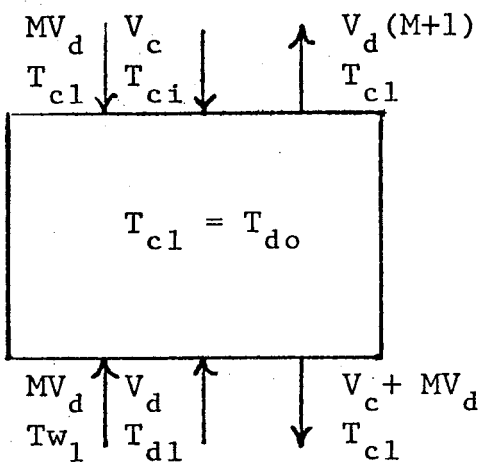

tion has been found to occur at Reynolds numbers from 200 to 500. It has also been found that wake shedding occurs at intervals of 0.05 to 0.08 seconds depending on the Reynolds number of the drop[16] which gives an indication of the amount of time required for a wake to form.

By assuming a transition velocity, V_s, the point at which wake shedding begins to occur can be calculated from a force balance around the drop and its wake. The force balance is given by:

Bouyant Force - Drag Force = Mass of Particle and Wake x Resulting Acceleration

or

$$\frac{1}{6}\pi d_p^3(\rho_c - \rho_d)\frac{g}{g_c} - f\frac{\pi}{8}d_p^2 \quad \rho_c V(t)^2 \frac{1}{g_c} = m_p \frac{a(t)}{g_c} \qquad (19)$$

where

$$m_p = \frac{\pi}{6} d_p^3 \rho_d + M_D \rho_c$$

Assuming that

$$\frac{M_D(t)}{M_{D_{MAX}}} \propto \frac{V(t)}{V_s}$$

equation 19 simplifies to

$$\frac{dV}{dt} = \frac{a^2 - b^2 V(t)^{1.4}}{c + d\,V(t)} \qquad Re_p < 500$$

or (20)

$$\frac{dV}{dt} = \frac{a^2 - b^2 V(t)^2}{c + d\,V(t)} \qquad Re_p > 500$$

where

$$a^2 = (\rho_c - \rho_d)g$$

$$b^2 = 13.88\left(\frac{\mu_c}{\rho_c d_p}\right)^{.6}\frac{\rho_c}{\rho_d} \qquad Re_p < 500$$

$$b^2 = .33 \frac{\rho_c}{d_p} \qquad Re_p > 500$$

$$c = \rho_d$$

$$d = \rho_c \frac{M}{V_s}$$

Integration for $Re_p > 500$ gives

$$t_s = \left[A \frac{1}{b} \ln \frac{a + bV_s}{a} - B \frac{1}{b} \ln \frac{a - bV_s}{a}\right] \qquad (21)$$

where

$$A = \frac{1}{2}\left[\frac{c}{a} + \frac{d}{b}\right]$$

$$B = \frac{1}{2}\left[\frac{c}{a} - \frac{d}{b}\right]$$

At this value of the Reynolds number the wake shedding velocity is about 5.8 cm/sec (0.20 ft/sec) and the time before shedding occurs is less than a tenth of a second. Based on this calculation it was decided that the wake formation zone is very short. The combined length of the wake formation zone and the intermediate zone in the present apparatus appeared to be approximately 25.4 cm (10 in.) judging from the axial continuous phase temperature profile.

Heat Loss and Radial Temperature Profile - Letan and Kehat ignored heat losses from the column and assumed that the radial temperature profile was flat. However, in this experiment an average of 12 percent of the heat was lost from the column and a radial temperature profile, shown in Figure 14, was observed. The gradual temperature drop toward the wall between b and a in Figure 14, was assumed due to heat loss. However, the sudden temperature drop at c could not be explained as a temperature gradient due to radial heat loss.

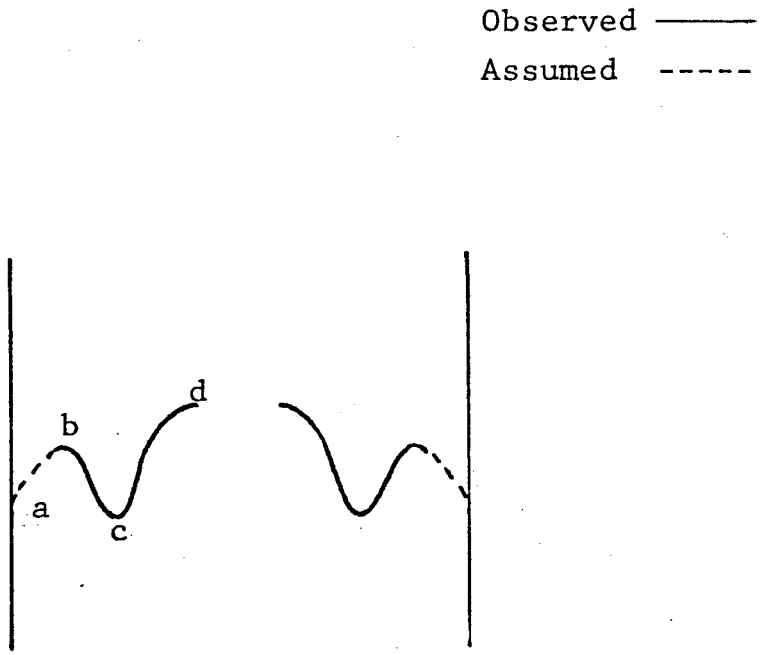

Figure 14. Radial temperature Profile

It has been observed that under certain conditions, particles in a Poiseuille flow field will migrate to a specific radial location near the wall. Jacobsen[17] solved for the resultant radial axial and torsional forces on a particle in a specified Poiseuille flow field. He found that it is possible to set the axial velocity, rotational velocity, and the radial position such that the forces on the particle are zero. The temperature drop at point c in Figure 14 could be due to a collection of dispersed phase droplets at that radial position; although, the kerosene droplets are more buoyant than the particles in suspension. The outputs of only the thermocouples located in further than point d, which is a region of no radial gradient, were compared to the model.

Axial Temperature Profiles - A plot of the present experimental profiles (corrected for time response is shown with those predicted by the model of Letan and Kehat in Figure 15 (refer to Appendix A for explanation). The remaining plots are shown in Appendix A. It can be seen that the experimental continuous phase wake temperature profiles agree with the model to within at least 13 and 18 percent respectively. The predicted temperature was usually less than the experimental temperature for both profiles. Uncertainties such as the location of the start of the wake shedding zone and the values of the wake parameters could account for the difference. The parameters that were used to apply the time response correction for the thermocouple, such as the hold up, the thermocouple time constant, and the frequency of the actual temperature sequence were also subject to uncertainty.

The values of the wake parameters suggested by Letan and Kehat

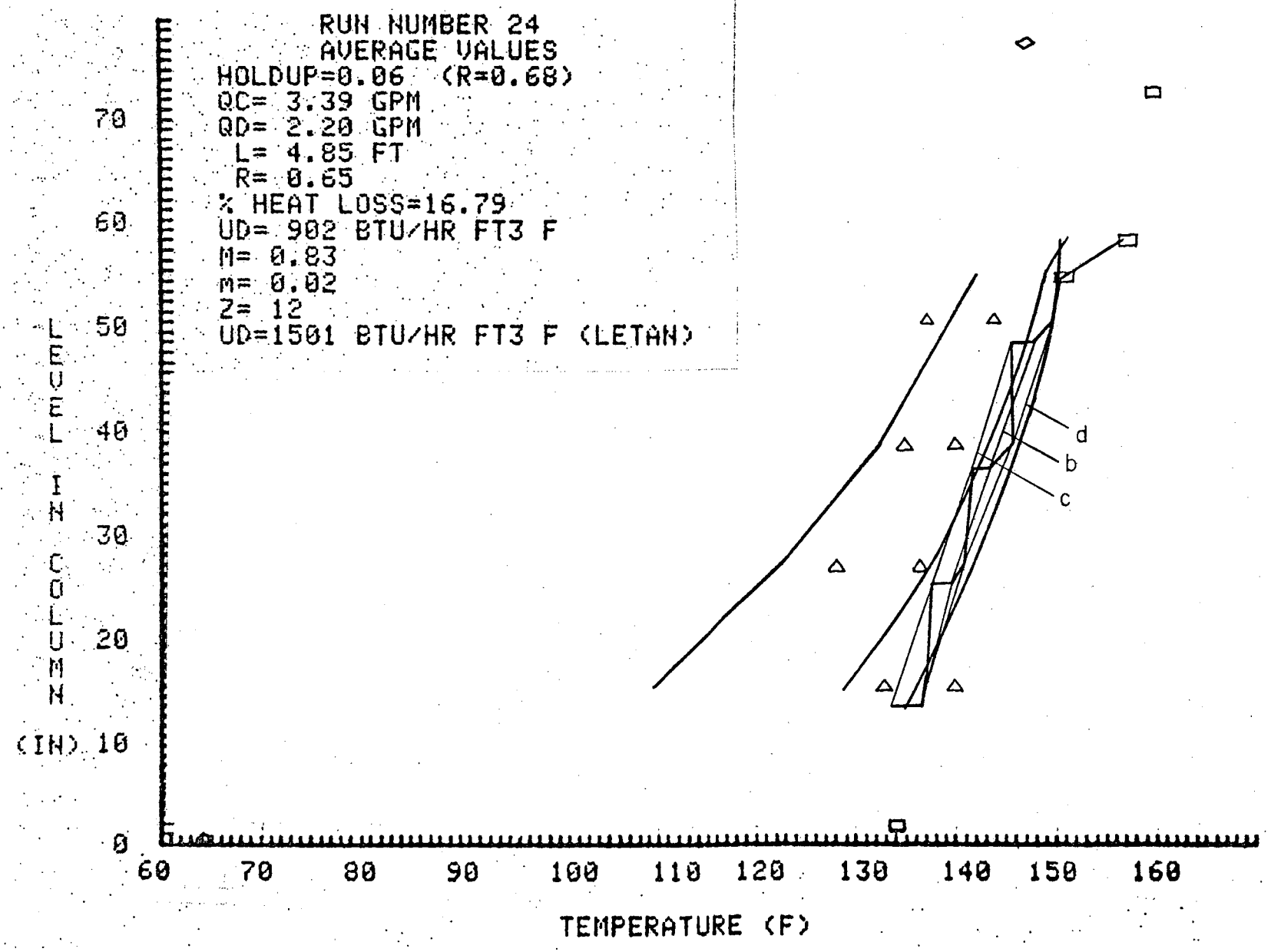

Figure 15. Temperature Values, Run Number 24

were used:

ϕ	M	m
0.06	1.0	0.023
0.06-0.4	0.83	0.03
> 0.4	0.83	0.023

Hendrix, Shashikant, and Johnson[15] find that the amount of backmixing in a column decreases as the flow rates of both phases are increased so perhaps the wake parameters are also functions of the flow rates.

Overall Volumetric Heat Transfer Coefficient

The experimental overall volumetric heat transfer coefficients are tabulated in Table 1 along with those predicted by the correlations of Plass and Letan and Kehat.* It should be noted that Plass used Equation (7) to calculate hold up, and although, Equation (7) did not predict the present experimental hold up, it was used in Equation (3) for the purpose of comparing the present results to those of Plass.

Table 1 shows that the correlation of Plass fits the present data to within 30 percent for values of R greater than .7 and less than 1.4. For values of R outside of this range the fit was poor. The experimental setup used by Plass was identical to the present one except for the method of flow rate measurement, the size and number of holes in the distribution plate, and the working fluid. However, the insulating oil was found to have a density-heat capacity product nearly the same as that of kerosene. Scatter in the agreement could

---

* Due to the difficulty of maintaining steady state operations with this apparatus, the experimental coefficients varied as much as 15 percent during a particular run , so the averages were tabulated.

Table 1a. Spray Column: Overall Volumetric Heat Transfer Coefficient

(.204 ≤ Q_c ≤ .225 lit/sec) (.56 ≤ R ≤ 1.42)

Run	ϕ (exper)	ϕ (Calc)	R	Q_c (lit/sec)	U_v (kcal/m^3hr°C)		
					U_v (exper)	U_v (Letan and Kehat)	U_v (Plass)
24	0.06	0.06	0.65	0.214	19736	24046	13601
25	0.14	0.10	0.98	0.225	37150	32136	30230
26	?	0.11	1.18	0.208	45464	33050	50078
27	0.11	0.09	0.97	0.213	36509	30342	26209
28	0.11	0.10	1.08	0.208	36926	31223	29088
29	0.03	0.06	0.69	0.206	22364	24158	12047
30	?	0.14	1.42	0.204	58537	36205	38497
31	0.08	0.04	0.60	0.199	19496	21259	8651
32	0.16	0.10	1.00	0.224	34336	34284	29989
33	0.08	0.05	0.56	0.217	18567	21675	9612
34	0.13	0.07	0.85	0.206	26065	27042	18487

Table 1b. Spray Column: Comparison of Results to Letan and Kehat, and Plass

Run	ϕ (exper)	ϕ (calc)	R	$\frac{U_V = \text{Letan and Kehat}}{U_V \text{ (exper)}}$	$\frac{U_{VT} \text{ (Plass)}}{U_{VT} \text{ (exper)}}$
24	0.06	0.06	0.65	1.22	0.69
25	0.14	0.10	0.98	0.87	0.81
26	?	0.11	1.18	0.73	1.10
27	0.11	0.09	0.97	0.83	0.72
28	0.11	0.10	1.08	0.85	0.79
29	0.03	0.05	0.69	1.08	0.54
30	?	0.14	1.42	0.62	0.66
31	0.08	0.04	0.60	1.09	0.44
32	0.16	0.10	1.00	0.93	0.87
33	0.08	0.05	0.56	1.17	0.52
34	0.13	0.07	0.85	1.04	0.71

be a result of experimental error in flow rate measurement. Differences in the distribution plate and the working fluid would be more likely to result in a constant offset in the agreement. In the present experiment, the distribution plate contained more holes which would increase the number of droplets and therefore the surface area available for heat transfer.

The coefficient predicted by the model of Letan and Kehat is also shown in Table 1. The agreement in this case is within 20 percent excluding the run with R = 1.40. This larger value of R possibly approached the dense packed mode in which the model does not apply. The agreement was best (within 17 percent) for R values between 0.85 and 1.10.

Letan and Kehat modeled an insulated column. However, in the present case the heat loss varied from 7 to 18 percent of the heat input. This loss would seem to result in a constant offset in the agreement by overestimating the experimental heat transfer coefficient. The experimental coefficient can be corrected for this loss as shown below. The overall heat balance is

$$(\dot{m}_p C_p)_d (T_{do} - T_{di}) = (1 - H) (\dot{m}_p C_p)_c (T_{ci} - T_{co})$$

$$\text{or} = (\dot{m}_p C_p)_c (T^{ci} - T_{co}')$$

$$T_{co}' = (1 - H) T_{co} + H T_{ci}$$

By using the value of T_{co}' in place of the measured continuous phase outlet temperature in the log mean temperature difference, the corrected value of the heat transfer coefficient can be obtained. This correction reduces the experimental coefficients by something less than 10 percent, however, it can be seen that with this correction the agreement with the

model is still plus or minus about 17 percent.

Correlating Heat Transfer to Flow Rates and Holdup - The overall heat transfer coefficient appears to be a strong function of R and V_c or ϕ. For the present range of continuous phase flow rates (V_c = 0.204 - 0.225 lit/sec or 3.24 - 3.57 gal/min) relationship of U_v and R was found to be linear. The correlation shown below fits the experimental results within at least 14 percent.

$$U_v \text{ (kcal/m}^3\text{hr°C)} = 46264\ R - 9687 \qquad (22)$$

Experimental results are compared with the prediction of Letan and Kehat, Plass, and Equation (22) in Figure 16.

The heat transfer coefficient can be obtained in terms of the calculated holdup by writing Equation (2) in terms of R as shown,

$$R = \phi \left[\frac{V_T}{V_c} (1 - \phi)^m - (1 - \phi)^{-1}\right] \qquad (23)$$

The term in parentheses changes very little over the present range of holdups for a constant continuous phase velocity, making U_v also fairly linear function of the calculated holdup. The relationship between U_v and the experimental holdup was not obvious; however, it is suspected that the measured holdup was subject to experimental error due to the difficulty of seeing the exact interface in the present apparatus.

From earlier runs over a wider range of R values it appears that U_v increases with R up to a value of approximately R = 1.90. Above this value the opposite trend occurs. It was also noticed that for a constant value R < 1, heat transfer increased as continuous phase flow rate increased. For a value of R = 1.50 the heat transfer decreased as the continuous phase flow rate increased.

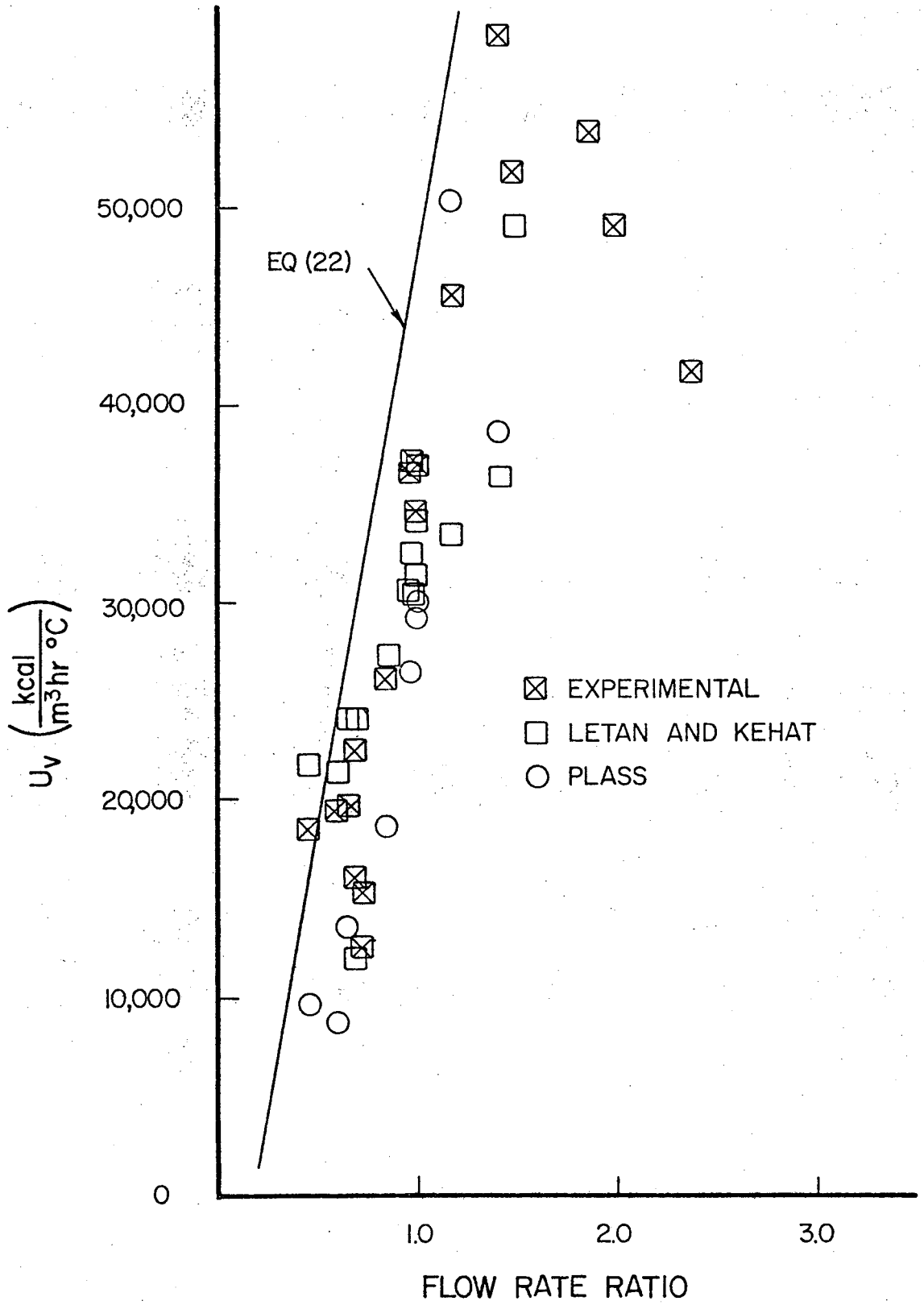

Figure 16. Comparison of Heat Transfer Results for Spray Column

Results from a preheater in a 500 kw pilot plant at Raft River, Utah are shown in Table 2. They agree with Plass's correlation to within 3 percent.

PERFORATED PLATE COLUMN

The perforated plates were designed such that the column could be operated in the same range of flow rates as the spray tower. Further the free area (of the down spout) was such that the velocity of the continuous phase in the down spout would never exceed the upward velocity of the drops. The depth of kerosene build up beneath each plate was calculated from a correlation by Treybal[18] relating the geometry, orifice velocities, and fluid properties. This length was found to be 11.0 cm (4.3 in.) and; therefore, the down spouts were made 15.2 cm (6.0 in.) long as a safety factor. The length of the wake formation zone was calculated to be so short that the only factor limiting the distance between a plate and the down spout above was smooth flow of the continuous phase. The distance was chosen to be 30.5 cm (12.0 in.) as that would be comparable to the length of the wake formation zone and the intermediate zone in the spray tower.

Experimental runs were made for values of R from .85 to 1.40. One set of runs was made with volumetric flow rates comparable to those used in the spary column, and the other set of runs was made with lower flow rates.

The effect of higher flow rates for all values of R was to increase the overall volumetric heat transfer coefficient and to decrease the approach temperature at the bottom of the column. For R values of one or greater, the intermediate water and kerosene temperatures were

Table 2. Pilot Plant Spray Column

R	ϕ (calc)	U_V ($cal/m^3 hr°C$)		
		(exper)	(Plass)	$\frac{U_V \text{ (Plass)}}{U_V \text{ (exper)}}$
1.81	.19	36648	36558	1.00
1.85	.13	23040	23824	0.97
1.94	.11	18607	19198	0.97

hotter for the higher flow rates. However, for smaller values of R the intermediate temperatures were not affected by the flow rates.

Comparing perforated plate to spray tower performance for similar operating conditions; in all cases the overall volumetric heat transfer coefficient was improved. The water outlet temperature was 13 to 18°F colder and the kerosene temperature at the interface was hotter.

Temperature Profiles

The kerosene temperature under each plate was cooler than the temperature that would exist at the top of the wake shedding zone as predicted by the model of Letan and Kehat. It is proposed that between each plate the wake formation zone is followed by an intermediate zone in which no heat transfer occurs.* Then near the kerosene interface is a zone where partial mixing occurs. As they slow down to coalesce, the drops are assumed to transfer heat back to the wakes until their temperatures have equilized. A temperature jump of the continuous phase occurs at this point as the down coming fluid mixes with these wakes which are still cooler.

The notation used for this model is shown in Figure 17. The energy balance for the wake formation zone is shown in Figure 18a. Equations (11) and (12) still give the drop and wake temperatures at the top of this zone and they are restated below in the new notation.

$$T_{dsj} = (T_{dj+1} - T_{cj+1}) \exp\left(\frac{-M}{r}\right) + T_{cj+1} \qquad (23)$$

$$T_{wsj} = \frac{r}{M}(T_{dj+1} - T_{dsj}) + T_{cj+1} \qquad (24)$$

---

* With the perforated plate column this zone could be due to stagnant regions of the continuous phase caused by the obstruction of the plates.

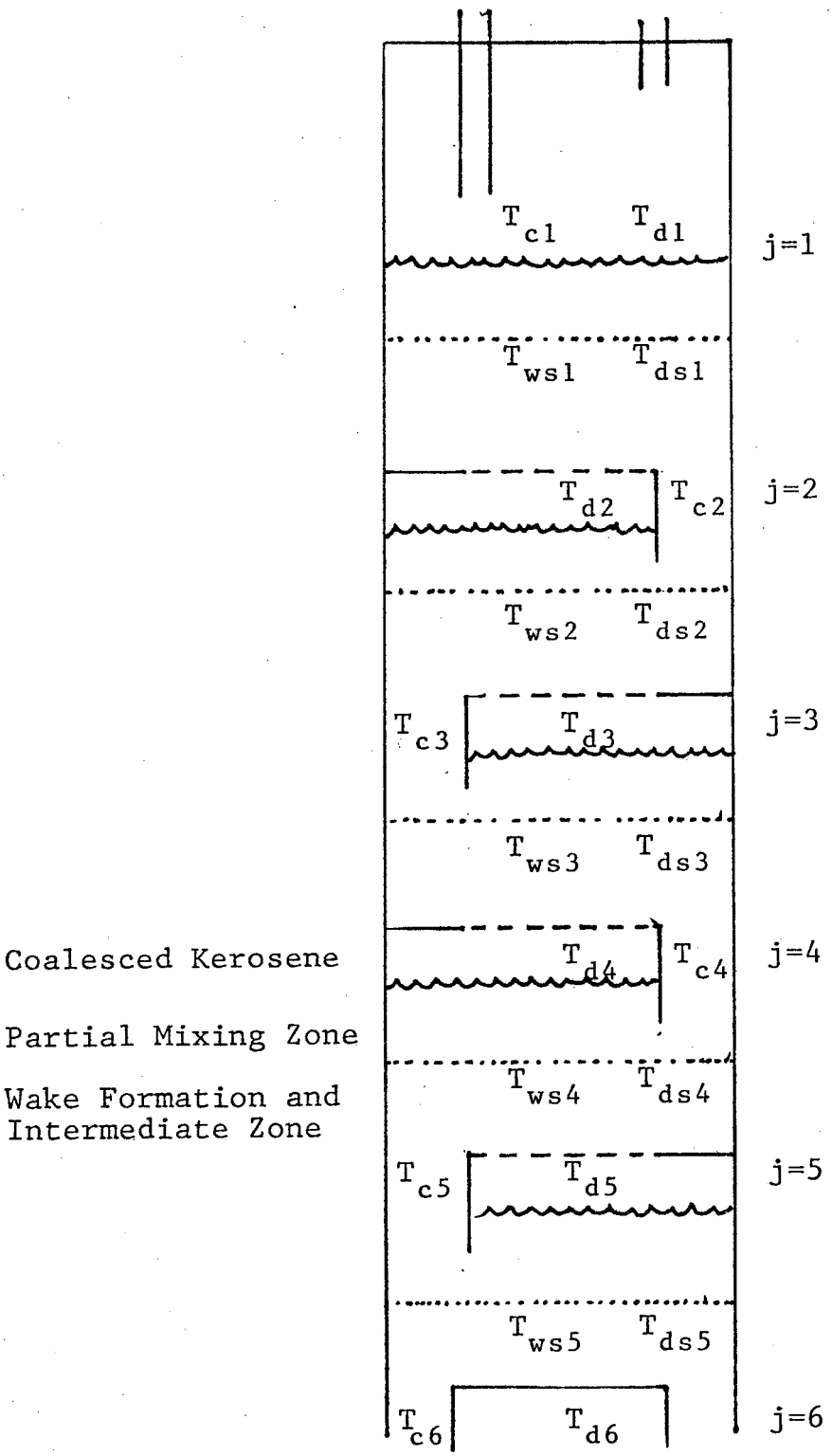

Figure 17. Notation Used for Perforated Plate Colum Model

Figure 18b shows the energy balance in the top zone. The heat that is transferred from the drops back to the wakes in this zone is given by

$$V_d\ (\rho\ C_p)_d\ (T_{dsj} - T_{dj}) = MV_d\ (\rho\ C_p)_c\ (T_{dj} - T_{wsj}). \qquad (25)$$

An overall heat balance is shown in Figure 18c. Energy is conserved in the model if the temperature of the kerosene held up under the plate is given by

$$T_{dj} = [MT_{wsj} + rT_{dsj}]/(M + r). \qquad (26)$$

Finally the continuous phase temperature in the down spout, given below, is found from the overall balance.

$$T_{cj} = Rr\ (T_{dj} - T_{dj+1}) + T_{cj+1} \qquad (27)$$

The continuous phase, droplet, and wake temperature profiles were calculated from Equations (23), (24), (26), and (27). This model fit the experimental profiles to within 5 percent in the region of the top three plates. The fit was within 15 percent at the bottom plate. A plot comparing the profiles is shown in Figure 19 (refer to Appendix B for explanation), and the remaining plots are shown in Appendix B and C for M = 0.83 and 0.50 respectively. It can be seen that more heat is transferred below the bottom plate than is predicted by the model. A possible reason for this deviation is that the dispersed phase appeared to consist of smaller droplets (resulting in a larger surface area and improved heat transfer) as it came out of the distribution plate than were formed coming out of any of the succeeding plates.

Comparing Appendix B, where the fast response thermocouple time constants were calculated using an estimated holdup, to Appendix C, where the calculations were made using the holdup from Equation (7), it can be seen that the resulting temperatures are more reasonable for

Energy Balances for Model of Perforated Plate Column

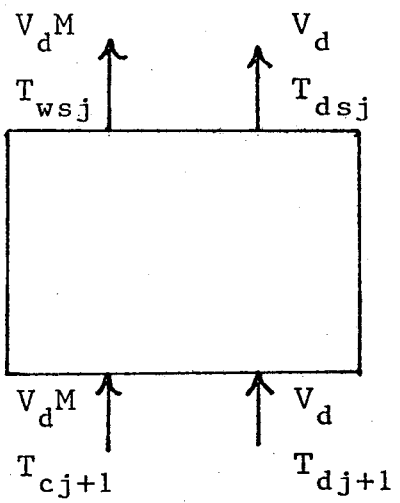

$$V_dM(\rho C_p)_c(T_{cj+1} - T_{wsj}) + V_d(\rho C_p)_d(T_{dj+1} - T_{dsj}) = 0$$

Figure 18a. Wake Formation Zone: Overall Balance

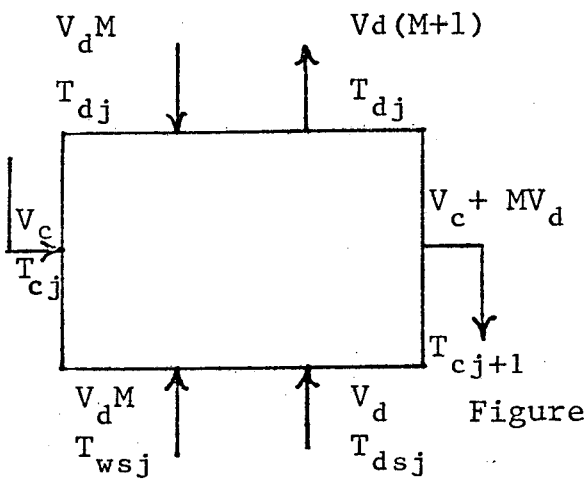

$$V_dM(\rho C_p)_c(T_{wsj} - T_{cj+1}) + V_d(\rho C_p)_d(T_{dsj} -$$
$$+ V_c(\rho C_p)_c(T_{cj} - T_{cj+1}) = 0$$

Figure 18b. Partial Mixing Zone: Overall Balan

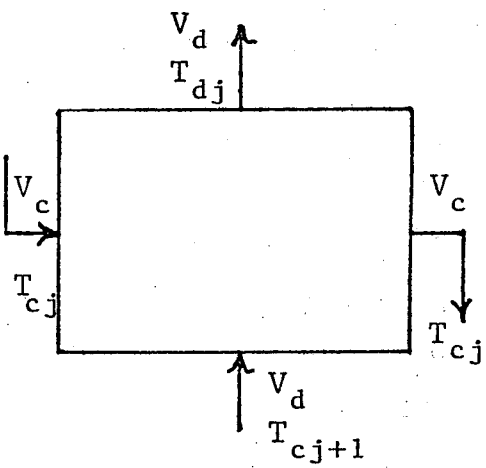

$$V_d(\rho C_p)_c(T_{cj} - T_{cj+1}) + V_d(\rho C_p)_d(T_{dj+1} - T_{dj}) = 0$$

Figure 18c. Entire Region Between Plates

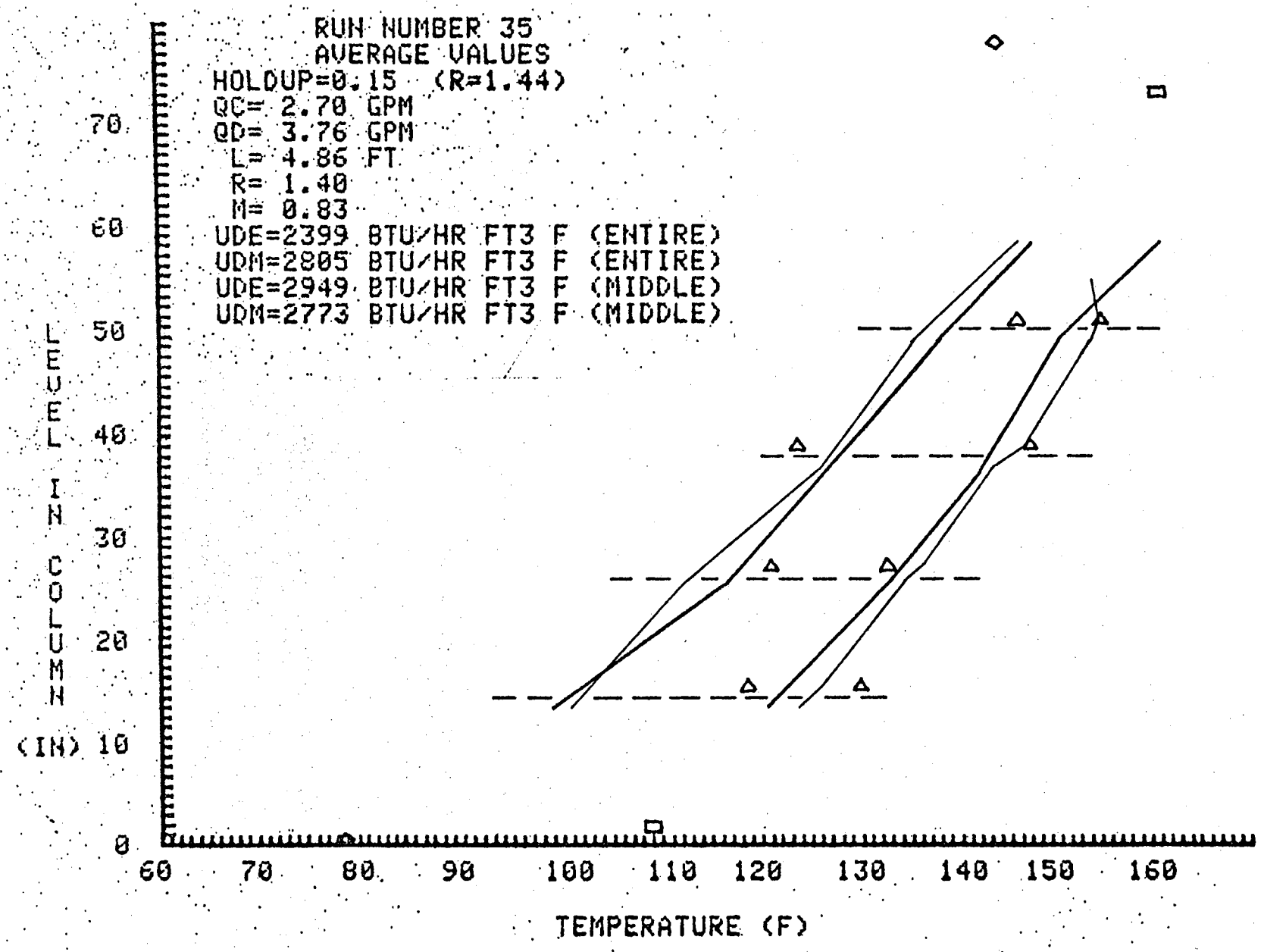

Figure 19. Temperature Values, Run Number 35

the estimated holdup which was generally higher than the calculated value.

Overall Volumetric Heat Transfer Coefficient

The overall volumetric heat transfer coefficients are tabulated in Tables 3 and 4 for M = 0.83 and 0.50 respectively. Coefficients for the perforated plate column are considerably greater than those for corresponding conditions in the spray column as shown in Table 5. Based on the volume below the interface in the column, the model predicts the coefficient to be within 11 to 28 percent of the experimental result for M = 0.83 and from 2 to 11 percent for M = 0.50. Also tabulated in Tables 3 and 4 is a comparison of calculated and experimental coefficients based on the volume between the middle two plates as this region is not influenced as much by end effects. Here the agreement was between 2 and 17 percent for both values of M. It is apparent that the model is not strongly affected by the value of M; however, the actual value of M could have been different in the perforated plate column due to the increase droplet sizes noticed above the perforated plate baffles as compared to those above the distribution plate. It should be noted that the heat transfer between the two middle plates was considerably better in every case than in the region between the distribution plate and the first perforated plate. The heat transfer also drops off above the top perforated plate.

Correlating Heat Transfer and Flow Rate - Within the operating range of the present experiments the overall volumetric heat transfer coefficient was shown to be a linear function of the flow rate ratio and the continuous phase flow rate. The function shown below fits the data to within 3 to 14 percent, as shown in Table 6.

Table 3a. Perforated Plate Column: Overall Volumetric Heat Transfer Coefficient

(M = 0.83)

Run	ϕ (est.)	R	Q_c (lit/sec)	U_v (kcal/m^3hr°C)			
				From Interface		Between Two Middle Plates	
				(exper)	(model)	(exper)	(mode)
35	0.15	1.40	2.70	38432	44936	47243	44423
36	0.11	1.08	2.72	29733	32873	48669	40354
38	0.14	0.95	3.53	41908	53475	47130	54068
39	0.11	0.83	3.79	43302	50912	45369	50303
40	0.14	1.23	3.12	54532	65970	57207	58153

Table 3b. Perforated Plate Column: Comparison of Results to Mode

Run	ϕ (est.)	R	Q_r (lit/sec)	U_v (model)/U_v (exper)	
				From Interface	Between Two Middle Plates
35	0.15	1.40	2.70	1.17	0.94
36	0.11	1.08	2.72	1.11	0.83
38	0.14	0.95	3.53	1.28	1.15
39	0.11	0.83	3.79	1.18	1.11
40	0.14	1.23	3.12	1.21	1.02

Table 4a. Perforated Plate Column: Overall Volumetric Heat Transfer Coefficient

(M = 0.05)

Run	ϕ (calc)	R	Q_c (lit/sec)	U_v ($cal/m^3 hr°C$) From Interface (exper)	(model)	U_v ($cal/m^3 hr°C$) Between Two Middle Plates (exper)	(model)
35	0.11	1.40	0.170	38432	36044	47243	44423
36	0.08	1.08	0.171	29734	26382	48668	40354
38	0.09	0.95	0.222	41909	42893	49229	51601
39	0.09	0.83	0.239	93303	40837	45368	50303
40	0.11	1.23	0.197	54532	52916	57207	58153

Table 4b. Perforated Plate Column: Comparison of Results to Model

(M = 0.50)

Run	ϕ (calc)	R	Q_c (lit/sec)	U_v (model)/U_v(exper) From Interface	Between Two Middle Plates
35	0.11	1.40	2.70	0.94	0.94
36	0.08	1.08	2.72	0.89	0.83
38	0.09	0.95	3.53	1.02	
39	0.09	0.83	3.79	0.94	1.11
40	0.11	1.23	3.12	0.97	1.02

Table 5. Comparison of Spray Column to Perforated Plate Column for Similar Operating Conditions

SPRAY COLUMN				PERFORATED PLATE COLUMN				$\frac{U_V \text{ (spray)}}{U_V \text{(plate)}}$
Run	R	Q_c (lit/sec)	U_V(kcal/m^3hr°C)	Run	R	Q_c (lit/sec)	U_V (kcal/m^3hr°C)	
34	0.85	0.206	26065	39	0.83	0.239	43303	.60
25	0.98	0.225	37150	38	0.95	0.222	41909	.89
26	1.18	0.208	45464	40	1.23	0.197	54532	.83

Table 6. Perforated Plate Column: Comparison of Experimental Results to Calculated Values (Equation 28)

Run	R	V_c (cm/sec)	U_v (Eqn. 28)(kcal/m^3hr°C)	U_v (Eqn. 28)/U_v (exper)
35	1.40	1.01	43985	1.16
36	1.08	1.02	28771	0.97
38	0.95	1.32	43606	1.04
39	0.83	1.42	44806	1.03
40	1.23	1.17	46898	0.86

$$U_V \text{ (kcal/m}^3\text{hr°C)} = -95015 + 48845\ R + 69640\ V_c \text{ (cm/sec)} \quad (28)$$

CONCLUSION

With the present apparatus it was found that the heat transfer performance of the perforated plate column was significantly improved over that in a spray column for similar operating conditions. It was also found that the heat transfer between the two middle plates in the column was better than that for the entire column indicating that end effects in the column reduce heat transfer.

Overall volumetric heat transfer coefficients in the range of 19,000 to 58,000 (kcal/m^{3}hr°C) [1200 to 4000 (Btu/ft^{3}hr°F)] were obtained in a 183.0 cm (6.0 ft) tall, 15.2 cm (6.0 in.) diameter column. Due to unavoidable fluctuations in operating parameters, heat transfer results varied as much as 15 percent during some runs. Considering this uncertainty the agreement between experimental results and theoretical models was considered to be good.

Spray Column

The wake and continuous phase temperature profiles of Letan and Kehat were within at least 18 percent of the experimental profiles measured in the center of the column. Although Letan and Kehat ignored the radial temperature profile, it was observed in the experimental results.

Predictions of the overall volumetric heat transfer coefficient from the correlation of Plass were within 10 to 28 percent of the results for R values between 0.70 and 1.20. The coefficient calculated from the model of Letan and Kehat was within 4 to 27 percent of the

experimental result for values of R less than 1.2. The agreement for R values outside of this range was poor. At a flow rate ratio of 1.40 the model predicted a coefficient much less than that which was obtained.

For a relatively constant continuous phase flow rate of approximately 0.215 lit/sec (3.40 gal/min) the heat transfer was found to be linear with respect to R ($R < 1.90$) as given below

$$U_V \text{ (kcal/m}^3\text{hr°C)} = 46264\ R - 9687$$

For higher values of R ($R > 1.90$) it was found that the heat transfer decreased as R was increased. It was also observed that constant values of R less than one, heat transfer increased as the continuous phase flow rate was increased. However for larger values of R ($R > 1.50$) the opposite trend occurred.

Perforated Plate Column

A hydrodynamic model was proposed for the volume between plates. The model proposes a wake formation zone and intermediate zone, like those of Letan and Kehat, followed by a partial mixing zone where the drops are cooled by their own wakes as they slow down to coalesce under the upper plate. The temperature profiles predicted by the model were within 5 percent of the experimental profiles. The overall heat transfer coefficient was normally within plus or minus 17 percent of the experimental value.

In the current range of operation ($R \leq 1.40$), the overall volumetric heat transfer was increased as the flow rates of both phases were increased and the approach temperature at the bottom of the column was decreased. The heat transfer in this range was found to be a

linear function of the flow rate ratio and the continuous phase flow rate as shown.

$$U_V \text{ (kcal/m}^3\text{hr°C)} = -95015 + 48845\ R + 69649\ V_C \text{ (cm/sec)}$$

Further Work

It is suggested that further work be done with a glass column to facilitate accurate measurement of interface levels holdup, and drop size. Variation in the two phase flow pattern with operating parameters could also be observed. More fast response and shielded (slow response) thermocouples should be installed to obtain detailed experimental temperature profiles for use in modeling the apparatus. Also a level indicator should be installed to keep the level of the interface constant by automatically adjusting flow valves.

The perforated plate column should be run over a wider range of operating conditions to determine the optimum and the number of plates should be varied as well. A larger tower might facilitate a wide range of operation by allowing for greater throughput.

REFERENCES

1. Greider, B., "Geothermal Energy Task Force Testimony," Geothermal Energy, Vol. 2, No. 6, Feb. 1978, p. 25.

2. Jacobs, H. R., Boehm, R. F., "Direct Contact Binary Cycles," UTEC ME-78-086, p. 1.

3. Jacobs, H. R., Boehm R. F., Hanson, A. C., "Application of Direct Contact Heat Exchangers to Geothermal Power Production Cycles," IDO/1549-8, VC-66d.

4. Letan, R., "Design of a Particulate Direct Contact Heat Exchanger: Uniform Countercurrent Flow," ASME 76-HT-27, p. 5.

5. Plass, S. B., Jacobs, H. R., Boehm, R. F., "Operational Characteristics of a Spray Column Type Direct Contact Preheater," AIChE Symp. Ser., Vol. 75, No. 189, (1979).

6. Letan, R., Kehat, E., "The Mechanism of Heat Transfer in a Spray Column Heat Exchanger," AIChE J, Vol. 14, No. 3, 1968, p. 401.

7. Letan R., "A Parametric Study of a Direct Contact Heat Exchanger," p. 9.

8. Richardson, J. F., Zaki, W. N., "Sedimentation and Fluidization: Part I," Trans. Instn. Chem. Engrs., Vol. 33, (1954), p. 35-53.

9. Lapidus, L., Elgin J. C., "Mechanisms of Verticle-Moving Fluidized Systems," AIChE J, Vol. 3, No. 1, (1957) p. 33.

10. Letan, R., "A Parametric Study of a Direct Contact Heat Exchanger," p. 4.

11. Letan, R., Kehat, E., "The Mechanism of Heat Transfer in a Spray Column Heat Exchanger," AIChE J., Vol. 14, no. 3, 1968, p. 398.

12. Letan R., Kehat E., "Mechanism of Heat Transfer in a Spray Column Heat Exchanger: Dense Packing of Drops," AIChE J, Vol. 16, No. 6, (1970), p. 955.

13. Kreith, F., "Principles of Heat Transfer," Third Edition, Intext Educational Publishers (1973), p. 473.

14. Letan, R., Kehat, E., "The Mechanism of Heat Transfer in a Spary Column Heat Exchanger," AIChE J, Vol. 14, No. 3, 1968, p. 400.

15. Hendrix, C. D., Shashikant, B. D., Homer, F. J., "Translation of Continuous Phase in the Wakes of Single Rising Drops," AIChE J, Vol. 13, No. 3, (1967), p. 1072.

16. Magarvey, R. H., Bishop, R. L., "Wakes in Liquid-Liquid Systems," The Physics of Fluids, Vol. 4, No. 7, (1968), p. 804.

17. Jacobsen, S. C., "Particle Migration in a Poiseuille Flow Field," Thesis University of Utah, June 1970.

18. Treybal, R. E., "Liquid Extraction," 2nd Ed. McGraw Hill, (1963), p. 503.

APPENDIX A

SPRAY COLUMN TEMPERATURE PROFILES

In the following plots the experimental radial temperature as determined from the slow response thermocouples is shown by three fine lines labeled b, c, and d, in order of increasing distance from the column wall (refer to Figure 14). The three profiles shown by thick lines were calculated from the model of Letan and Kehat and represent the wake droplet and continuous phase temperatures listed from coldest to hottest. Triangular shapes mark the maximum and minimum temperatures seen by each fast response thermocouple. Other experimental continuous phase and dispersed phase temperatures are shown by rectangles and diamonds respectively.

Following each plot is a page giving a numerical comparison of the model and the experimental results. These comparisons are made at the level of each fast response thermocouple in the column with number 14 being the lowest in the column. Also given are durations in seconds that the fast response thermocouples are exposed to the continuous phase, droplets, and wakes denoted R1, R2, and R3 respectively, and defined in Equation (10). The corresponding fast and slow response thermocouple time constants in seconds^{-1} are given by A1, A2, and A3.

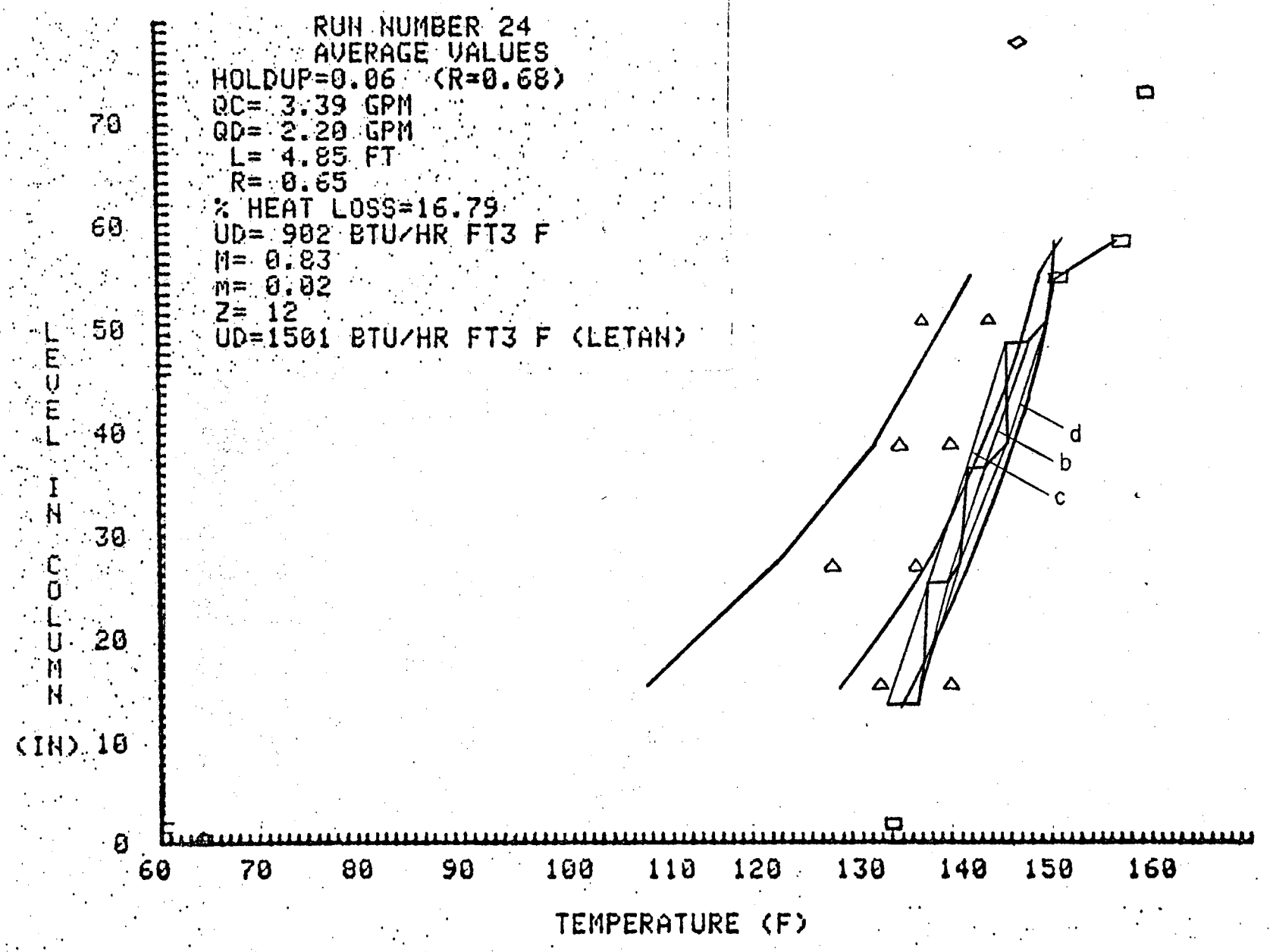

Temperature Values, Run Number 24

RUN NUMBER 24
EXPERIMENTAL TEMP MINUS VALUE CALCULATED FROM LETANS MODEL
COLUMN A -- DIFFERENCE
COLUMN B -- % DIFFERENCE

CONTINUOUS PHASE TEMP

T.C.#	A(F)	B(%)
14.	3.6	97.4
11.	-5.9	104.3
8.	-6.8	104.9
5.	-6.1	104.2

WAKE TEMP

T,C,#	A(F)	B(%)
14.	23.2	82.5
11.	5.5	95.7
8.	2.6	98.1
5.	-2.5	101.8

REPITITION TIME= 0.5
R1= 0.44000 R2= 0.03000 R3= 0.03000

A1f= 8.69606 A2f= 2.91327 A3f= 13.87741
A1s= 0.05064 A2s= 0.02997 A3s= 0.13955

LENGTH OF WAKE FORMATION AND INTERMEDIATE ZONE= 12

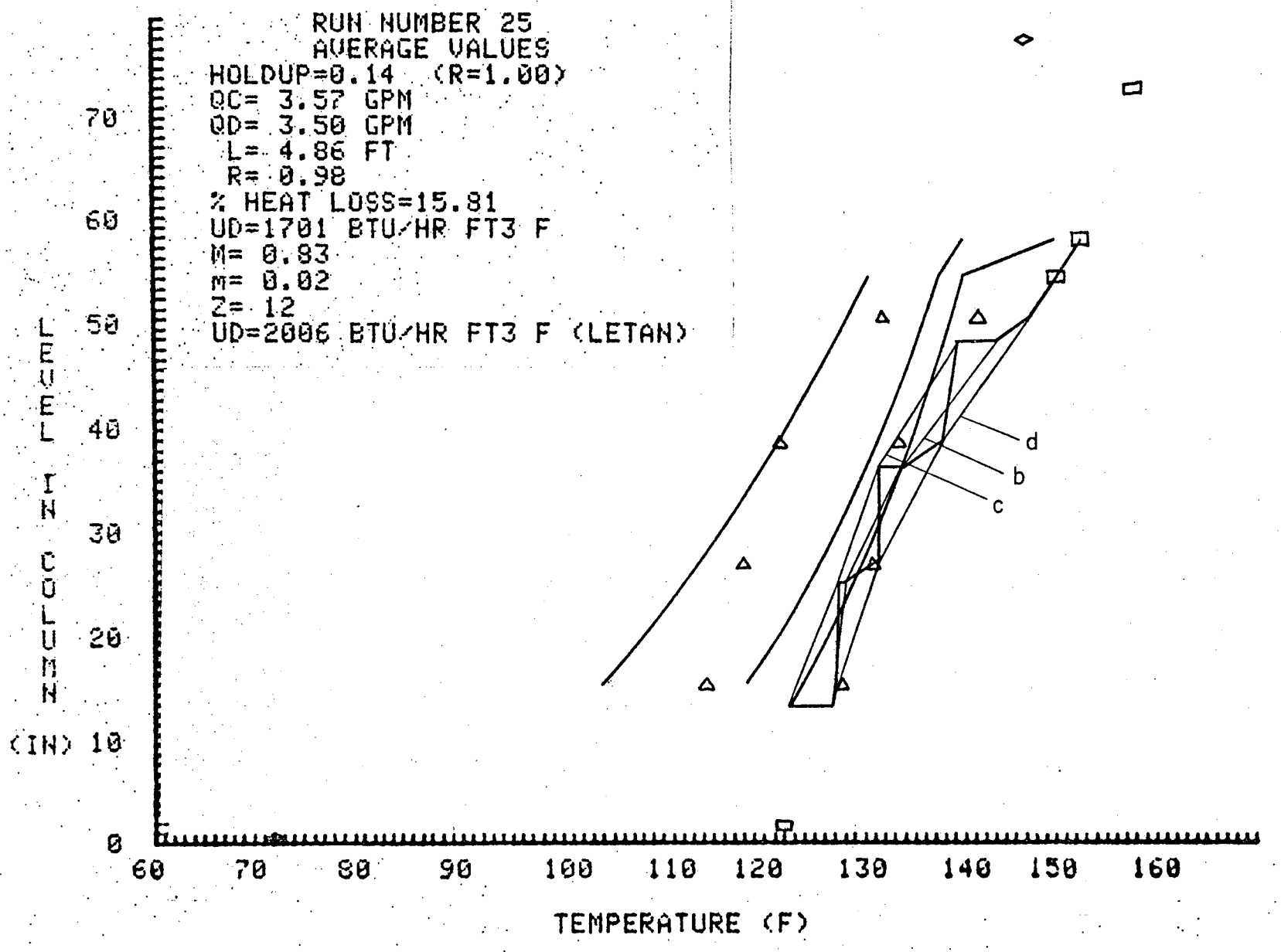

Temperature Values, Run Number 25

RUN NUMBER 25
EXPERIMENTAL TEMP MINUS VALUE CALCULATED FROM LETANS MODEL
COLUMN A -- DIFFERENCE
COLUMN B -- % DIFFERENCE

CONTINUOUS PHASE TEMP

T.C.#	A(F)	B(%)
14.	3.8	97.1
11.	0.9	99.3
8.	-1.4	101.0
5.	2.5	98.2

WAKE TEMP

T,C,#	A(F)	B(%)
14.	10.3	91.1
11.	4.4	96.3
8.	-0.1	100.1
5.	3.5	97.4

REPITITION TIME= 0.5
R1= 0.37190 R2= 0.07000 R3= 0.05810

A1f= 8.84432 A2f= 2.59535 A3f= 12.42257
A1s= 0.05310 A2s= 0.02454 A3s= 0.11449

LENGTH OF WAKE FORMATION AND INTERMEDIATE ZONE= 12

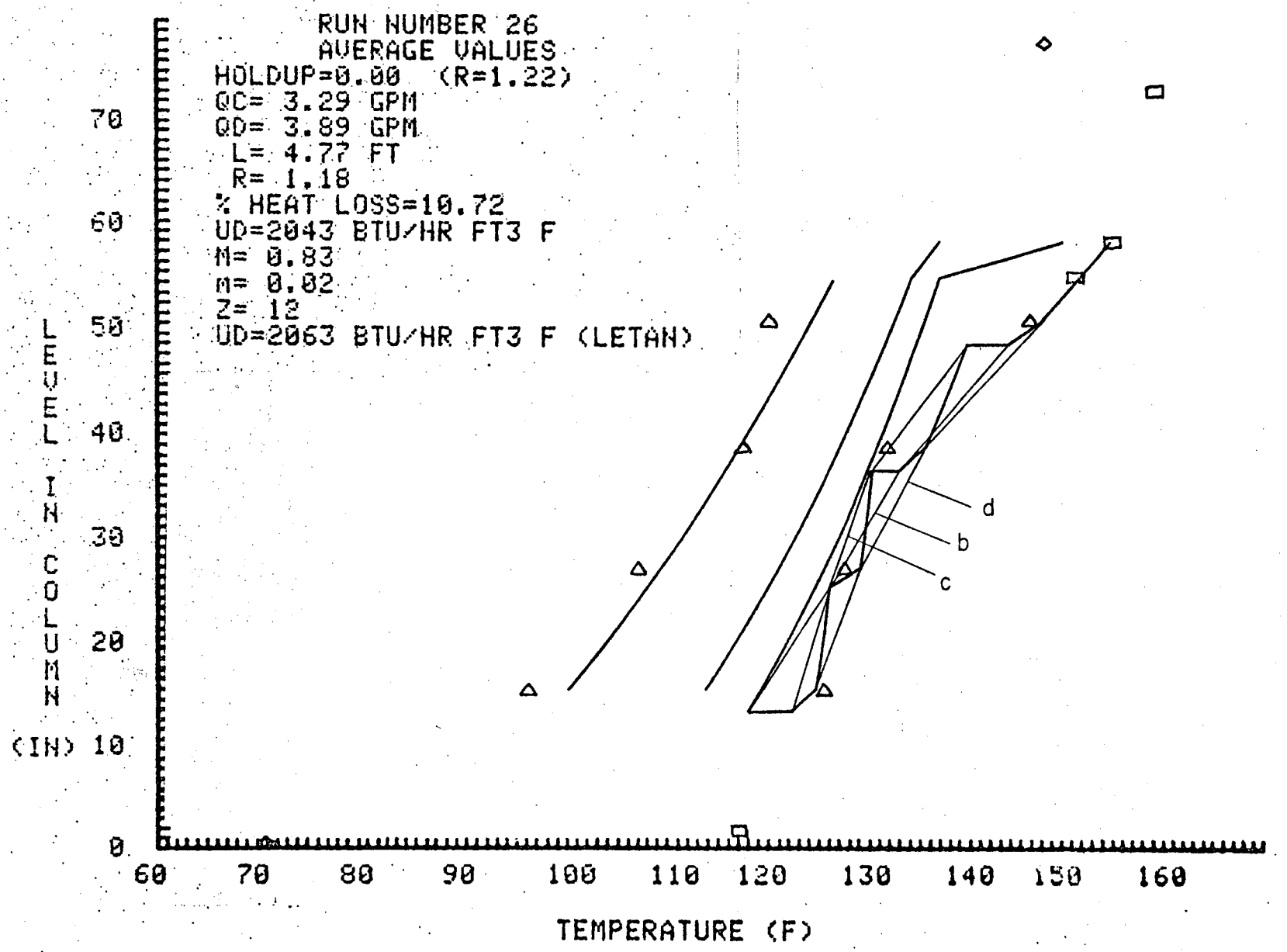

Temperature Values, Run Number 26

RUN NUMBER 26
EXPERIMENTAL TEMP MINUS VALUE CALCULATED FROM LETANS MODEL
COLUMN A -- DIFFERENCE
COLUMN B -- % DIFFERENCE

CONTINUOUS PHASE TEMP

T.C.#	A(F)	B(%)
14.	6.2	95.1
11.	1.9	98.5
8.	0.8	99.4
5.	10.3	93.0

WAKE TEMP

T,C,#	A(F)	B(%)
14.	-4.3	104.4
11.	-2.5	102.3
8.	0.1	100.0
5.	-4.3	103.5

REPITITION TIME= 0.5
R1= 0.43595 R2= 0.03500 R3= 0.02905

A1f= 8.67677 A2f= 3.02143 A3f= 14.37281
A1s= 0.05032 A2s= 0.03182 A3s= 0.14810

LENGTH OF WAKE FORMATION AND INTERMEDIATE ZONE= 12

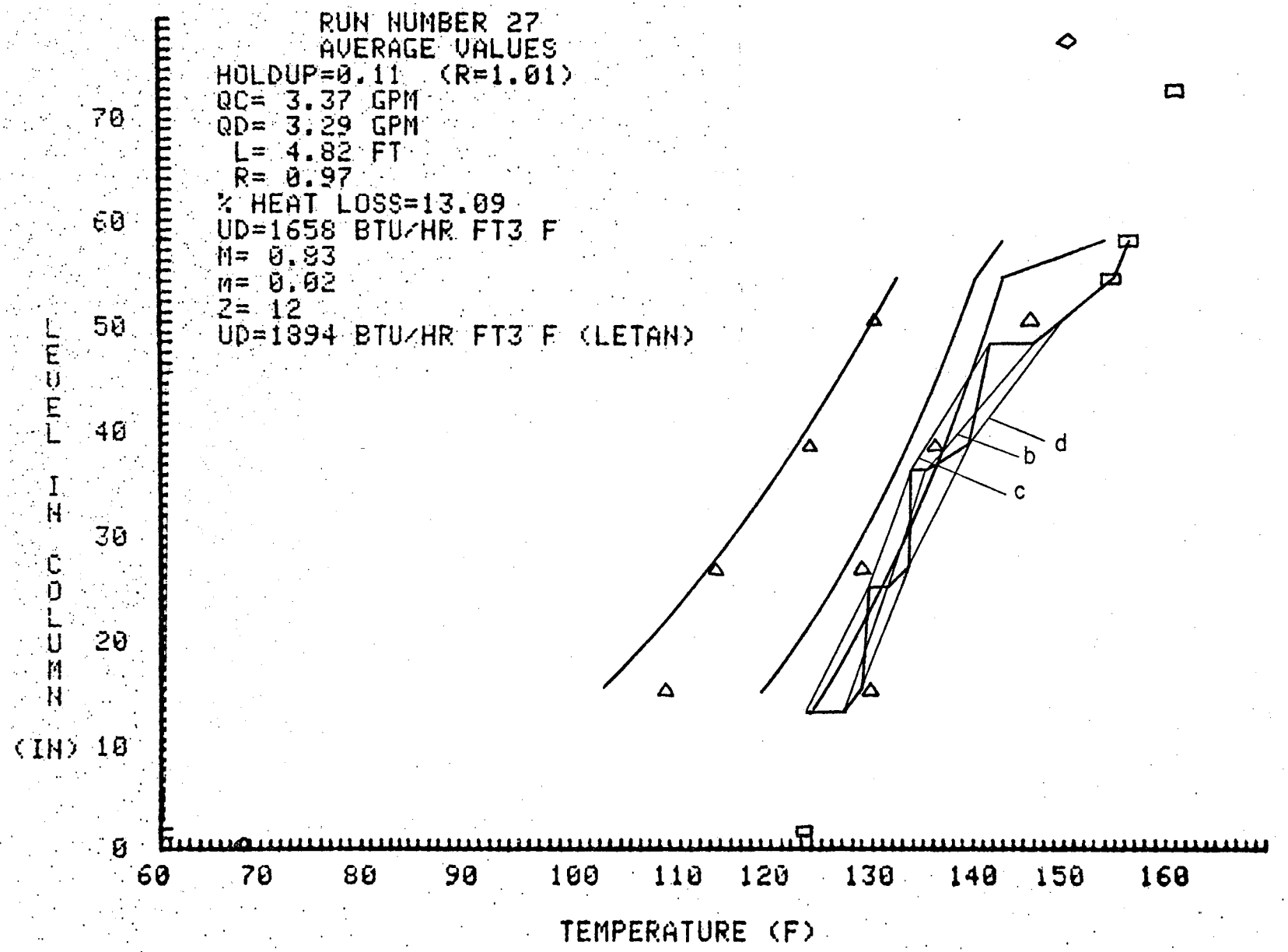

Temperature Values, Run Number 27

RUN NUMBER 27
EXPERIMENTAL TEMP MINUS VALUE CALCULATED FROM LETANS MODEL
COLUMN A -- DIFFERENCE
COLUMN B -- % DIFFERENCE

CONTINUOUS PHASE TEMP

T.C.#	A(F)	B(%)
14.	4.2	96.8
11.	-3.2	102.5
8.	-1.2	100.9
5.	3.9	97.3

WAKE TEMP

T.C.#	A(F)	B(%)
14.	6.1	94.5
11.	0.1	99.9
8.	0.9	99.3
5.	-0.1	100.1

REPITITION TIME= 0.5
R1= 0.39935 R2= 0.05500 R3= 0.04565

A1f= 8.74596 A2f= 2.73465 A3f= 13.05974
A1s= 0.05147 A2s= 0.02691 A3s= 0.12545

LENGTH OF WAKE FORMATION AND INTERMEDIATE ZONE= 12

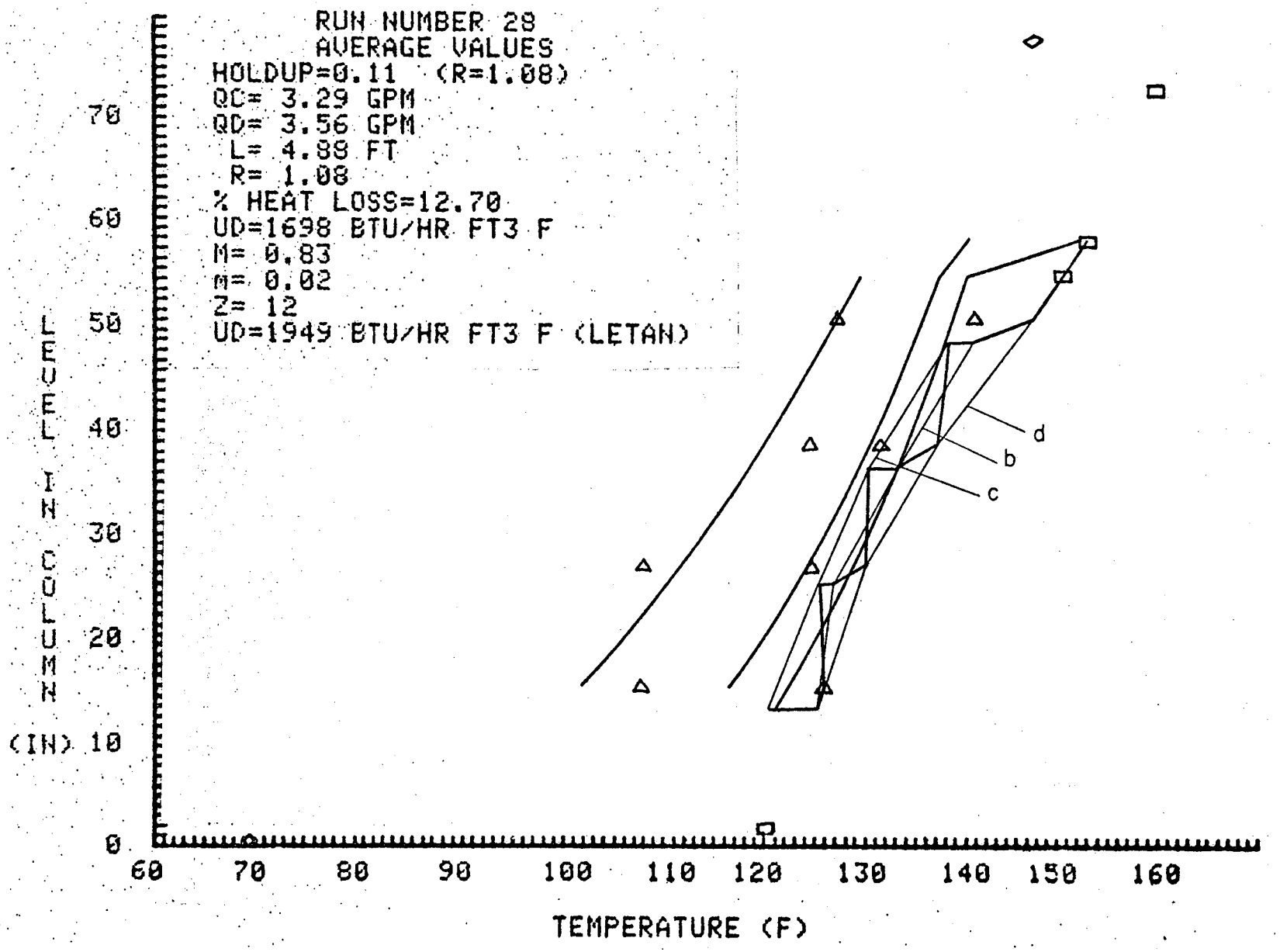

Temperature Values, Run Number 28

```
 RUN NUMBER 28
 EXPERIMENTAL TEMP MINUS VALUE CALCULATED FROM LETANS MODEL
    COLUMN A -- DIFFERENCE
    COLUMN B -- % DIFFERENCE

CONTINUOUS PHASE TEMP

T.C.#      A(F)       B(%)

14.           3.5       97.2
11.          -4.3      103.4
 8.          -2.8      102.1
 5.           2.1       98.5

WAKE TEMP

T.C.#      A(F)       B(%)

14.           5.7       94.7
11.          -3.9      103.6
 8.           4.2       96.6
 5.          -0.2      100.2

REPITITION TIME= 0.5
R1= 0.39935   R2= 0.05500   R3= 0.04565

A1f=  8.72117   A2f=  2.80110   A3f= 13.36385
A1s=  0.05105   A2s=  0.02805   A3s=  0.13069

LENGTH OF WAKE FORMATION AND INTERMEDIATE ZONE= 12
```

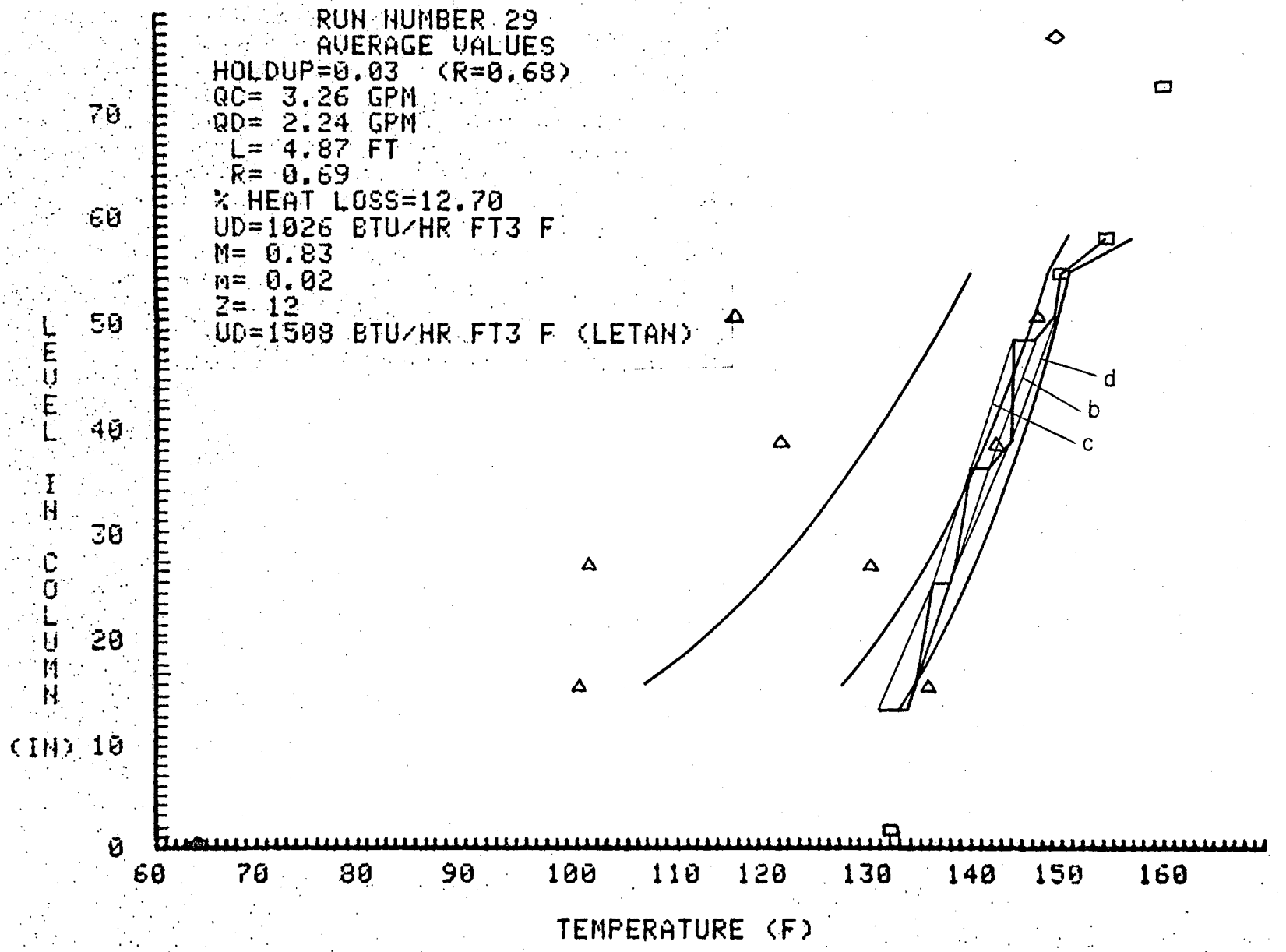

Temperature Values, Run Number 29

RUN NUMBER 29
EXPERIMENTAL TEMP MINUS VALUE CALCULATED FROM LETANS MODEL
COLUMN A -- DIFFERENCE
COLUMN B -- % DIFFERENCE

CONTINUOUS PHASE TEMP

T.C.#	A(F)	B(%)
14.	1.4	99.0
11.	-10.6	108.0
8.	-2.7	101.9
5.	-2.2	101.5

WAKE TEMP

T.C.#	A(F)	B(%)
14.	-6.5	106.4
11.	-18.5	117.9
8.	-9.2	107.5
5.	-21.3	118.1

REPITITION TIME= 0.5
R1= 0.47000 R2= 0.01500 R3= 0.01500

A1f= 8.62650 A2f= 3.75264 A3f= 17.72679
A1s= 0.04949 A2s= 0.04439 A3s= 0.20622

LENGTH OF WAKE FORMATION AND INTERMEDIATE ZONE= 12

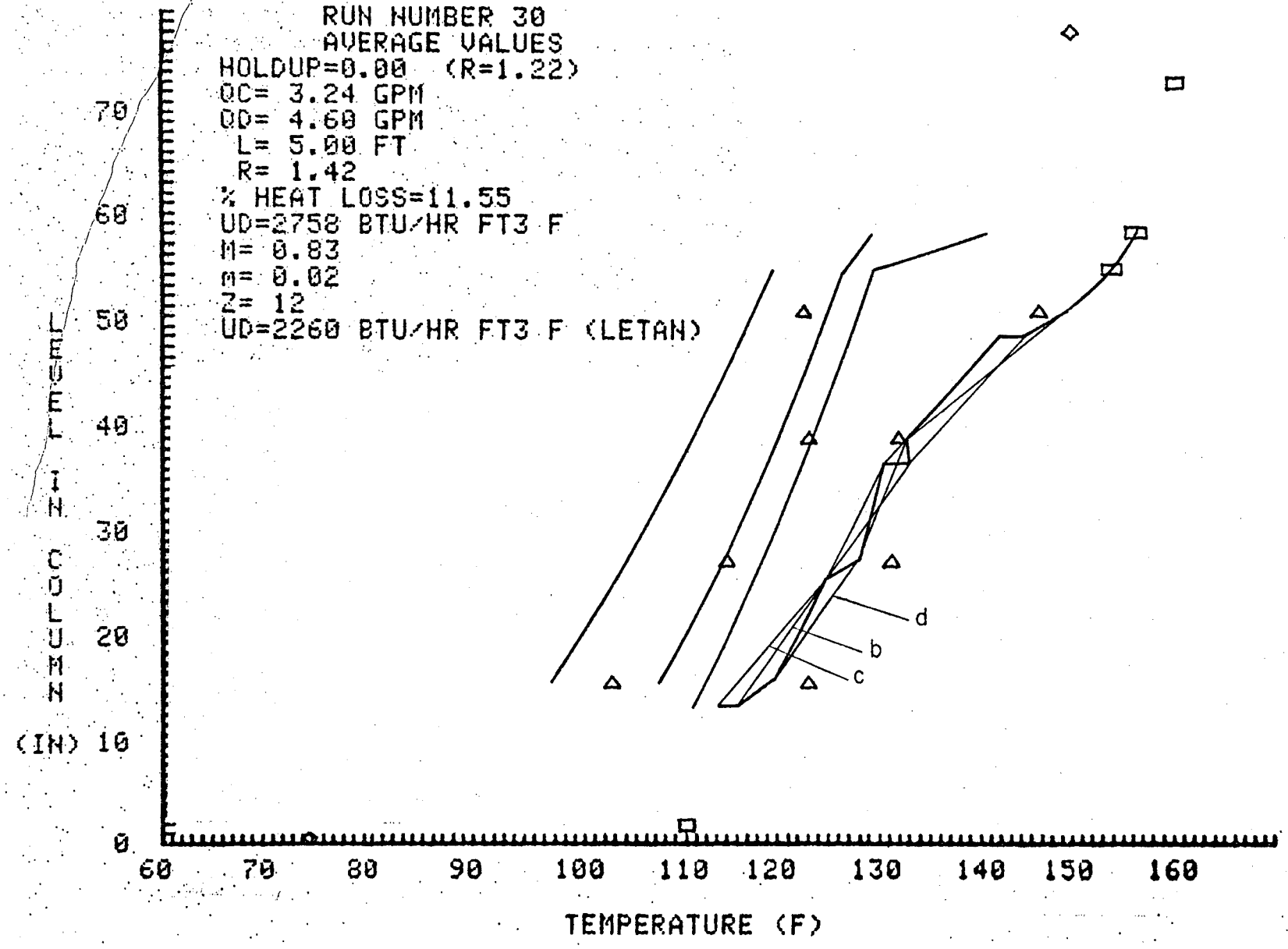

Temperature Values, Run Number 30

RUN NUMBER 30
EXPERIMENTAL TEMP MINUS VALUE CALCULATED FROM LETANS MODEL
COLUMN A -- DIFFERENCE
COLUMN B -- % DIFFERENCE

CONTINUOUS PHASE TEMP

T.C.#	A(F)	B(%)
14.	10.2	91.8
11.	12.7	90.4
8.	9.4	93.7
5.	17.8	87.9

WAKE TEMP

T,C,#	A(F)	B(%)
14.	5.8	94.5
11.	9.8	91.5
8.	11.4	90.9
5.	4.9	96.1

REPITITION TIME= 0.5
R1= 0.36275 R2= 0.07500 R3= 0.06225

A1f= 8.75288 A2f= 2.75536 A3f= 13.15455
A1s= 0.05158 A2s= 0.02727 A3s= 0.12708

LENGTH OF WAKE FORMATION AND INTERMEDIATE ZONE= 12

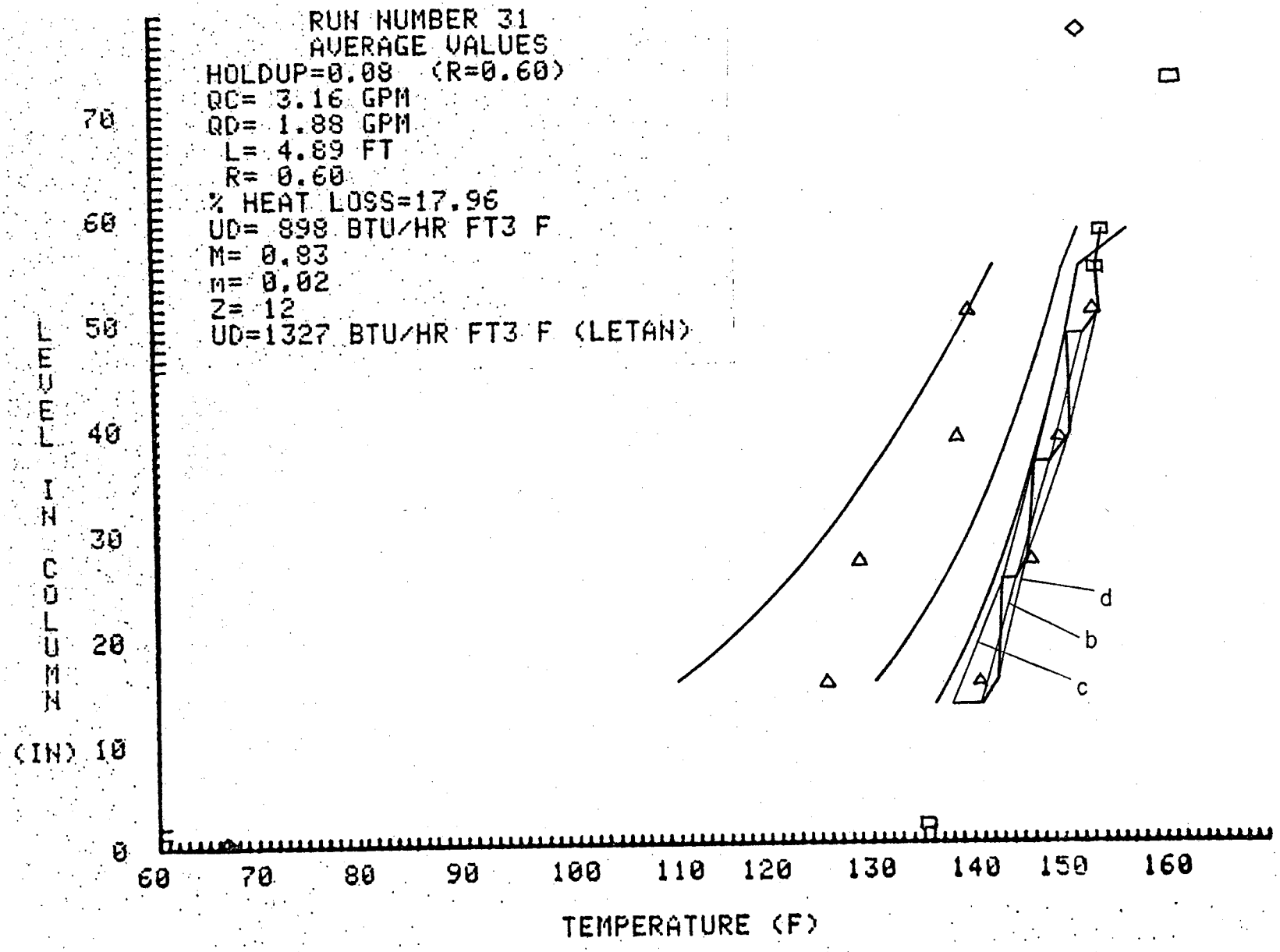

Temperature Values, Run Number 31

RUN NUMBER 31
EXPERIMENTAL TEMP MINUS VALUE CALCULATED FROM LETANS MODEL
COLUMN A -- DIFFERENCE
COLUMN B -- % DIFFERENCE

CONTINUOUS PHASE TEMP

T.C.#	A(F)	B(%)
14.	3.1	97.8
11.	2.7	98.1
8.	1.6	98.9
5.	2.1	98.6

WAKE TEMP

T,C,#	A(F)	B(%)
14.	14.7	88.4
11.	5.3	95.9
8.	5.6	96.0
5.	-0.4	100.3

REPITITION TIME= 0.5
R1= 0.42314 R2= 0.04200 R3= 0.03486

A1f= 8.65088 A2f= 2.51720 A3f= 12.06531
A1s= 0.04989 A2s= 0.02321 A3s= 0.10835

LENGTH OF WAKE FORMATION AND INTERMEDIATE ZONE= 12

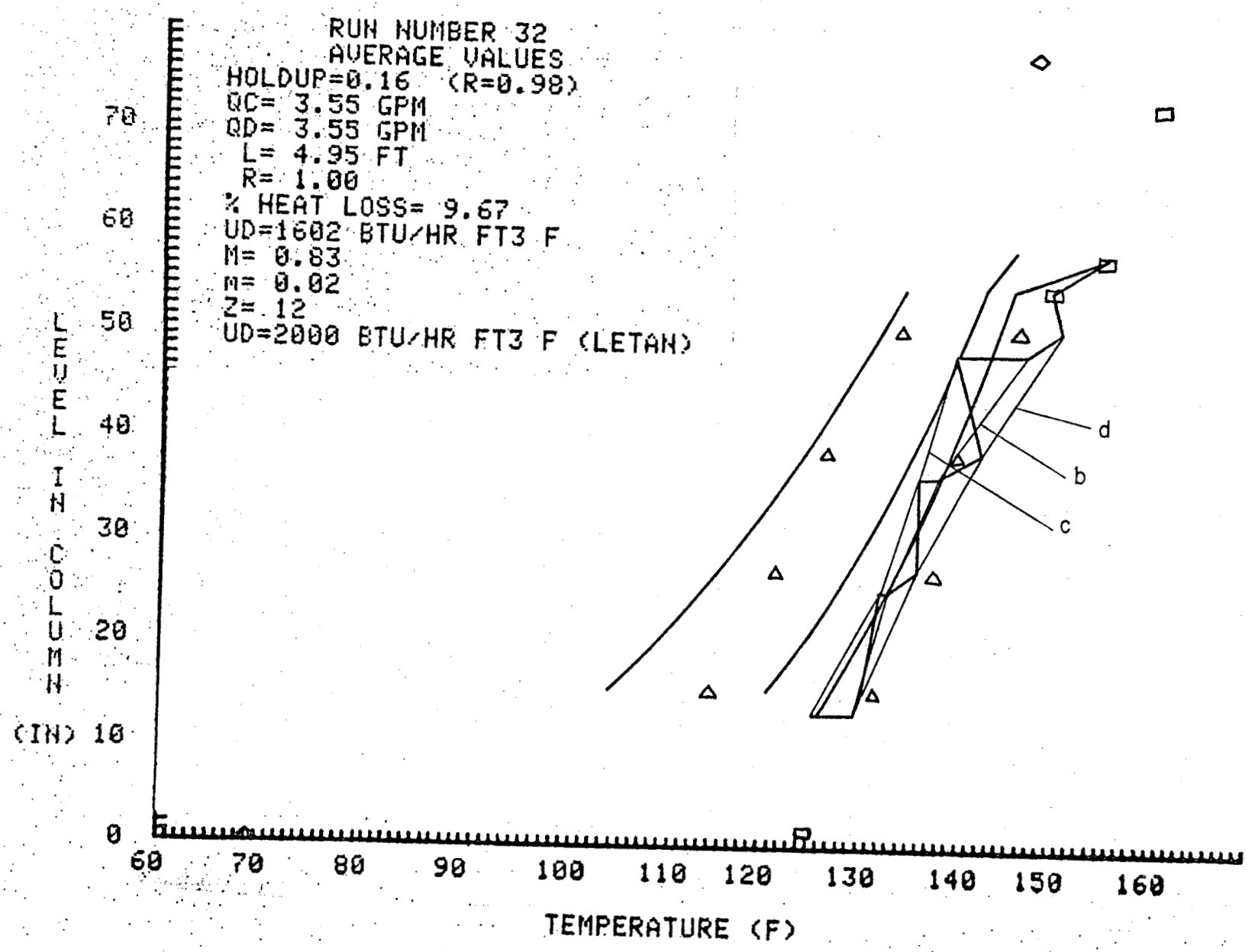

Temperature Values, Run Number 32

RUN NUMBER 32
EXPERIMENTAL TEMP MINUS VALUE CALCULATED FROM LETANS MODEL
COLUMN A -- DIFFERENCE
COLUMN B -- % DIFFERENCE

CONTINUOUS PHASE TEMP

T.C.#	A(F)	B(%)
14.	4.3	96.7
11.	3.4	97.5
8.	0.2	99.8
5.	1.8	98.8

WAKE TEMP

T.C.#	A(F)	B(%)
14.	10.1	91.3
11.	5.8	95.3
8.	1.9	98.5
5.	1.8	98.7

REPITITION TIME= 0.5
R1= 0.35177 R2= 0.08100 R3= 0.06723

A1f= 8.86785 A2f= 2.50207 A3f= 11.99616
A1s= 0.05349 A2s= 0.02295 A3s= 0.10717

LENGTH OF WAKE FORMATION AND INTERMEDIATE ZONE= 12

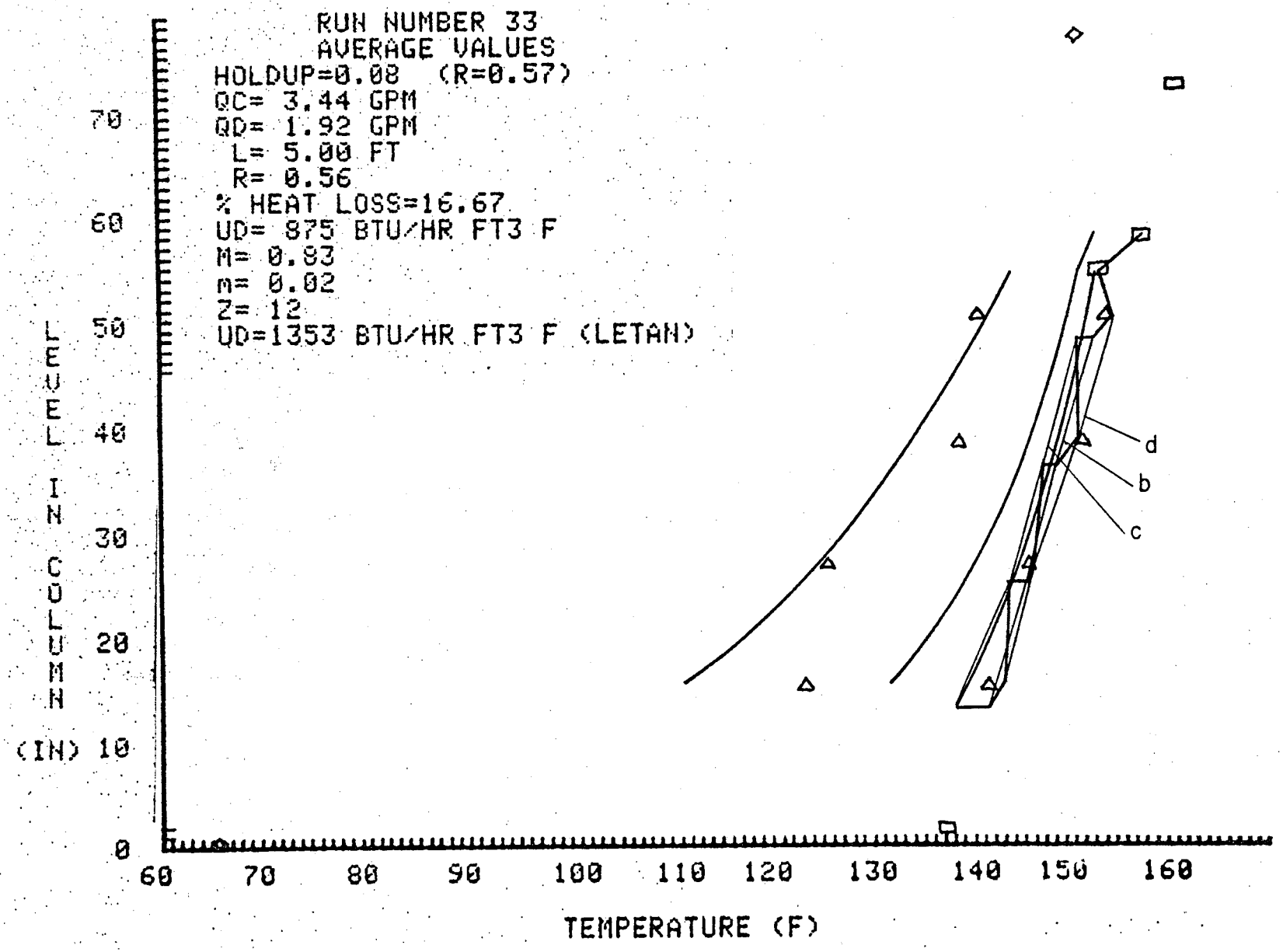

Temperature Values, Run Number 33

RUN NUMBER 33
EXPERIMENTAL TEMP MINUS VALUE CALCULATED FROM LETANS MODEL
COLUMN A -- DIFFERENCE
COLUMN B -- % DIFFERENCE

CONTINUOUS PHASE TEMP

T.C.#	A(F)	B(%)
14.	2.0	98.6
11.	0.7	99.5
8.	2.2	98.6
5.	1.7	98.9

WAKE TEMP

T,C,#	A(F)	B(%)
14.	11.6	90.7
11.	0.5	99.6
8.	4.0	97.2
5.	-1.3	100.9

REPITITION TIME= 0.5
R1= 0.42680 R2= 0.04000 R3= 0.03320

A1f= 8.73292 A2f= 2.56484 A3f= 12.28308
A1s= 0.05125 A2s= 0.02402 A3s= 0.11209

LENGTH OF WAKE FORMATION AND INTERMEDIATE ZONE= 12

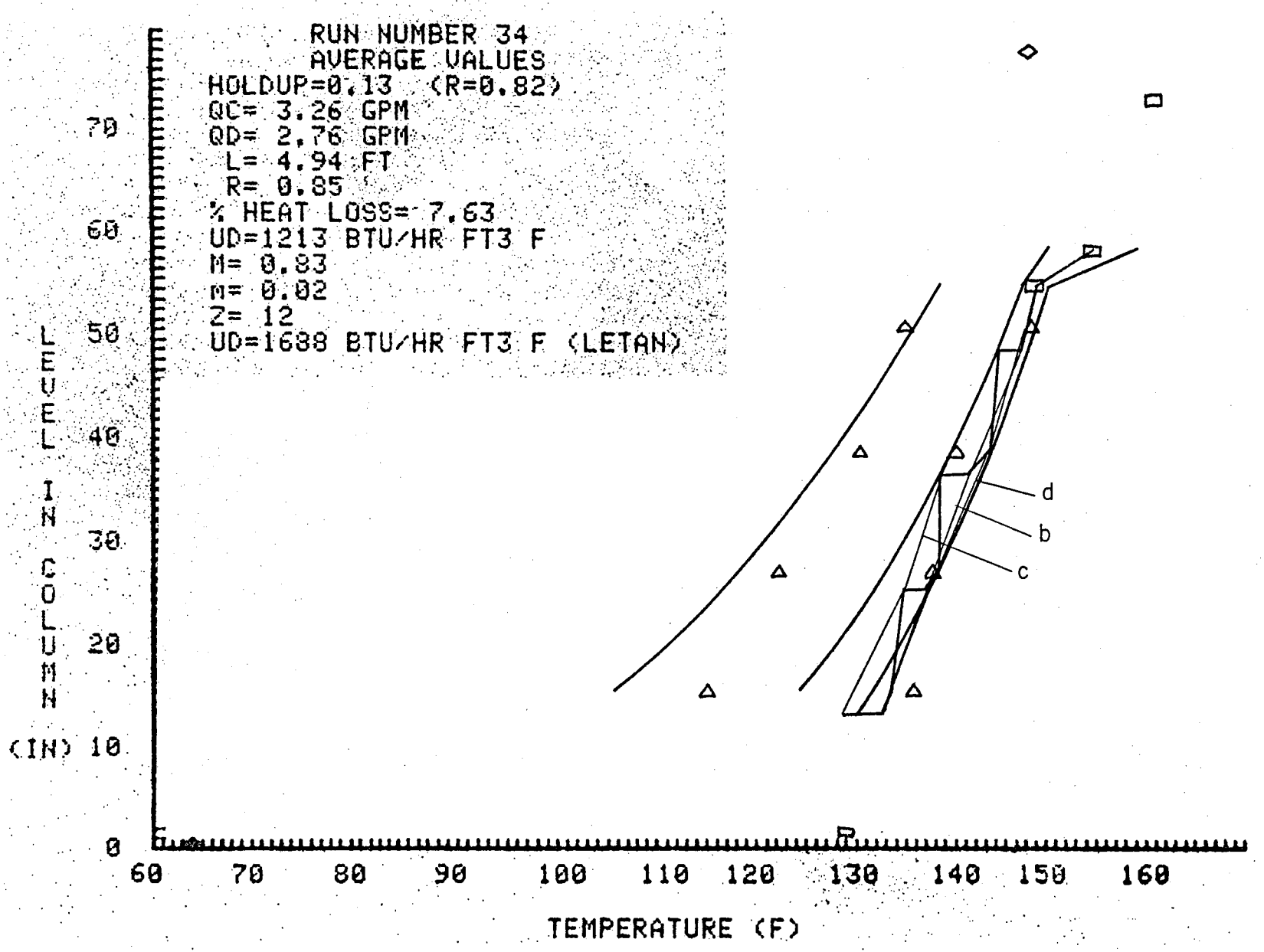

Temperature Values, Run Number 34

RUN NUMBER 34
EXPERIMENTAL TEMP MINUS VALUE CALCULATED FROM LETANS MODEL
COLUMN A -- DIFFERENCE
COLUMN B -- % DIFFERENCE

CONTINUOUS PHASE TEMP

T.C.#	A(F)	B(%)
14.	4.2	96.9
11.	-0.8	100.5
8.	-3.9	102.8
5.	-0.6	100.4

WAKE TEMP

T,C,#	A(F)	B(%)
14.	9.3	92.0
11.	4.1	96.7
8.	2.4	98.2
5.	-1.2	100.9

REPITITION TIME= 0.5
R1= 0.38105 R2= 0.06500 R3= 0.05395

A1f= 8.73486 A2f= 2.48237 A3f= 11.90616
A1s= 0.05128 A2s= 0.02261 A3s= 0.10562

LENGTH OF WAKE FORMATION AND INTERMEDIATE ZONE= 12

APPENDIX B

PERFORATED PLATE COLUMN TEMPERATURE PROFILES: M = 0.83

In these plots the experimental profiles are shown by thin lines and the profiles calculated from the model are shown by thick lines. Triangular shapes mark the maximum and minimum temperatures seen by each fast response thermocouple. Other continuous phase and dispersed phase temperatures are shown by rectangles and diamonds respectively. Horizontal dashed lines indicate the level of each plate.

Following each plot is a page giving a numerical comparison of the model and the experimental results. The comparisons are made just below the level of each plate with the first one being below the lowest plate. Also given are the durations in seconds that the fast response thermocouples were exposed to the continuous phase droplet, and wakes denoted R1, R2, and R3 respectively. The corresponding fast and slow response thermocouple time constants in seconds^{-1} are given by A1, A2, and A3.

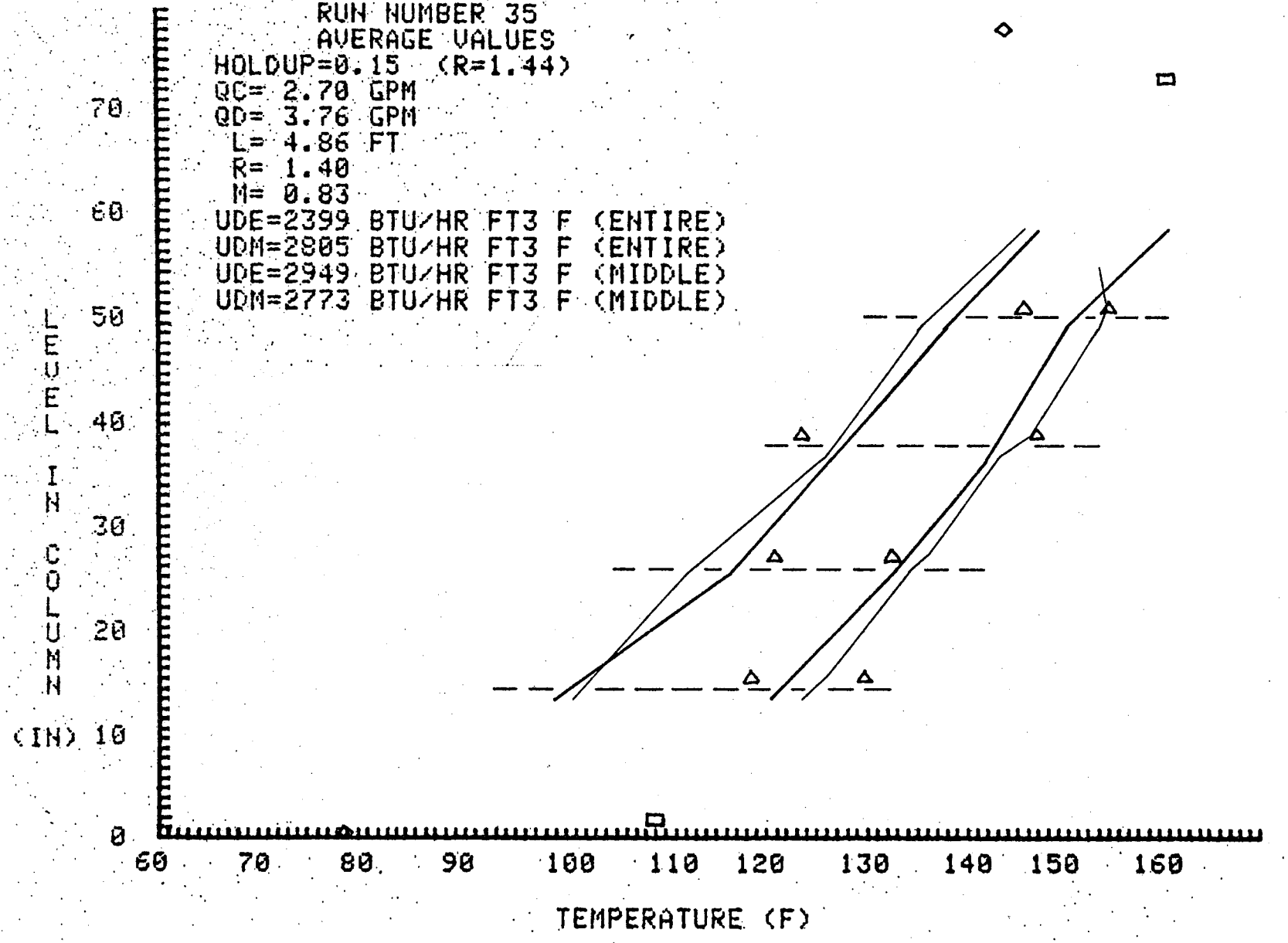

Temperature Values, Run Number 35

RUN NUMBER 35
EXPERIMENTAL TEMP MINUS VALUE CALCULATED FROM MODEL
COLUMN A -- DIFFERENCE
COLUMN B -- % DIFFERENCE

WATER TEMP

T.C.#	A(F)	B(%)
15.	3.1	97.5
12.	1.5	98.9
9.	1.0	99.3
6.	3.4	97.8

KEROSENE TEMP

T.C.#	A(F)	B(%)
16.	1.9	98.1
13.	-4.3	103.8
10.	-1.0	100.8
7.	-2.6	101.9

REPITITION TIME= 0.5
R1= 0.36275 R2= 0.07500 R3= 0.06225

A1f= 8.57128 A2f= 2.59763 A3f= 12.43300
A1s= 0.04857 A2s= 0.02458 A3s= 0.11467

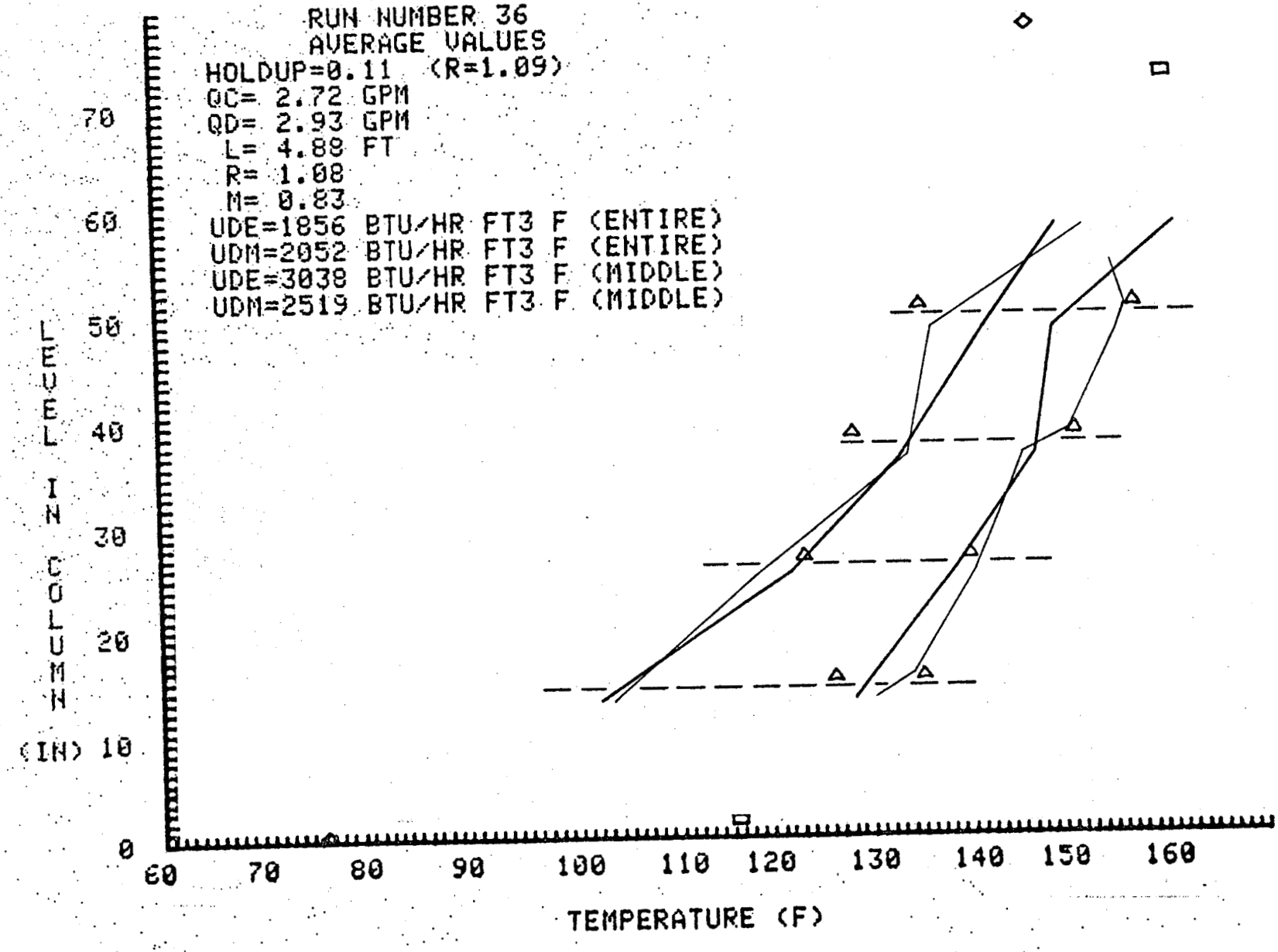

Temperature Values, Run Number 36

RUN NUMBER 36
EXPERIMENTAL TEMP MINUS VALUE CALCULATED FROM MODEL
COLUMN A -- DIFFERENCE
COLUMN B -- % DIFFERENCE

WATER TEMP

T.C.#	A(F)	B(%)
15.	2.2	98.3
12.	2.1	98.5
9.	-1.3	100.9
6.	6.4	95.9

KEROSENE TEMP

T.C.#	A(F)	B(%)
16.	1.1	98.9
13.	-3.0	102.5
10.	0.5	99.6
7.	-5.2	103.8

REPITITION TIME= 0.5
R1= 0.39935 R2= 0.05500 R3= 0.04565

A1f= 8.53580 A2f= 2.64173 A3f= 12.63469
A1s= 0.04799 A2s= 0.02533 A3s= 0.11814

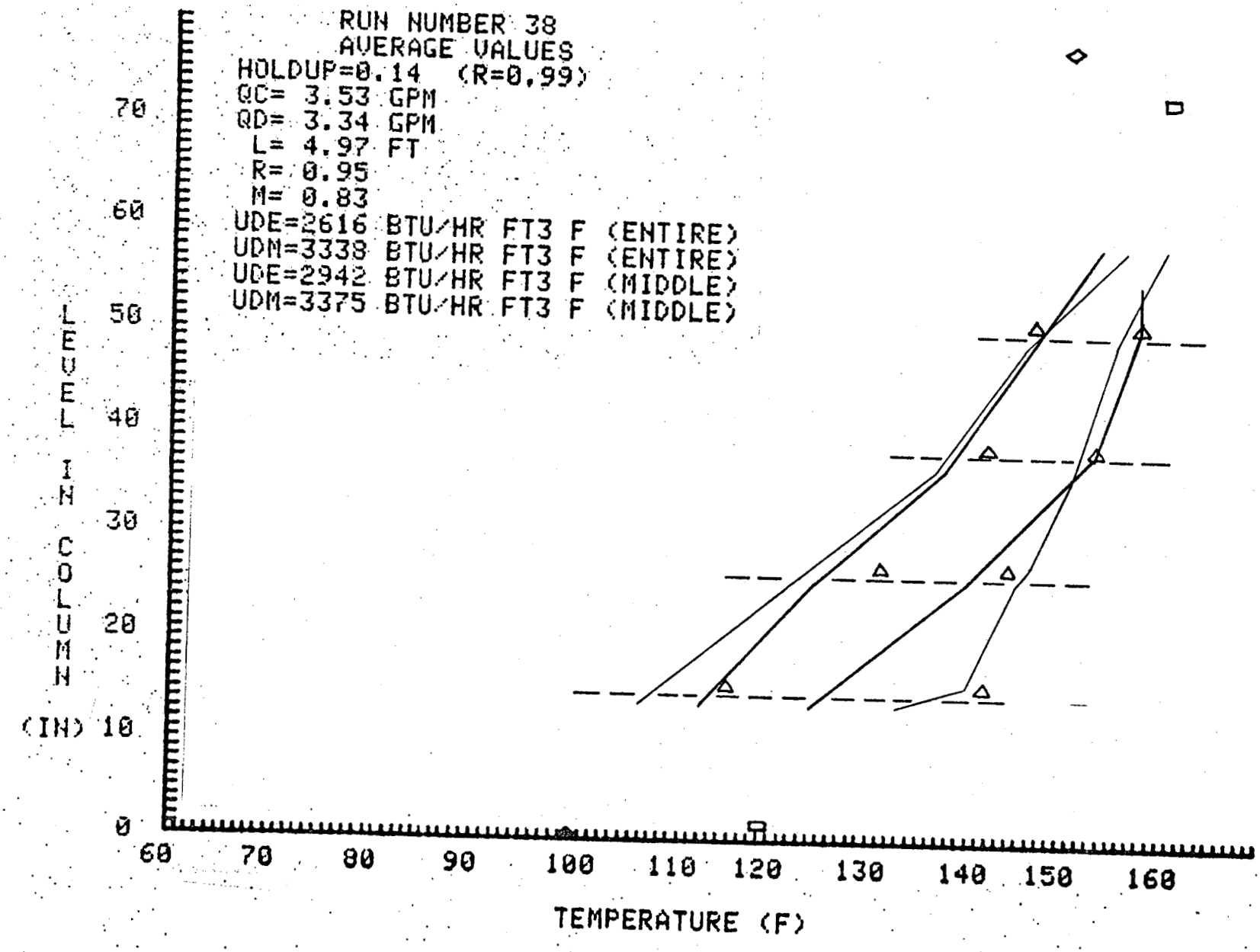

Temperature Values, Run Number 38

```
RUN NUMBER 38
EXPERIMENTAL TEMP MINUS VALUE CALCULATED FROM MODEL
   COLUMN A -- DIFFERENCE
   COLUMN B -- % DIFFERENCE

WATER TEMP

T.C.#      A(F)       B(%)

15.           8.8        93.4
12.           5.2        96.5
 9.           0.3        99.8
 6.           2.0        98.7

KEROSENE TEMP

T,C,#      A(F)       B(%)

16.          -6.0       105.6
13.          -2.4       102.0
10.          -0.8       100.6
 7.          -0.8       100.5

REPITITION TIME= 0.5
R1= 0.39500    R2= 0.07000    R3= 0.03500

A1f=  8.83299    A2f=  2.56222    A3f= 12.27110
A1s=  0.05291    A2s=  0.02397    A3s=  0.11189
```

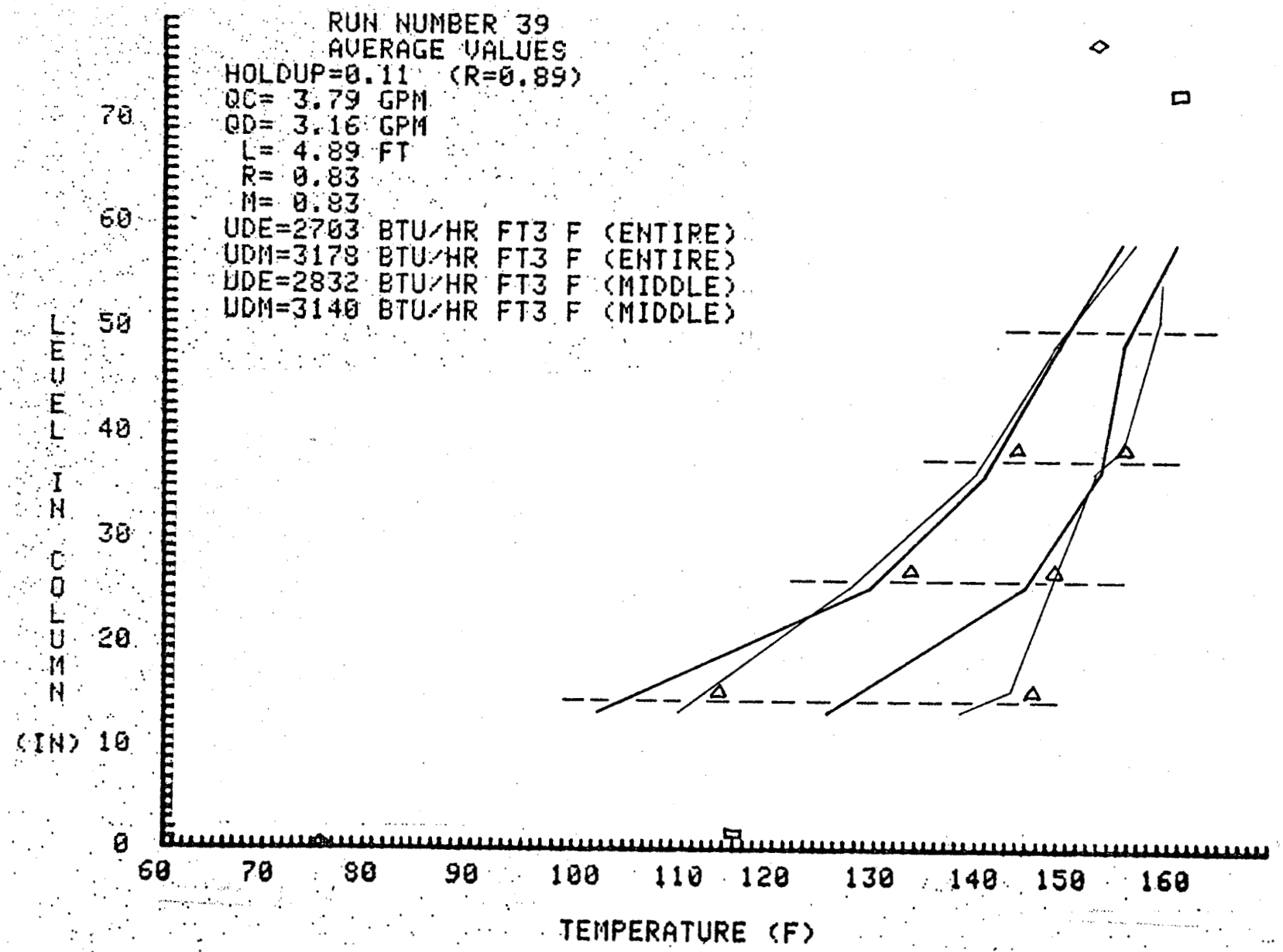

Temperature Values, Run Number 39

RUN NUMBER 39
EXPERIMENTAL TEMP MINUS VALUE CALCULATED FROM MODEL
COLUMN A -- DIFFERENCE
COLUMN B -- % DIFFERENCE

WATER TEMP

T.C.#	A(F)	B(%)
15.	13.1	90.6
12.	3.0	98.0
9.	-0.4	100.3
6.	2.9	98.2

KEROSENE TEMP

T.C.#	A(F)	B(%)
16.	7.8	93.0
13.	-1.9	101.5
10.	-1.0	100.7
7.	-0.2	100.2

REPITITION TIME= 0.5
R1= 0.39935 R2= 0.05500 R3= 0.04565

A1f= 8.87337 A2f= 2.70299 A3f= 12.91492
A1s= 0.05358 A2s= 0.02637 A3s= 0.12296

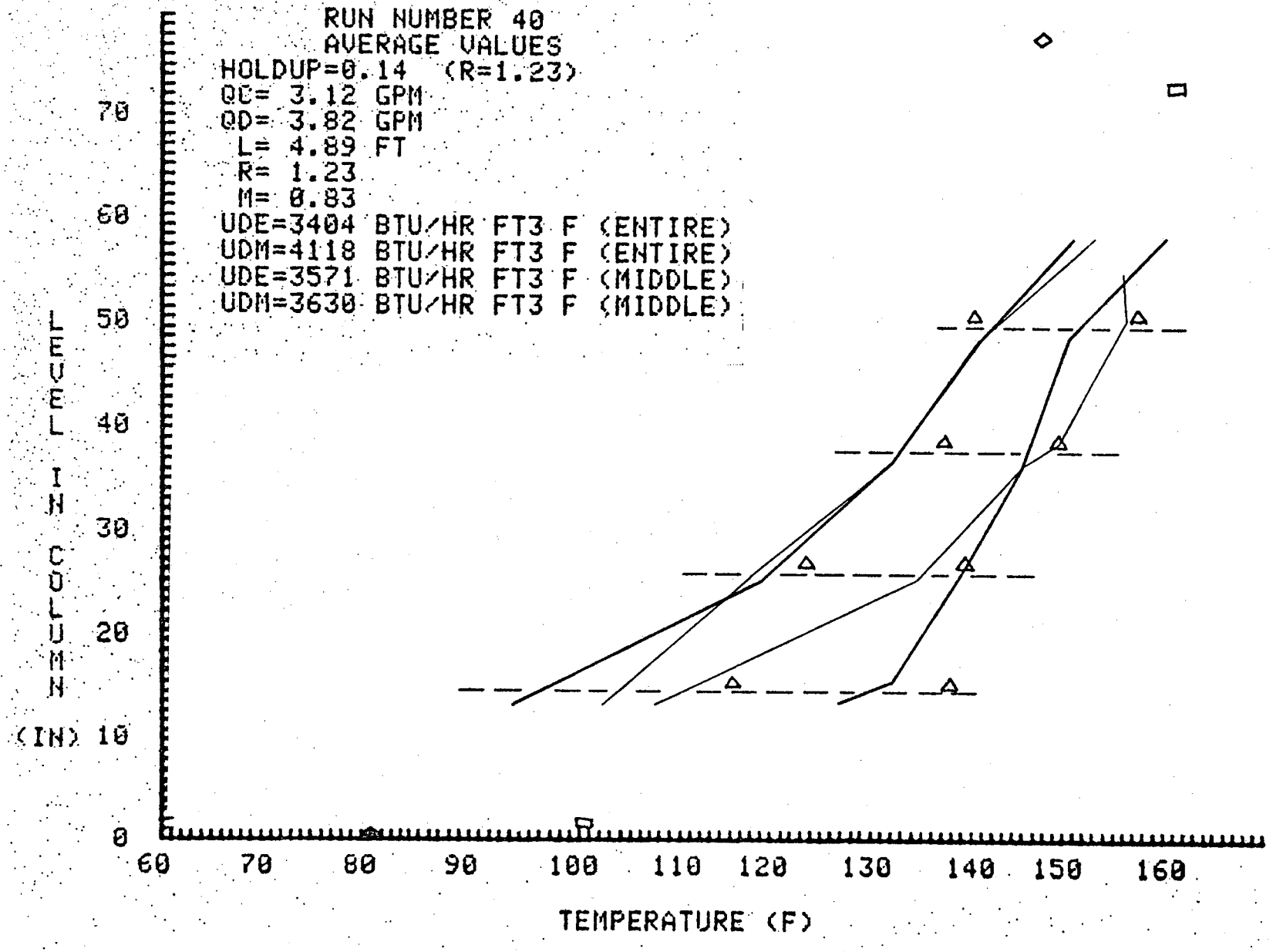

Temperature Values, Run Number 40

RUN NUMBER 40
EXPERIMENTAL TEMP MINUS VALUE CALCULATED FROM MODEL
COLUMN A -- DIFFERENCE
COLUMN B -- % DIFFERENCE

WATER TEMP

T.C.#	A(F)	B(%)
15.	18.2	85.7
12.	3.8	97.3
9.	0.0	100.0
6.	4.9	96.9

KEROSENE TEMP

T,C,#	A(F)	B(%)
16.	8.9	91.5
13.	-1.5	101.3
10.	0.2	99.8
7.	-0.1	100.1

REPITITION TIME= 0.5
R1= 0.37190 R2= 0.07000 R3= 0.05810

A1f= 8.70207 A2f= 2.66220 A3f= 12.72832
A1s= 0.05074 A2s= 0.02568 A3s= 0.11975

APPENDIX C

PERFORATED PLATE COLUMN TEMPERATURE PROFILES: M = 0.50

In these plots the experimental profiles are shown by thin lines and the profiles calculated from the model are shown by thick lines. Triangular shapes mark the maximum and minimum temperatures seen by each fast response thermocouple. Other continuous phase and dispersed phase temperatures are shown by rectangles and diamonds respectively. Horizontal dashed lines indicate the level of each plate.

Following each plot is a page giving a numerical comparison of the model and the experimental results. The comparisons are made just below the level of each plate with the first one being below the lowest plate. Also given are the durations in seconds that the fast response thermocouples were exposed to the continuous phase droplet, and wakes denoted R1, R2, and R3 respectively. The corresponding fast and slow response thermocouple time constants in seconds^{-1} are given by A1, A2, and A3.

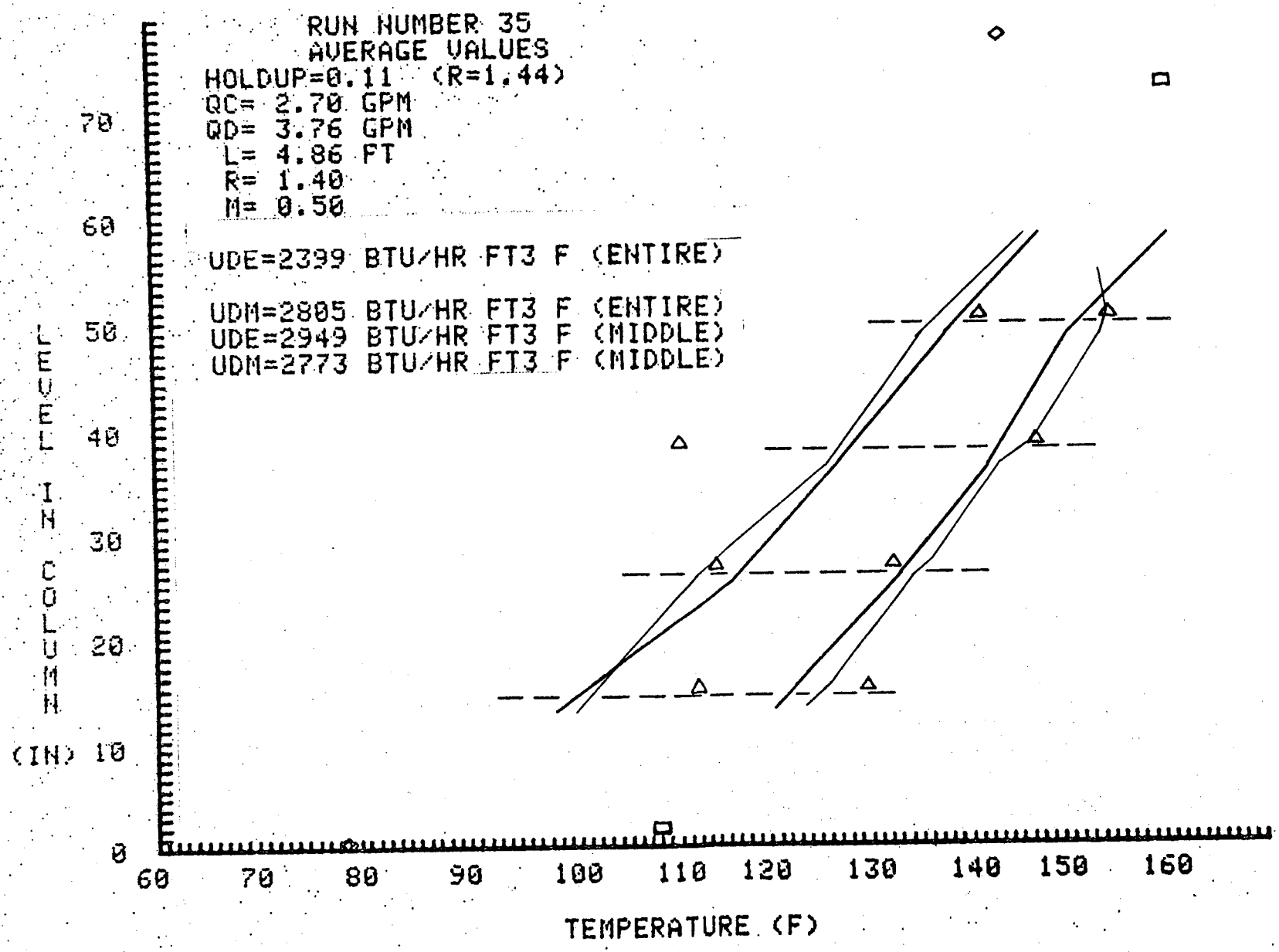

Temperature Values, Run Number 35

RUN NUMBER 35
EXPERIMENTAL TEMP MINUS VALUE CALCULATED FROM MODEL
COLUMN A -- DIFFERENCE
COLUMN B -- % DIFFERENCE

WATER TEMP

T.C.#	A(F)	B(%)
15.	3.1	97.5
12.	1.5	98.9
9.	1.0	99.0
6.	3.4	97.8

KEROSENE TEMP

T,C,#	A(F)	B(%)
16.	1.9	98.1
13.	-4.3	103.8
10.	-1.0	100.8
7.	-2.6	101.9

REPITITION TIME= 0.5
R1= 0.42125 R2= 0.05250 R3= 0.02625

A1f= 8.52404 A2f= 2.89174 A3f= 13.77881
A1s= 0.04779 A2s= 0.02960 A3s= 0.13784

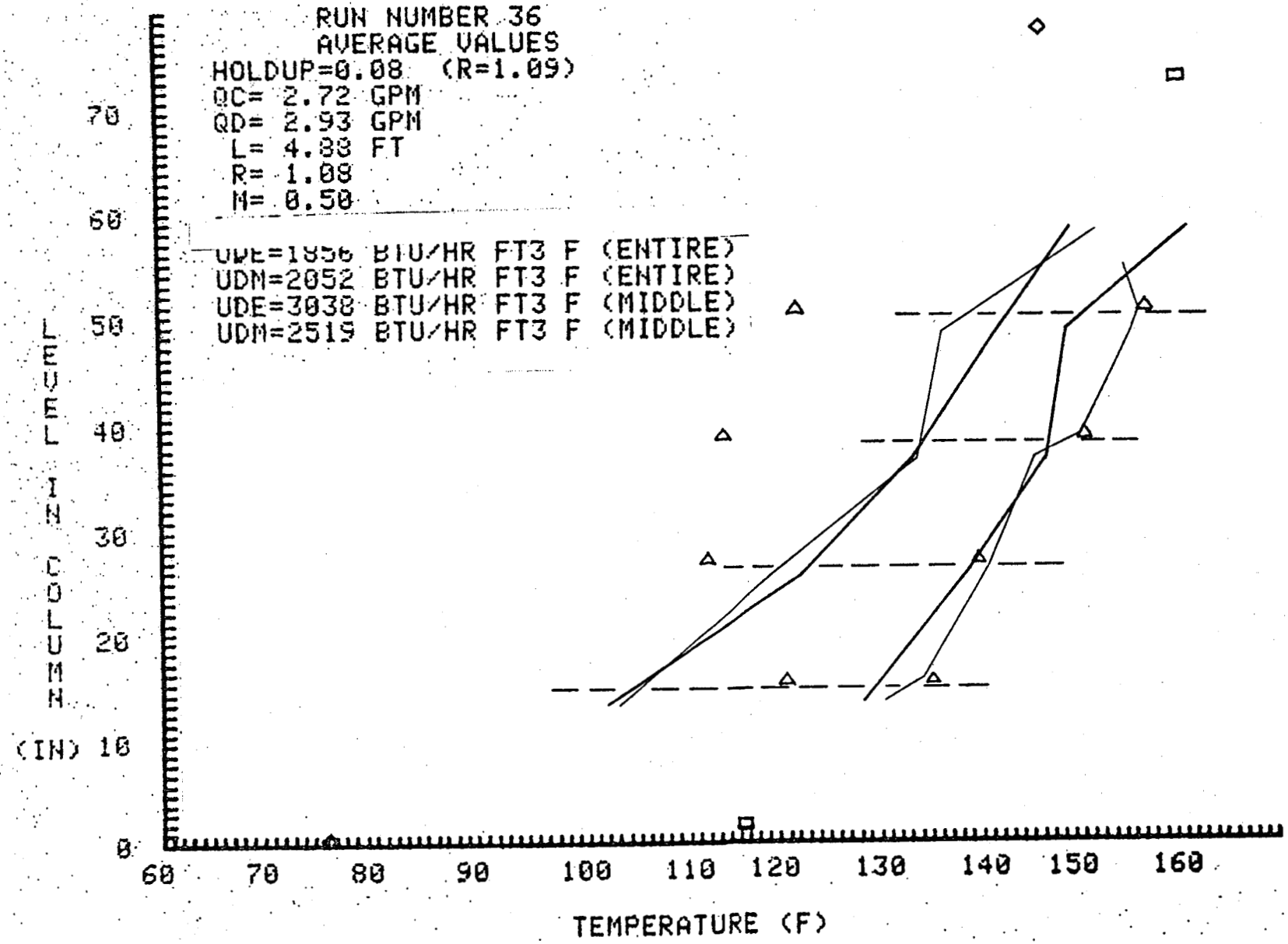

Temperature Values, Run Number 36

RUN NUMBER 36
EXPERIMENTAL TEMP MINUS VALUE CALCULATED FROM MODEL
COLUMN A -- DIFFERENCE
COLUMN B -- % DIFFERENCE

WATER TEMP

T.C.#	A(F)	B(%)
15.	2.2	98.3
12.	2.1	98.5
9.	-1.3	100.9
6.	6.4	95.9

KEROSENE TEMP

T.C.#	A(F)	B(%)
16.	1.1	98.9
13.	-3.0	102.5
10.	0.5	99.6
7.	-5.2	103.8

REPITITION TIME= 0.5
R1= 0.44375 R2= 0.03750 R3= 0.01875

A1f= 8.50118 A2f= 2.97233 A3f= 14.14793
A1s= 0.04741 A2s= 0.03098 A3s= 0.14422

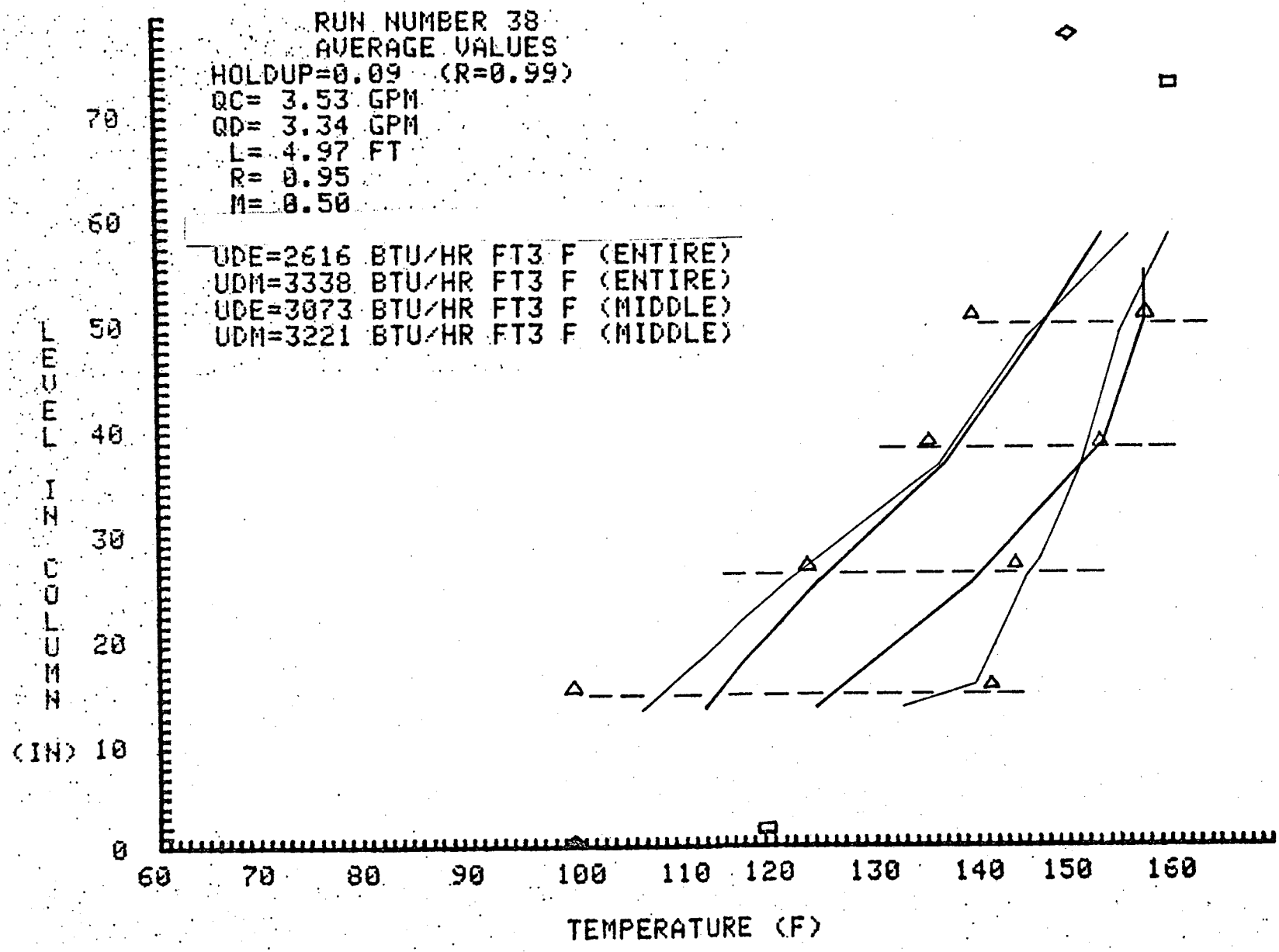

Temperature Values, Run Number 38

RUN NUMBER 38
EXPERIMENTAL TEMP MINUS VALUE CALCULATED FROM MODEL
COLUMN A -- DIFFERENCE
COLUMN B -- % DIFFERENCE

WATER TEMP

T.C.#	A(F)	B(%)
15.	8.8	93.4
12.	5.2	96.5
9.	0.0	100.0
6.	2.0	98.7

KEROSENE TEMP

T.C.#	A(F)	B(%)
16.	-6.0	105.6
13.	-3.4	102.8
10.	-0.5	100.4
7.	-0.8	100.5

REPITITION TIME= 0.5
R1= 0.43025 R2= 0.04650 R3= 0.02325

A1f= 8.77575 A2f= 2.89493 A3f= 13.79345
A1s= 0.05196 A2s= 0.02965 A3s= 0.13810

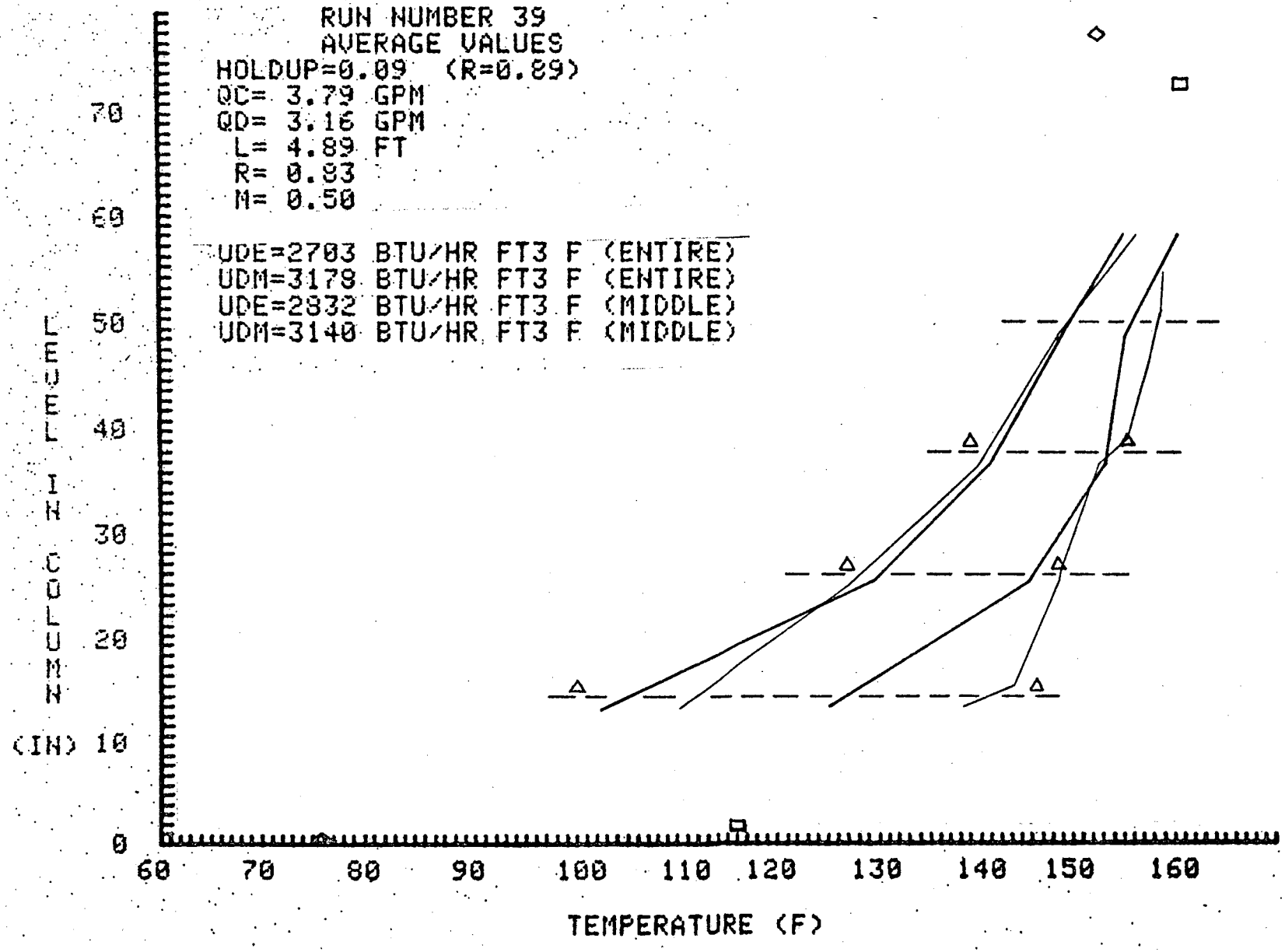

Temperature Values, Run Number 39

RUN NUMBER 39
EXPERIMENTAL TEMP MINUS VALUE CALCULATED FROM MODEL
COLUMN A -- DIFFERENCE
COLUMN B -- % DIFFERENCE

WATER TEMP

T.C.#	A(F)	B(%)
15.	13.1	90.6
12.	3.0	98.0
9.	-0.4	100.3
6.	2.9	98.2

KEROSENE TEMP

T,C,#	A(F)	B(%)
16.	7.8	93.0
13.	-1.9	101.5
10.	-1.0	100.7
7.	-0.2	100.2

REPITITION TIME= 0.5
R1= 0.43250 R2= 0.04500 R3= 0.02250

A1f= 8.84867 A2f= 2.87451 A3f= 13.69992
A1s= 0.05317 A2s= 0.02930 A3s= 0.13648

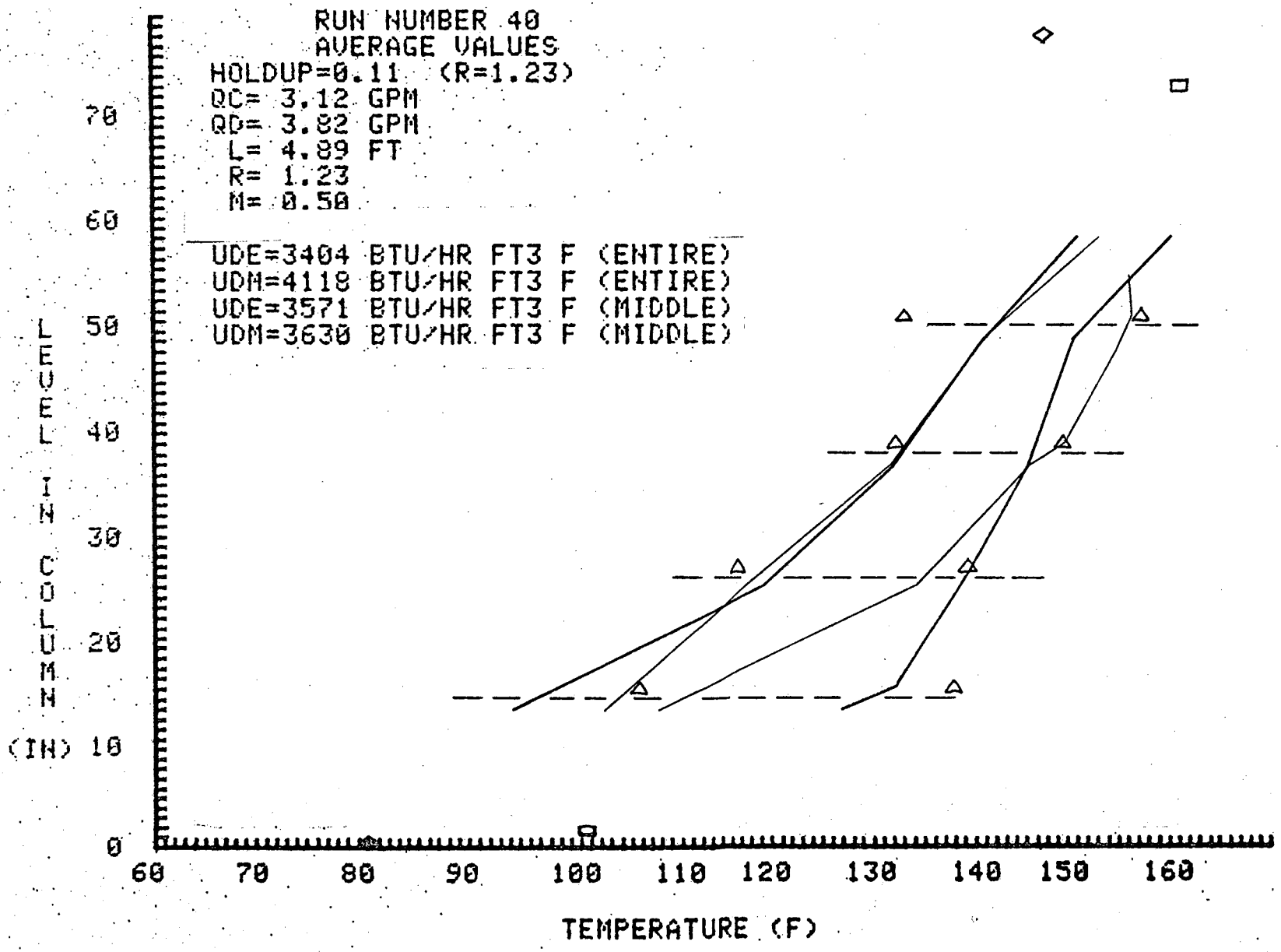

Temperature Values, Run Number 40

RUN NUMBER 40
EXPERIMENTAL TEMP MINUS VALUE CALCULATED FROM MODEL
COLUMN A -- DIFFERENCE
COLUMN B -- % DIFFERENCE

WATER TEMP

T.C.#	A(F)	B(%)
15.	18.2	85.7
12.	3.8	97.3
9.	0.0	100.0
6.	4.9	96.9

KEROSENE TEMP

T,C,#	A(F)	B(%)
16.	8.9	91.5
13.	-1.5	101.3
10.	0.2	99.8
7.	-0.1	100.1

REPITITION TIME= 0.5
R1= 0.41750 R2= 0.05500 R3= 0.02750

A1f= 8.66774 A2f= 2.86433 A3f= 13.65334
A1s= 0.05017 A2s= 0.02913 A3s= 0.13568

APPENDIX D

DATA

The averaged data for each run is given in this Appendix. The thermocouples are numbered 1 through 18 on all computer printouts. Refer to Figure 10 for the location of these thermocouples.

RUN NUMBER 24 SPRAY COLUMN
AVERAGE VALUES
HOLDUP=0.06 (R=0.68)
QC= 3.39 GPM
QD= 2.20 GPM
L= 4.85 FT
R= 0.65
M= 0.70
% HEAT LOSS=16.79
UDE=1196 BTU/HR FT3 F (ENTIRE)

SLOW RESPONSE THERMOCOUPLES

1	159.9	10	141.9
2	146.9	11	141.0
3	150.6	12	139.9
4	150.9	13	137.6
5	150.1	14	136.9
6	148.2	15	136.4
7	145.8	16	133.5
8	145.9	17	64.3
9	143.5	18	134.1

FAST RESPONSE THERMOCOUPLES

	MAX	MIN
1	140.0	137.2
5	136.5	133.2
9	140.0	138.0
13	144.0	141.3

RUN NUMBER 25 SPRAY COLUMN
AVERAGE VALUES

HOLDUP=0.06 (R=0.68)
QC= 3.39 GPM
QD= 2.20 GPM
L= 4.85 FT
R= 0.65
M= 0.70
% HEAT LOSS=16.79
UDE=1196 BTU/HR FT3 F (ENTIRE)

SLOW RESPONSE THERMOCOUPLES

1	159.9	10	141.9
2	146.9	11	141.0
3	150.6	12	139.9
4	150.9	13	137.6
5	150.1	14	136.9
6	148.2	15	136.4
7	145.8	16	133.5
8	145.9	17	64.3
9	143.5	18	134.1

FAST RESPONSE THERMOCOUPLES

	MAX	MIN
1	140.0	137.2
5	136.5	133.2
9	140.0	138.0
13	144.0	141.3

RUN NUMBER 26 SPRAY COLUMN
AVERAGE VALUES

HOLDUP=0.06 (R=0.68)
QC= 3.39 GPM
QD= 2.20 GPM
L= 4.85 FT
R= 0.65
M= 0.70
% HEAT LOSS=16.79
UDE=1196 BTU/HR FT3 F (ENTIRE)

SLOW RESPONSE THERMOCOUPLES

1	159.9	10	141.9
2	146.9	11	141.0
3	150.6	12	139.9
4	150.9	13	137.6
5	150.1	14	136.9
6	148.2	15	136.4
7	145.8	16	133.5
8	145.9	17	64.3
9	143.5	18	134.1

FAST RESPONSE THERMOCOUPLES

	MAX	MIN
1	140.0	137.2
5	136.5	133.2
9	140.0	138.0
13	144.0	141.3

RUN NUMBER 27 SPRAY COLUMN
AVERAGE VALUES

HOLDUP=0.06 (R=0.68)
QC= 3.39 GPM
QD= 2.20 GPM
L= 4.85 FT
R= 0.65
M= 0.70
% HEAT LOSS=16.79
UDE=1196 BTU/HR FT3 F (ENTIRE)

SLOW RESPONSE THERMOCOUPLES

1	159.9	10	141.9
2	146.9	11	141.0
3	150.6	12	139.9
4	150.9	13	137.6
5	150.1	14	136.9
6	148.2	15	136.4
7	145.8	16	133.5
8	145.9	17	64.3
9	143.5	18	134.1

FAST RESPONSE THERMOCOUPLES

	MAX	MIN
1	140.0	137.2
5	136.5	133.2
9	140.0	138.0
13	144.0	141.3

RUN NUMBER 28 SPRAY COLUMN
AVERAGE VALUES
HOLDUP=0.06 (R=0.68)
QC= 3.39 GPM
QD= 2.20 GPM
L= 4.85 FT
R= 0.65
M= 0.70
% HEAT LOSS=16.79
UDE=1196 BTU/HR FT3 F (ENTIRE)

SLOW RESPONSE THERMOCOUPLES

1	159.9	10	141.9
2	146.9	11	141.0
3	150.6	12	139.9
4	150.9	13	137.6
5	150.1	14	136.9
6	148.2	15	136.4
7	145.8	16	133.5
8	145.9	17	64.3
9	143.5	18	134.1

FAST RESPONSE THERMOCOUPLES

	MAX	MIN
1	140.0	137.2
5	136.5	133.2
9	140.0	138.0
13	144.0	141.3

RUN NUMBER 29 SPRAY COLUMN
AVERAGE VALUES

HOLDUP=0.06 (R=0.68)
QC= 3.39 GPM
QD= 2.20 GPM
L= 4.85 FT
R= 0.65
M= 0.70
% HEAT LOSS=16.79
UDE=1196 BTU/HR FT3 F (ENTIRE)

SLOW RESPONSE THERMOCOUPLES

1	159.9	10	141.9
2	146.9	11	141.0
3	150.6	12	139.9
4	150.9	13	137.6
5	150.1	14	136.9
6	148.2	15	136.4
7	145.8	16	133.5
8	145.9	17	64.3
9	143.5	18	134.1

FAST RESPONSE THERMOCOUPLES

	MAX	MIN
1	140.0	137.2
5	136.5	133.2
9	140.0	138.0
13	144.0	141.3

RUN NUMBER 30 SPRAY COLUMN
AVERAGE VALUES

HOLDUP=0.06 (R=0.68)
QC= 3.39 GPM
QD= 2.20 GPM
L= 4.85 FT
R= 0.65
M= 0.70
% HEAT LOSS=16.79
UDE=1196 BTU/HR FT3 F (ENTIRE)

SLOW RESPONSE THERMOCOUPLES

1	159.9	10	141.9
2	146.9	11	141.0
3	150.6	12	139.9
4	150.9	13	137.6
5	150.1	14	136.9
6	148.2	15	136.4
7	145.8	16	133.5
8	145.9	17	64.3
9	143.5	18	134.1

FAST RESPONSE THERMOCOUPLES

	MAX	MIN
1	140.0	137.2
5	136.5	133.2
9	140.0	138.0
13	144.0	141.3

RUN NUMBER 31 SPRAY COLUMN
AVERAGE VALUES

HOLDUP=0.06 (R=0.68)
QC= 3.39 GPM
QD= 2.20 GPM
L= 4.85 FT
R= 0.65
M= 0.70
% HEAT LOSS=16.79
UDE=1196 BTU/HR FT3 F (ENTIRE)

SLOW RESPONSE THERMOCOUPLES

1	159.9	10	141.9
2	146.9	11	141.0
3	150.6	12	139.9
4	150.9	13	137.6
5	150.1	14	136.9
6	148.2	15	136.4
7	145.8	16	133.5
8	145.9	17	64.3
9	143.5	18	134.1

FAST RESPONSE THERMOCOUPLES

	MAX	MIN
1	140.0	137.2
5	136.5	133.2
9	140.0	138.0
13	144.0	141.3

RUN NUMBER 32 SPRAY COLUMN
AVERAGE VALUES
HOLDUP=0.06 (R=0.68)
QC= 3.39 GPM
QD= 2.20 GPM
L= 4.85 FT
R= 0.65
M= 0.70
% HEAT LOSS=16.79
UDE=1196 BTU/HR FT3 F (ENTIRE)

SLOW RESPONSE THERMOCOUPLES

1	159.9	10	141.9
2	146.9	11	141.0
3	150.6	12	139.9
4	150.9	13	137.6
5	150.1	14	136.9
6	148.2	15	136.4
7	145.8	16	133.5
8	145.9	17	64.3
9	143.5	18	134.1

FAST RESPONSE THERMOCOUPLES

	MAX	MIN
1	140.0	137.2
5	136.5	133.2
9	140.0	138.0
13	144.0	141.3

RUN NUMBER 33 SPRAY COLUMN
AVERAGE VALUES
HOLDUP=0.06 (R=0.68)
QC= 3.39 GPM
QD= 2.20 GPM
L= 4.85 FT
R= 0.65
M= 0.70
% HEAT LOSS=16.79
UDE=1196 BTU/HR FT3 F (ENTIRE)

SLOW RESPONSE THERMOCOUPLES

1	159.9	10	141.9
2	146.9	11	141.0
3	150.6	12	139.9
4	150.9	13	137.6
5	150.1	14	136.9
6	148.2	15	136.4
7	145.8	16	133.5
8	145.9	17	64.3
9	143.5	18	134.1

FAST RESPONSE THERMOCOUPLES

	MAX	MIN
1	140.0	137.2
5	136.5	133.2
9	140.0	138.0
13	144.0	141.3

RUN NUMBER 34 SPRAY COLUMN
AVERAGE VALUES
HOLDUP=0.06 (R=0.68)
QC= 3.39 GPM
QD= 2.20 GPM
L= 4.85 FT
R= 0.65
M= 0.70
% HEAT LOSS=16.79
UDE=1196 BTU/HR FT3 F (ENTIRE)

SLOW RESPONSE THERMOCOUPLES

1	159.9	10	141.9
2	146.9	11	141.0
3	150.6	12	139.9
4	150.9	13	137.6
5	150.1	14	136.9
6	148.2	15	136.4
7	145.8	16	133.5
8	145.9	17	64.3
9	143.5	18	134.1

FAST RESPONSE THERMOCOUPLES

	MAX	MIN
1	140.0	137.2
5	136.5	133.2
9	140.0	138.0
13	144.0	141.3

RUN NUMBER 35 PERFORATED PLATE COLUMN
AVERAGE VALUES

QC= 3.39 GPM
QD= 2.20 GPM
L= 4.85 FT
R= 0.65
M= 0.70
UDE=1196 BTU/HR FT3 F (ENTIRE)

SLOW RESPONSE THERMOCOUPLES

1	159.9	10	141.9
2	146.9	11	141.0
3	150.6	12	139.9
4	150.9	13	137.6
5	150.1	14	136.9
6	148.2	15	136.4
7	145.8	16	133.5
8	145.9	17	64.3
9	143.5	18	134.1

FAST RESPONSE THERMOCOUPLES

	MAX	MIN
1	140.0	137.2
5	136.5	133.2
9	140.0	138.0
13	144.0	141.3

RUN NUMBER 36 PERFORATED PLATE COLUMN
AVERAGE VALUES

QC= 3.39 GPM
QD= 2.20 GPM
L= 4.85 FT
R= 0.65
M= 0.70
UDE=1196 BTU/HR FT3 F (ENTIRE)

SLOW RESPONSE THERMOCOUPLES

1	159.9	10	141.9
2	148.9	11	141.0
3	150.6	12	139.9
4	150.9	13	137.6
5	150.1	14	136.9
6	148.2	15	136.4
7	145.8	16	133.5
8	145.9	17	64.3
9	143.5	18	134.1

FAST RESPONSE THERMOCOUPLES

	MAX	MIN
1	140.0	137.2
5	136.5	133.2
9	140.0	138.0
13	144.0	141.3

RUN NUMBER 37 PERFORATED PLATE COLUMN
AVERAGE VALUES

QC= 3.39 GPM
QD= 2.20 GPM
L= 4.85 FT
R= 8.65
M= 0.70
UDE=1196 BTU/HR FT3 F (ENTIRE)

SLOW RESPONSE THERMOCOUPLES

1	159.9	10	141.9
2	146.3	11	141.0
3	150.6	12	139.9
4	150.9	13	137.6
5	150.1	14	136.9
6	148.2	15	136.4
7	145.8	16	133.5
8	145.9	17	64.3
9	143.5	18	134.1

FAST RESPONSE THERMOCOUPLES

	MAX	MIN
1	140.0	137.2
5	136.5	133.2
9	140.0	138.0
13	144.0	141.3

RUN NUMBER 38 PERFORATED PLATE COLUMN
AVERAGE VALUES

QC= 3.39 GPM
QD= 2.20 GPM
L= 4.85 FT
R= 0.65
M= 0.70
UDE=1196 BTU/HR FT3 F (ENTIRE)

SLOW RESPONSE THERMOCOUPLES

1	159.9	10	141.9
2	146.9	11	141.0
3	150.6	12	139.9
4	150.9	13	137.6
5	150.1	14	136.9
6	148.2	15	136.4
7	145.8	16	133.5
8	145.9	17	64.3
9	143.5	18	134.1

FAST RESPONSE THERMOCOUPLES

	MAX	MIN
1	140.0	137.2
5	136.6	133.2
9	140.0	138.0
13	144.0	141.3

RUN NUMBER 39 PERFORATED PLATE COLUMN
AVERAGE VALUES

QC= 3.39 GPM
QD= 2.20 GPM
L= 4.85 FT
R= 0.65
M= 0.70
UDE=1196 BTU/HR FT3 F (ENTIRE)

SLOW RESPONSE THERMOCOUPLES

1	159.9	10	141.9
2	146.9	11	141.0
3	150.6	12	139.9
4	150.9	13	137.6
5	150.1	14	136.9
6	148.2	15	136.4
7	145.8	16	133.5
8	145.9	17	64.3
9	143.5	18	134.1

FAST RESPONSE THERMOCOUPLES

	MAX	MIN
1	140.0	137.2
5	136.5	133.2
9	140.0	138.0
13	144.0	141.3

RUN NUMBER 40 PERFORATED PLATE COLUMN
AVERAGE VALUES

QC= 3.39 GPM
QD= 2.20 GPM
L= 4.85 FT
R= 0.65
M= 0.70
UDE=1196 BTU/HR FT3 F (ENTIRE)

SLOW RESPONSE THERMOCOUPLES

1	159.9	10	141.9
2	146.9	11	141.0
3	150.6	12	139.9
4	150.9	13	137.6
5	150.1	14	136.9
6	148.2	15	136.4
7	145.8	16	133.5
8	145.9	17	64.3
9	143.5	18	134.1

FAST RESPONSE THERMOCOUPLES

	MAX	MIN
1	140.0	137.2
5	136.5	133.2
9	140.0	138.0
13	144.0	141.3